J Neurophysiol 93: 2194–2232, 2005.
First published November 3, 2004; doi:10.1152/jn.00983.2004.

Single-Column Thalamocortical Network Model Exhibiting Gamma Oscillations, Sleep Spindles, and Epileptogenic Bursts

Roger D. Traub,[1] Diego Contreras,[2] Mark O. Cunningham,[3] Hilary Murray,[3] Fiona E. N. LeBeau,[3] Anita Roopun,[3] Andrea Bibbig,[1] W. Bryan Wilent,[2] Michael J. Higley,[2] and Miles A. Whittington[3]

[1]*Departments of Physiology and Pharmacology, and Neurology, State University of New York, Downstate Medical Center, Brooklyn, New York;* [2]*Department of Neuroscience, University of Pennsylvania School of Medicine, Philadelphia, Pennsylvania; and* [3]*School of Biomedical Sciences, University of Leeds, Leeds, United Kingdom*

Submitted 20 September 2004; accepted in final form 3 November 2004

Traub, Roger D., Diego Contereas, Mark O. Cunningham, Hilary Murray, Fiona E. N. LeBeau, Anita Roopun, Andrea Bibbig, W. Bryan Wilent, Michael Higley, and Miles A. Whittington. Single-column thalamocortical network model exhibiting gamma oscillations, sleep spindles, and epileptogenic bursts. *J Neurophysiol* 93: 2194–2232, 2005. First published November 3, 2004; doi:10.1152/jn.00983.2004. To better understand population phenomena in thalamocortical neuronal ensembles, we have constructed a preliminary network model with 3,560 multicompartment neurons (containing soma, branching dendrites, and a portion of axon). Types of neurons included superficial pyramids (with regular spiking [RS] and fast rhythmic bursting [FRB] firing behaviors); RS spiny stellates; fast spiking (FS) interneurons, with basket-type and axoaxonic types of connectivity, and located in superficial and deep cortical layers; low threshold spiking (LTS) interneurons, which contacted principal cell dendrites; deep pyramids, which could have RS or intrinsic bursting (IB) firing behaviors, and endowed either with nontufted apical dendrites or with long tufted apical dendrites; thalamocortical relay (TCR) cells; and nucleus reticularis (nRT) cells. To the extent possible, both electrophysiology and synaptic connectivity were based on published data, although many arbitrary choices were necessary. In addition to synaptic connectivity (by AMPA/kainate, NMDA, and $GABA_A$ receptors), we also included electrical coupling between dendrites of interneurons, nRT cells, and TCR cells, and—in various combinations—electrical coupling between the proximal axons of certain cortical principal neurons. Our network model replicates several observed population phenomena, including *1*) persistent gamma oscillations; *2*) thalamocortical sleep spindles; *3*) series of synchronized population bursts, resembling electrographic seizures; *4*) isolated double population bursts with superimposed very fast oscillations (>100 Hz, "VFO"); *5*) spike-wave, polyspike-wave, and fast runs (about 10 Hz). We show that epileptiform bursts, including double and multiple bursts, containing VFO occur in rat auditory cortex in vitro, in the presence of kainate, when both $GABA_A$ and $GABA_B$ receptors are blocked. Electrical coupling between axons appears necessary (as reported previously) for persistent gamma and additionally plays a role in the detailed shaping of epileptogenic events. The degree of recurrent synaptic excitation between spiny stellate cells, and their tendency to fire throughout multiple bursts, also appears critical in shaping epileptogenic events.

INTRODUCTION

The greatest scientific challenge, perhaps, in all of brain research is how to understand the cooperative behavior of large numbers of neurons. Such cooperative behavior is necessary for sensory processing and motor control, planning, and in the case of humans, at least, for thought and language. Yet it is a truism to observe that single neurons are complicated little machines, as well as to observe that not all neurons are alike—far from it; and finally to observe that the connectional anatomy and synaptology of complex networks, in the cortex for example, have been studied long and hard, and yet are far from worked out. Any model, even of a small bit of cortex, is subject to difficulties and hazards: limited data, large numbers of parameters, criticisms that models with complexity comparable to the modeled system cannot be scientifically useful, the expense and slowness of the necessary computations, and serious uncertainties as to how a complex model can be compared with experiment and shown to be predictive.

The above difficulties and hazards are too real to be dismissed readily. In our opinion, the only way to proceed is through a state of denial that any of the difficulties need be fatal. The reader must then judge whether the results, preliminary as they must be, help our understanding.

Previous models of cortical or thalamocortical circuits have been developed, usually with specific applications in mind (Bal et al. 2000; Bazhenov et al. 2002, 2004; Bush and Sejnowski 1996; Contreras et al. 1996; Destexhe et al. 1996, 1999; Douglas and Martin 1991; Golomb and Amitai 1997; Lytton et al. 1997; Pinto et al. 2003; Wang and Rinzel 1993). These previous models tend to use small numbers of cells and usually represent each cell with one or a few compartments. We are not aware of a previous model that has a multiplicity of cell types and firing behaviors in cortical cells, including regular spiking (RS), fast rhythmic bursting (FRB) (Gray and McCormick 1996; Steriade et al. 1998), and intrinsic bursting (IB) (McCormick et al. 1982; Nowak et al. 2003). It has been unusual to include electrical coupling, particularly between the axons of principal cells, a form of coupling that appears to be essential for persistent gamma and for very fast oscillations (>70 Hz) (Cunningham et al. 2004a,b; Traub et al. 2002, 2003a,b).

We have attempted here to construct a thalamocortical circuit model that has applicability to the study of a range of emergent behaviors in the thalamocortical network. Our attempt hinges on an effort to be faithful to a range of intrinsic properties in different neuronal types (Llinás 1988) and to

Address for reprint requests and other correspondence: R. D. Traub at Departments of Physiology and Pharmacology, and Neurology, State University of New York, Downstate Medical Center, 450 Clarkson Ave., Box 31, Brooklyn, NY 11203 (E-mail: roger.traub@downstate.edu).

The costs of publication of this article were defrayed in part by the payment of page charges. The article must therefore be hereby marked "*advertisement*" in accordance with 18 U.S.C. Section 1734 solely to indicate this fact.

include a variety of between-cell interactions, both chemical synaptic and gap junction-mediated. Although the model does indeed describe, predictively, several sorts of network behaviors (as will be seen below), it is insufficient to describe many others: for reasons that include, but are not limited to, the omission of many cell types, the requirement to make many guesses about structural details, the absence of mechanisms to simulate synaptic plasticity (either short-term or long-term), and the restriction of the model to a single column. In particular, the present model is best suited to address the physiology of network oscillations and epileptogenesis.

A major question to be addressed here concerns the role of axonal gap junctions (Schmitz et al. 2001) in epilepsy. A number of experimental studies suggest a role of gap junctions in epileptogenesis (Gajda et al. 2003; Jahromi et al. 2002; Köhling et al. 2001; Pais et al. 2003; Perez-Velazquez et al. 1994; Ross et al. 2000; Schweitzer et al. 2000; Szente et al. 2002; Traub et al. 2001, 2002). Earlier modeling studies of hippocampal pyramidal cell networks (Traub et al. 1999) predicted that gap junctions, if located between the axons of pyramidal cells, are expected to have 2 effects on epileptogenesis: *1*) they would lower the extent of recurrent chemical synaptic excitation required for population synchronization of bursts of action potentials; *2*) they would introduce a very fast oscillation (>70 Hz, "VFO") on top of the interictal field potential. [Earlier studies of such a superimposed very fast oscillation in hippocampus (Snow and Dudek 1984) had considered the possibility of field-effect–induced synchronization.] In the cortex, VFO is of interest not only because of its association with human epilepsy (Bragin et al. 1999; Staba et al. 2004), but also because of the appearance of VFO in somatosensory evoked potentials in rat barrel cortex (Jones and Barth 1999, 2002; Jones et al. 2000).

We have paid particular attention to electrical coupling between principal cell axons because of the necessity to include such an effect, to account for experimental recordings of kainate-induced persistent gamma in superficial layers of auditory cortex in vitro (Cunningham et al. 2004), and also because of clinical data documenting, in human epilepsy patients, the presence of VFO superimposed on seizure burst complexes, and on interictal spikes (Traub et al. 2001): earlier work in hippocampus (Traub and Bibbig 2000) had shown that the postulate of axonal coupling between hippocampal pyramidal cells could account for the occurrence of VFO on top of physiological sharp waves (Ylinen et al. 1995), even though the sharp waves are primarily mediated by a synaptically coupled network. Further details suggesting that axonal coupling could occur in cortex are discussed in APPENDIX B.

Topics covered in this paper include: kainate-induced persistent gamma oscillations and sleep spindles; then epileptogenesis, with illustrations of patterns resembling interictal spikes, fast runs, spike-wave, and polyspike-wave. These topics were selected because they are logically related: they are all associated with slow sleep oscillations, and its transition to seizures, in vivo (Steriade 2003). We include some experimental recordings that are consistent with some of the model predictions, particularly on the presence of very fast oscillations superimposed on epileptiform field potentials, and on firing patterns of layer 4 spiny stellate cells during seizurelike events. Further topics are considered in the appendices. APPENDIX A describes how individual cell types were modeled. APPENDIX B describes between-cell interactions, both synaptic and by electrical coupling. APPENDIX C deals with technical issues of how the large computations were carried out.

A note on terminology: sleep spindles refer to a well-known in vivo population phenomenon (Steriade 2001, 2003), appearing in natural slow-wave sleep in addition to other states, and consisting of cellular oscillations (about 10 to about 15 Hz, depending on species) that involve thalamic relay cells, nucleus reticularis thalami (nRT) cells, and cortical cells. Network phenomena in vitro, which exhibit a similar appearance in terms of cellular oscillations, shall be called simply "spindles."

METHODS

Simulation methods

We confine ourselves here to general comments on our philosophy of modeling and the overall network architecture. Specific details on single-cell properties are described in APPENDIX A; on synaptic and gap-junctional interactions (connectivity, kinetics, and conductance amplitudes) in APPENDIX B; and on programming issues and the use of the parallel computer in APPENDIX C. [In addition, interested readers may obtain copies of the Fortran code and Linux compilation and execution scripts by writing to roger.traub@downstate.edu.]

The approach to modeling single neurons grew out of 2 earlier studies (Traub et al. 1994, 2003c). The code described in the latter reference was the basis for simulating 2 of the cell types here. The approach is to use an electrotonic architecture containing dozens of compartments, but nowhere near the number of compartments used to model an anatomically reconstructed neuron. Network simulations, on a large scale anyway, are not practical with such detailed neurons. Dozens of compartments are sufficient to capture certain aspects of neuronal function, including differences in electrogenesis between axon, soma, and dendrites; action potential initiation in the axon; dendritic calcium spikes and bursts; spike backpropagation; and to allow for axons and/or dendrites to be electrically coupled between neurons.

The structure of a particular neuron is described by its compartmental topology; the values of electrotonic parameters such as specific membrane capacitance, membrane resistivity, and internal resistivity (some of which can be different in the axon compared with soma/dendrites); the densities of a fixed repertoire of ionic conductances, where the same repertoire of conductances was used, for the sake of simplicity, in *all* cell types; and by parameters describing the kinetics of $[Ca^{2+}]$ concentration in a thin submembrane shell. Again for the sake of simplicity, the first-order kinetic scheme for submembrane $[Ca^{2+}]$ concentration was the same for all cell types; only the particular parameters were different. Submembrane $[Ca^{2+}]$ concentration is used to gate the slow AHP conductance, and (along with membrane voltage) one of the fast K conductances—the "C" conductance. All neurons of a given type (e.g., layer 2/3 RS pyramidal neurons) have the same parameter set: heterogeneity can be introduced by the use of slightly different bias currents. A final simplification is to use, wherever possible, identical kinetics for voltage-sensitive channels between different neuron types. Exceptions to this latter rule include the use of different fast g_{Na} and delayed rectifier $g_{K(DR)}$ kinetics in pyramidal cells versus cells with stellate or interneuron-like morphology; and the use of different T-channel kinetics in nRT versus thalamocortical relay (TCR) neurons. Our experience has been that using 50 to 100 or so compartments is sufficient to capture many detailed aspects of neuronal firing behavior (Traub et al. 1994, 2003c).

The "standard repertoire" of active ionic conductances are these: fast, transient, g_{Na}; persistent g_{Na}; K conductances of delayed rectifier, A (transient, inactivating), slow AHP, C (fast voltage- and calcium-

dependent), "K2," and "M" types; high- and low-threshold g_{Ca}; and a relatively slow anomolous rectifier, or "h," conductance.

The cell types and cell locations of the 3,560-neuron model are shown in Fig. 1. The cortical portion of the model is one-dimensional, the dimension being cortical depth: dimensions parallel to the pia are not represented, so that the structure can be thought of as a column. Space is not defined within the thalamic portion. The reader should note the following: there is no layer 1; layers 2 and 3 are lumped together; a large variety of neuronal types are omitted, including but not limited to: neurogliaform cells, double bouquet cells, multipolar bursting neurons (Blatow et al. 2003), and numerous other sorts of interneurons; there are no pyramidal cells in layer 4; synaptic inhibition in layer 4 derives primarily from deep interneurons; there are no FRB cells in deep layers nor FRB interneurons (which were shown to exist by Steriade et al. 1998); there is homogeneity of cell structure within layers. Considerations in choosing the repertoire that we used were these: we began with a model of layer 2/3 circuitry that included RS and FRB pyramidal cells, as well as superficial fast-spiking (FS) and low-threshold spiking (LTS) interneurons (Cunningham et al. 2004a). We needed layer 4 stellate cells as the major recipient of thalamic inputs. Tufted pyramids in layer 5 are a major neuronal type, much studied, and important for cortical outputs not headed for the thalamus; and both IB and occasionally RS firing patterns have been described in these cells (Williams and Stuart 1999). Layer 6 pyramids were needed as an interface to the thalamus. Deep interneurons were necessary because, for among other reasons, we know that in vitro gamma/beta oscillations have different structure in deep versus superficial layers (A. Roopun and M. A. Whittington, unpublished data). Finally, both nRT and TCR thalamic neurons are essential for the understanding of thalamic oscillations, including sleep spindles, as presented here, but also for subsequent work including delta waves and the slow (<1 Hz) oscillation of sleep (Steriade et al. 1993).

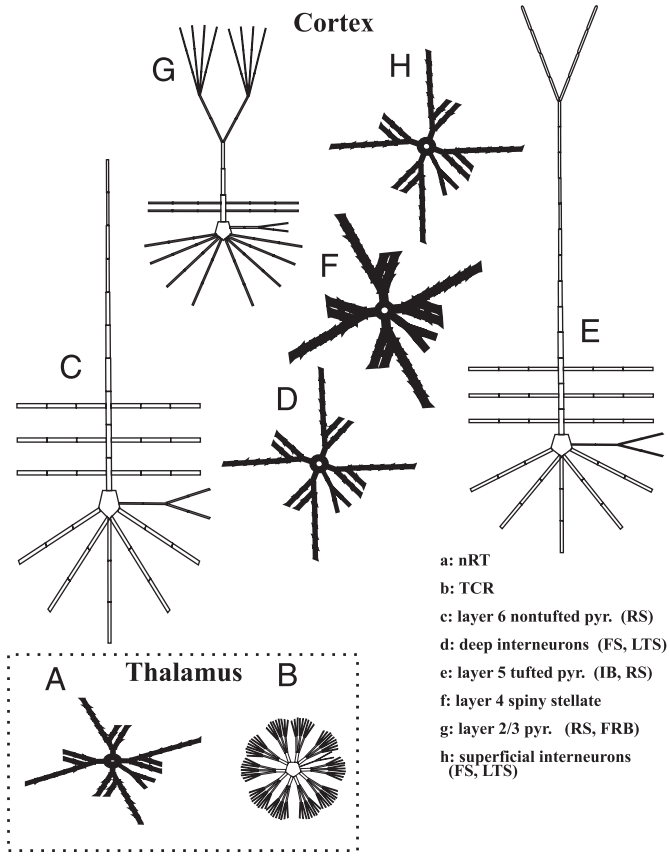

FIG. 1. General architecture of the model. All neurons are multicompartmental, with soma, branching dendrites, and a short branching axon. *Thalamic* portion of the network contains (a) 100 nucleus reticularis thalami (nRT) cells [each with low-threshold g_{Ca}, and lacking intrinsic gamma oscillatory properties (Contreras et al. 1993; Pinault and Deschênes 1992)], as well as (b) 100 "typical" thalamocortical relay (TCR) cells [i.e., also lacking intrinsic gamma oscillations (Steriade et al. 1993)]. *Cortical* portion contains the following cell types: (c) 500 layer 6 nontufted pyramidal neurons that connect intracortically, as well as to nRT and TCR neurons (the only model cortical cells to connect to the thalamus); (d) 100 deep fast-spiking (FS) basket interneurons, 100 deep axoaxonic interneurons, 100 deep low threshold spiking (LTS) dendrite-contacting interneurons; (e) 800 layer 5 tufted intrinsic bursting (IB) pyramidal neurons and 200 layer 5 tufted regular spiking (RS) pyramidal neurons; (f) 240 layer 4 spiny stellate cells, the major (but not only) recipients of thalamic inputs; (g) 1,000 layer 2/3 RS pyramidal cells and 50 layer 2/3 fast rhythmic bursting (FRB) pyramidal cells; (h) 90 superficial basket interneurons, 90 superficial axoaxonic interneurons, and 90 LTS interneurons.

APPENDIX A provides further details on the structure of the individual cell models and illustrates examples of some of their firing behaviors, considered as single neurons in isolation from other neurons.

The neurons were connected together *1*) by chemical synapses, using AMPA and NMDA receptors, and γ-aminobutyric acid-A ($GABA_A$; but not $GABA_B$) receptors; and *2*) gap junctions, that were nonrectifying and voltage-independent. Connections of both sorts were "wired up" randomly, subject to constraints on how many connections there were, and the possible locations of postsynaptic compartments. A given excitatory synapse activated both α-amino-3-hydroxy-5-methyl-4-isoxazolepropionic acid (AMPA) and *N*-methyl-D-aspartate (NMDA) receptors. Gap junctions were located between dendrites of cortical interneurons, of nRT cells (Landisman et al. 2002), and of TCR cells (Hughes et al. 2002a). Gap junctions could also be located between the axons of *1*) the pool of superficial pyramids, RS and FRB; and/or *2*) the pool of spiny stellates; and/or *3*) the pool of layer 5 tufted pyramids; and/or *4*) the pool of layer 6 nontufted pyramids. It was a major assumption that only homologous sorts of glutamatergic neurons could be electrically coupled by their axons (see APPENDIX B).

We justified the use of axonal coupling as follows: *1*) it is necessary in models for the occurrence of gamma oscillations (Cunningham et al. 2004a); *2*) spikelets occur in cortical neurons (Cunningham et al. 2004a; Deschênes,1981; Thomson and Bannister 2004; however, the Deschênes study attributed the spikelets to synaptic activation); *3*) there is staining for pannexin 2 [a putative component of the electrical coupling substrate between axons (Bruzzone et al. 2003)] throughout cortical layers 2–6 (Cunningham et al. 2004a); *4*) very fast oscillations occur in the cortex (Traub et al. 2001; this paper).

Certain important state variables could not be included, such as fluctuations in extracellular ion concentrations. In addition, we did not allow for afferent inputs (coming from outside the model network), or for specific effects of neuromodulators on membrane properties, although we did depolarize selected neuronal subpopulations (including FRB neurons, and at times pyramidal neurons in layers 5 and 6), using steady bias currents. All collective behaviors simulated are thus essentially "autonomous" in the model network.

The effects of the many simplifications made here will become known as progressively more detailed models are constructed and their behaviors analyzed. It is to be hoped that—as the model incorporates further cell types, membrane currents, metabotropic effects, more accurate synaptic connectivity, and so forth—then it will be possible to study a broader range of network phenomena, including the slow oscillation of sleep, gamma oscillations in deep cortical layers, and cortical responses to thalamic activation.

In APPENDIX B, we list the set of "baseline" synaptic conductance scaling constants. These, and details of connectivity, were arrived at after extensive (dozens) of preliminary simulations. (Many dozens of preliminary simulations were also necessary for each individual cell model.) Then, for this paper, we can list modifications in synaptic conductances relative to the baseline values. APPENDIX B also describes between-cell connectivity (synaptic and gap junctional), methods for

estimating field potentials, and other matters related to ensemble activity.

APPENDIX C describes computer science and numerical integration aspects of how our large calculations were performed on a parallel computer (Linux cluster). (For questions about these issues and copies of the code, or portions thereof, the reader can contact roger.traub@downstate.edu.)

The parameters of greatest interest in the RESULTS will be these: which populations of cortical principal cells are electrically coupled; how cortical inhibitory postsynaptic conductances (IPSCs) are scaled; steady depolarizing currents to particular subpopulations of neurons; the properties of AMPA and NMDA conductances at synapses between layer 4 spiny stellate cells; the effects on cortical activity of disconnecting the thalamus.

In vitro experimental methods

Horizontal slices (450 μm thick) were prepared from adult male Wistar rats (150–250 g). Neocortical slices containing primary and secondary auditory regions and secondary parietal regions were maintained at 34°C at the interface between warm wetted 95% O_2-5% CO_2 and artificial cerebrospinal fluid (CSF) containing (in mM): KCl 3; NaH_2PO_4 1.25; $MgSO_4$ 1; $CaCl_2$ 1.2; $NaHCO_3$ 24; glucose 10; NaCl 126. Extracellular recordings from primary auditory cortex were obtained by using glass micropipettes containing artificial CSF (resistance $<$0.5 MΩ). Intracellular recordings were obtained with sharp microelectrodes filled with potassium acetate (resistance 30–90 MΩ), and, in some cases, with the addition of 2% biocytin. For identification of biocytin-filled cells, slices were immediately fixed in 4% paraformaldehyde (PFA) in phosphate-buffered saline, following the recording. Signals were analog filtered at 2 kHz and digitized at 10 kHz. Cells other than those in layer 4 were identified by physiological criteria (regular spiking, fast spiking, intrinsic bursting). Slices were bathed in 400 nM kainate (Tocris, Bristol, UK) and 40 μM picrotoxin (Tocris). In some cases, CGP55845A (10 μM, Sigma-Aldrich UK, Dorset, UK) was added as well, to block $GABA_B$ receptors. All procedures were carried out in accordance with the UK Animals (Scientific Procedures) Act of 1986.

In vivo experimental methods

Experiments were conducted in accordance with the ethical guidelines of the National Institutes of Health and with the approval of the Institutional Animal Care and Use Committee of the University of Pennsylvania. Adult male Sprague–Dawley rats (350–450 g) were anesthetized with pentobarbital (50 mg/kg intraperitoneally). Buprenorphine (0.03 mg/kg subcutaneously) was administered to provide additional analgesia. Animals were paralyzed with gallamine triethiodide and artificially ventilated. End-tidal CO_2 (3.5–3.7%) and heart rate were continuously monitored. Body temperature was maintained at 37°C by servocontrolled heating blanket and rectal thermometer (Harvard Apparatus, Holliston, MA). The depth of anesthesia was maintained by supplemental doses of the same anesthetic to keep a constant heart rate and a constant high-amplitude, low-frequency electroencephalogram (EEG) as recorded from a bipolar electrode inserted into the cortex.

For cortical intracellular recordings, a craniotomy was made to expose the surface of the barrel cortex (1.0–3.0 mm posterior to bregma, 4.0–7.0 mm lateral to the midline). The dura was resected over the recording area and mineral oil was applied to prevent dessication. The stability of recordings was improved by drainage of the cisterna magna, hip suspension, and filling of the holes made for recording with a solution of 4% agar.

Intracellular recordings were performed with glass micropipettes filled with 3 M potassium acetate and DC resistances of 80–90 MΩ. A high-impedance amplifier (band-pass of 0–5 kHz) with active bridge circuitry (Cygnus Technology, Delaware Water Gap, PA) was used to record and inject current into the cells. Data were digitized at 10 kHz and stored on a Nicolet Vision (Nicolet Instrument Technologies, Madison, WI). A computer operating Labview (National Instruments, Austin, TX) was used for the on-line averaging of responses. All data analysis was done off-line using routines written in Igor Pro (Wavemetrics, Lake Oswego, OR).

RESULTS

Persistent gamma oscillation

Persistent, or pharmacologically induced, gamma oscillations occur in in vitro preparations and are called "persistent" because, once initiated, they continue as long as the slice remains healthy (Fisahn et al. 1998). In rat auditory cortex in vitro, kainate-induced gamma oscillations have their maximal amplitude in superficial layers (Cunningham et al. 2004a). Interestingly, two other sorts of in vitro gamma oscillations have maximal amplitude in the superficial layers: interneuron gamma evoked by stimulating metabotropic glutamate receptors, during pharmacological blockade of ionotropic glutamate receptors (Whittington et al. 1995); and thalamically evoked cortical gamma oscillations in thalamocortical slices in vitro (Metherate and Cruikshank 1999). [Not all gamma oscillations in vitro follow this rule, however: when gamma is evoked in somatosensory cortex in vitro, with carbachol plus a low concentration of kainate, then the gamma occurs in all cortical layers, with deep gamma 180° out of phase with superficial gamma (Buhl et al. 1998).]

Our earlier model of auditory cortex kainate-induced persistent gamma (Cunningham et al. 2004a) involved simulations of layer 2/3 only, with RS and FRB pyramidal cells, FS interneurons (basket and axoaxonic), and LTS interneurons. Electrical coupling, between axons, occurred within and between RS and FRB pyramidal cell populations; dendritic electrical coupling occurred between FS interneuron dendrites and between LTS interneuron dendrites. As in earlier models of persistent gamma in hippocampus (Traub et al. 2000, 2003a,b), the superficial neocortical model produced gamma as a result of axonal spiking percolating through the principal cell axonal plexus (in the neocortical case, having such spiking boosted by FRB bursting), with resultant bursts of orthrodromic activation of interneurons, and with the interneurons then interrupting the principal cell somata and axons for some tens of milliseconds, by GABAergic inhibition, thereby producing the gamma period.

Figure 2 demonstrates persistent gamma in a full-thickness model of neocortex (the thalamus being disconnected here), one that includes the cell types of the original superficial cortical model, but many other cell types as well: layer 4 spiny stellates, deep pyramids, deep interneurons. Different bias currents were applied to some of the neurons, particularly to superficial FRB neurons (see legend). (This applies to other simulations as well.) As before (compare Cunningham et al. 2004a), gamma is of highest amplitude in the superficial layers (Fig. 2*A*); and cells in the superficial layers have similar firing patterns to the previous model, and to in vitro experiment: sporadic somatic firing of superficial RS pyramids on a background of rhythmic synaptic potentials (Fig. 2*B*), superficial FRB pyramids discharging on approximately every other burst, superficial FS interneurons (e.g., the basket cell shown in *bottom right panel*) firing on a majority of the gamma waves,

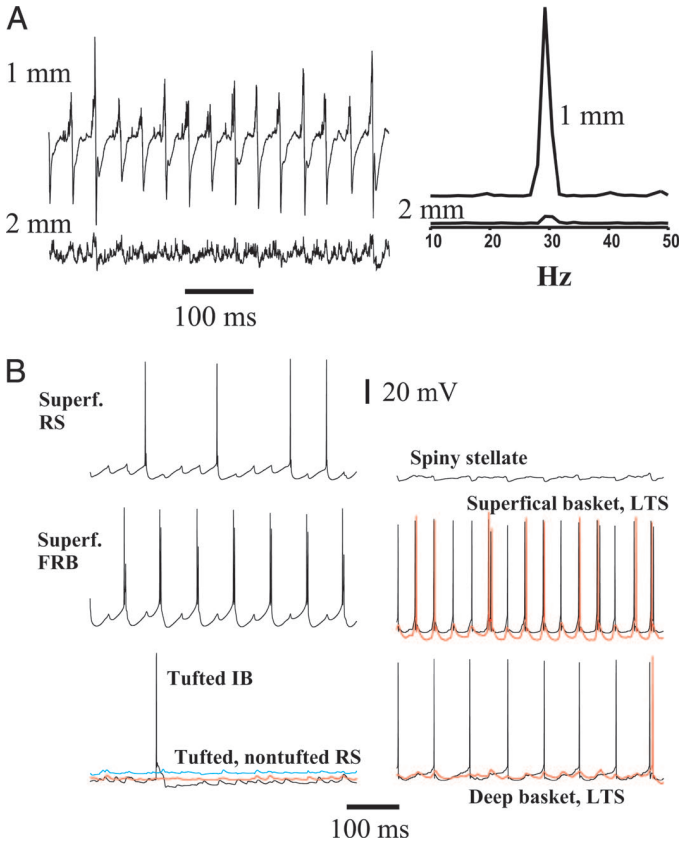

FIG. 2. Simulation of kainate-induced gamma oscillations. *A*: fields in superficial and deep sites, with corresponding power spectra. Note that the oscillations are generated in superficial layers. *B*: firing patterns of selected neurons (compare Cunningham et al. 2004a). (*LTS interneuron traces* are shown in red, *basket cell traces* in black; *tufted RS trace* is blue; *nontufted RS trace* is red.) This simulation was run with inhibitory postsynaptic conductances (IPSCs) 1.25 × baseline, and with "open" axonal gap junctions between cortical principal cells (conductance 4 nS for deep pyramids, and 3 nS for superficial pyramids and spiny stellates). Depolarizing currents were 0.25–0.35 nA for FRB neurons and were <0.1 nA for all other cortical principal cells.

and superficial LTS interneurons firing less than the FS cells. This simulation, however, is not sufficient to explain *why* the deep layers are not generating their own gamma, or at least being driven more strongly by the superficial gamma. The explanation could lie in differences in gap junctional connectivity between the two regions, in properties of interlaminar synaptic connections, in the model's lack of deep FRB neurons, or in other structural features. It is important to note that in vivo (in recordings from cat pericruciate gyri, anterior and posterior suprasylvian areas, and area 18 of the marginal gyrus), gamma oscillations occur in *both* superficial and deep layers with comparable amplitude (Steriade et al. 1996). In addition, FRB cells have been recorded in the infragranular layers of cat pericruciate and suprasylvian gyri (Steriade et al. 1998) and of cat primary visual cortex (J. Cardin and D. Contreras, unpublished data).

Sleep spindles generated in the thalamic network

Individual model thalamic relay cells, and model reticular neurons, fire in bursting and tonic modes, as occurs physiologically (Bal and McCormick 1993; Jahnsen and Llinás 1984a 1984b; Contreras et al. 1993; Deschênes et al. 1984) (APPENDIX A); model thalamic cells can generate rhythmic bursts at approximately 5 Hz during injection of a steady current (not shown). Figure 3 shows a simulated thalamic network spindle and its influence on the cortex. The spindle is initiated by a spontaneous burst in the reticular neurons (Fig. 3*A*). The spindle has a frequency of about 16 Hz (slightly above the frequency range for sleep spindles in cats, but at the upper limit for humans), and has a waxing/waning course (seen in the TCR average in Fig. 3*A*). The relatively fast spindle frequency shown here may be related to the relatively rapid time constants used for the decay of nRT cell-induced $GABA_A$ receptor-mediated IPSCs in TCR cells: 3.3 and 9 ms for the fast and slow components, respectively (APPENDIX B).

Interestingly, the spindle in Fig. 3 stops on its own; in the model case, cessation occurs without time- or calcium-dependent h-current kinetics in TCR neurons (Lüthi and McCormick 1998). Note that individual TCR neurons exhibit the expected sawtooth-like voltage fluctuations (resulting from rebound low-threshold calcium spikes), and each neuron fires on only a fraction of the waves. In contrast, nRT neurons discharge a burst on each spindle wave, as occurs in both in vivo (Contreras et al. 1993) sleep spindles and in vitro (Bal et al. 1995a,b) spindles. The nRT neurons do not, however, show a tonic depolarization as seen in vivo [perhaps attributable in part to persistent g_{Na} (Contreras and Steriade 1993)]; the model nRT neurons instead exhibit the slight tonic hyperpolarization that usually occurs in vitro in ferret slices (Bal et al. 1995a,b). [There are exceptions, however: sometimes nRT neurons in vitro do exhibit an underlying depolarization during a spindle oscillation, sustained by a persistent sodium conductance (Kim and McCormick 1998).] This spindle is generated entirely within the thalamic portion of the model, as corticothalamic excitatory postsynaptic conductances (EPSCs) (AMPA) in TCR (after the initial wave) are at most 0.2 nS.

Figure 3*B* illustrates the effects of the thalamic spindle on spiny stellate neurons: a series of synaptic depolarizations, sometimes with action potentials. Note further the coherent depolarizations in the spiny stellate cells, as shown in the middle trace in Fig. 3*B*, an inverted average of the somatic potentials of all layer 4 spiny stellates; this coherence is aided by the electrical coupling between spiny stellate axons used in the simulation. In addition, a small burst occurs (Fig. 3, *B* and *C*, *); this burst results because of the strong recurrent chemical synaptic excitation between the spiny stellates; when the coupling is weakened 8-fold, the burst does not occur (not shown). Multiphasic waves similar to the asterisk-marked burst in Fig. 3*C*, are on occasion observed in in vivo sleep spindles (Contreras and Steriade 1996; see also Beierlein et al. 2002).

Figure 3*C* shows (*top portion*) that cortical neurons, layer 5 tufted IB pyramids in particular, actually "see," at spindle frequency, a superimposition of synaptic excitation and inhibition; the inhibition results in the model because of strong feedforward excitation of interneurons by thalamic afferents (Swadlow 2003). Trains of IPSPs have been observed experimentally in vivo on the depolarizing phase of the slow oscillation in cortical neurons (Steriade et al. 1993).

Finally, Fig. 3*C* illustrates the behavior of superficial layer 2/3 RS pyramids, including the average of all of the layer 2/3 pyramids (note that the average signal is inverted, so as to approximate a local field potential). During the spindle itself,

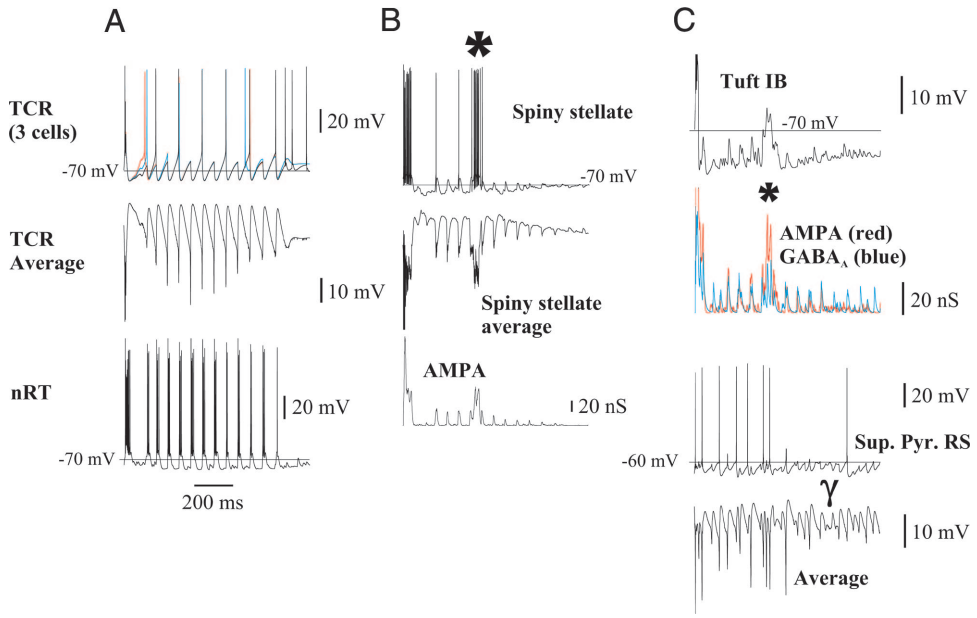

FIG. 3. Simulation of thalamic spindle, with its effects on the cortex. In this case, the corticothalamic input is small [peak α-amino-3-hydroxy-5-methyl-4-isoxazolepropionic acid (AMPA) conductance <0.2 nS in a TCR neuron during the spindle proper, i.e., after the first burst], so that the spindle is generated intrathalamically. Note (*A*) the spindlelike appearance in the mean behavior of thalamic neurons (waxing and waning), the intermittent firing of individual TCR neurons, and the bursting of the nRT cell on each spindle wave. [Compare with, for example, the sleep spindle in a decorticated, ketamine–xylazine anesthetized cat; Fig. 11 of Timofeev and Steriade (1996).] Spindle induces nearly simultaneous excitatory postsynaptic conductances (EPSCs) and IPSCs in cortical neurons (*B*, *C*) by the TCR excitation of both principal cells and interneurons. * marks the occurrence of a small synchronized burst among spiny stellates, dependent on the strong recurrent connections between spiny stellate cells in this simulation; complex synaptic potentials appear in other cortical neurons (e.g., tufted layer 5 IB pyramidal cell in *C*), coincident with the small burst in the spiny stellates. [Note that complex synaptic potentials can sometimes also occur in cortical neurons during in vivo sleep spindles: cf. Fig. 1*A* of Contreras and Steraide (1996).] The spindle is followed by gamma oscillation in superficial layers (*C*, *bottom trace*). Conditions: nRT cells biased by 0.17 to 0.18 nA, and TCR cells by −0.08 to −0.07 nA; axonal gap junction conductance = 3 nS for superficial pyramids and 0 nS for all other cortical principal cells; relative to "baseline conductances" (APPENDIX B), intrinsic nRT γ-aminobutyric acid (GABA) conductances × 0.2; TCR GABA conductances × 3; TCR → nRT AMPA × 3; layer 6 pyramids → nRT *N*-methyl-D-aspartate (NMDA) × 0.02; layer 6 pyramids → TCR NMDA × 0.2 and AMPA × 0.1.

there is a mixture of spindle intervals (about 16 Hz) and gamma intervals (about 30 Hz); gamma is possible in the superficial layers because, in this simulation, superficial pyramids are electrically coupled by their axons. As the spindle ends, gamma alone is present. In vivo as well (in cats) sleep spindles are often followed by a run of gamma oscillation (Steriade et al. 1996), although the gamma in vivo is in both cortex and thalamus. In our model, the gamma is only in the cortex. This difference from in vivo results may arise because the model does not include a mechanism for sustained depolarization of nRT and TCR neurons, such as occurs during the slow oscillation in vivo (Contreras and Steriade 1995; their Figs. 4 and 8), and which may be mediated by metabotropic glutamate receptors (Blethyn et al. 2003; Hughes et al. 2002), and/or by a persistent sodium conductance (Kim and McCormick 1998).

Our simulated spindles require synaptic interactions between nRT and TCR cells. Figure 4 shows that when nRT cells are isolated from other neurons—layer 6 pyramids and TCR neurons—but are not isolated from each other, then there is no spindling, either in the nRT population or elsewhere. (All other parameters in the simulation of Fig. 4 were as for Fig. 3.) Superficial layers (Fig. 4*B*) show continuous gamma oscillations. This model behavior corresponds to the behavior seen with the in vitro ferret slice model of spindles of Bal et al. (1995a,b), but is different from what has been described in vivo, wherein an isolated portion of nucleus reticularis appears to spindle on its own (Steriade et al. 1987). The model as now

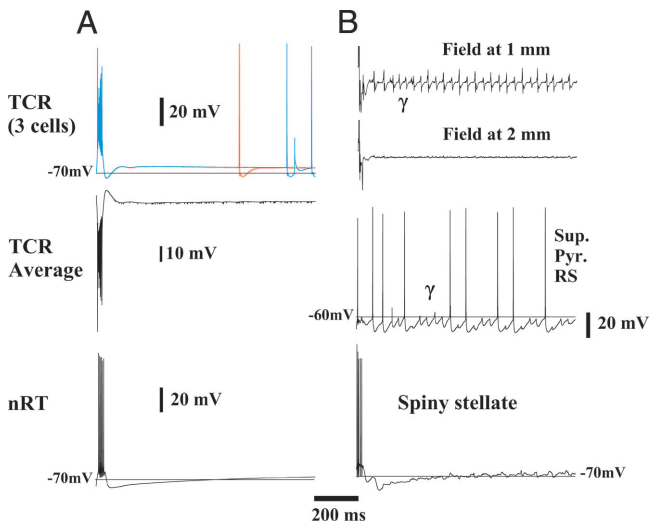

FIG. 4. Under the conditions of Fig. 3, but with nucleus reticularis isolated (i.e., corticoreticular connections are cut, as are connections from nRT neurons to TCR neurons, and vice versa), spindling does not occur. *A*: 3 superimposed TCR somatic voltages, the inverted average of all TCR somatic potentials, and an nRT somatic potential (as in Fig. 3*A*). *B*: cortical field potentials, somatic potential of a superficial RS pyramid and of a layer 4 spiny stellate cell. There are, in this simulation, continuous gamma oscillations in cortical superficial layers (note fields in *B*), reflecting the axonal coupling between pyramidal neurons there. Requirement for nRT/TCR interactions in this model for spindling to occur appears to be similar to in vitro ferret data (von Krosigk et al. 1993), and different from what has been reported for the cat in vivo (Steriade et al. 1987); but see Fig. 5.

constituted appears rather to be consistent with the notion of Ulrich and Huguenard (1997) that within-nRT synaptic inhibition subserves some purpose other than spindling, perhaps what they refer to as "lateral inhibition."

On the other hand, if we repeat the simulation of Fig. 4, isolating the nucleus reticularis, but now (Fig. 5) further depolarize nRT neurons (bias currents in Fig. 4 = 0.17 to 0.18 nA, in Fig. 5 bias currents = 0.27 to 0.28 nA), then a synchronized reticularis oscillation *does* occur (Fig. 5), at approximately 6 Hz. This simulated isolated nRT oscillation requires gap junctions to remain synchronized (Fig. 5*B*), but not within-nRT synaptic inhibition (Fig. 5*C*). Still further depolarization of the nRT neurons in the model resulted in rapid tonic firing; on the other hand, metabotropic effects such as reducing one or more K^+ conductances might have allowed a 10-Hz oscillation, a matter not further explored here. Landisman et al. (2002) observed oscillations in the reticular nucleus in vitro, that required gap junctional communication, but not synaptic transmission; their oscillations could occur at frequencies around 10 Hz. An in vivo study has also found evidence for electrical coupling between nRT neurons, in the form of halothane-sensitive spikelets, and simulations in that study showed that such coupling could contribute to the synchronization of sleep spindle oscillations (Fuentealba et al. 2004).

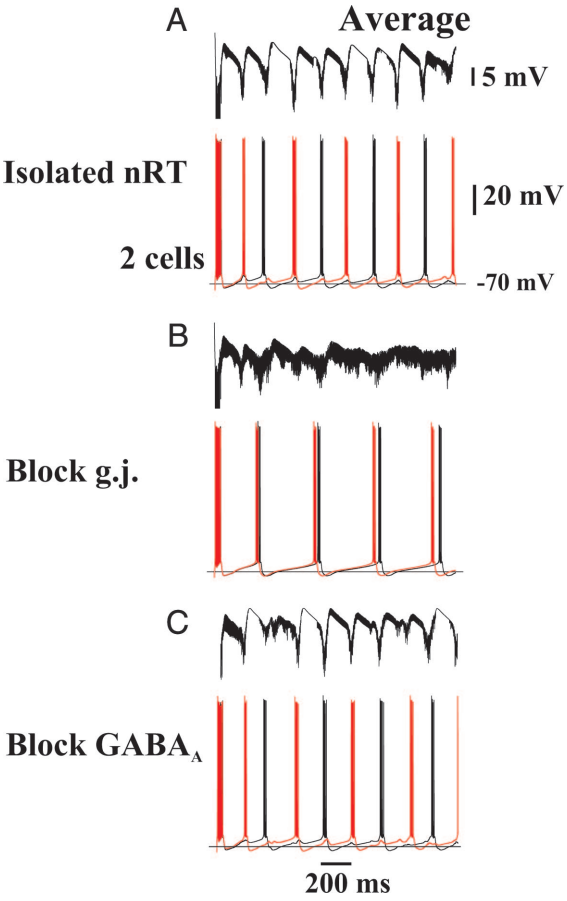

FIG. 5. Depolarization of nRT cells in the isolated model reticular nucleus leads to a 6-Hz synchronized oscillation that requires gap junctions (dendritic in this model, with conductance 1 nS and an average of 2.5 gap junctions on each cell), but that does not require recurrent inhibition. *A*: simulation of Fig. 4 was repeated, but with bias currents to the nRT cells increased by 0.1 nA. There is a 6-Hz population oscillation. *B*: same as *A*, but between-nRT gap junctions were blocked. *C*: same as *A* (with gap junctions intact), but between-nRT synaptic inhibition blocked.

Neocortical epileptogenesis in the presence of electrical coupling between subpopulations of principal neurons

In the monograph of Traub and Miles (1991), some of the basic principles of epileptogenesis in the disinhibited hippocampal CA3 region in vitro were analyzed. CA3 pyramidal cells are intrinsically bursting neurons, and are synaptically connected in such a way that an intrinsic burst in a single presynaptic neuron can evoke, with latency of tens of milliseconds, a burst in a monosynaptically connected postsynaptic neuron (Miles and Wong 1986, 1987). In addition, there is enough recurrent excitatory connectivity, even in vitro, so that on average bursting in one presynaptic neuron will actually evoke bursting in more than one postsynaptic neuron. Thus by a chain reaction, bursting in a single neuron can lead to bursting throughout the whole population, with latency from initial burst to peak number of cells firing dependent on the latency for bursting to spread from cell to cell, and on the density of connections. Although some of the excitatory synaptic connections between neocortical layer 5 tufted pyramids are extremely powerful (see APPENDIX B), we are not aware of data documenting the transmission of a burst from one neuron directly to another in neocortex, either for the case of layer 5 pyramids or for other pairs of neocortical neurons (either of homogeneous cell type or not). Thus it is not clear whether the above analysis of hippocampal bursts applies to cortex. It is certainly the case that during a synchronized burst in neocortex, each principal neuron "experiences" a very large EPSP (Gutnick et al. 1982), consistent with the synchronized discharge of many neurons, although this information is not sufficient to define how the synchrony comes about.

In Traub and Miles (1991), we also considered the case in which a homogeneous population of neurons were all regular spiking, and synaptic connections were not strong enough to transfer firing from a single neuron to another neuron (Fig. 6.11 of that monograph); we asked what sort of stimulus was necessary to synchronize the population. Clearly, firing in a single neuron will no longer suffice. It turns out that a threshold number of cells needs to be discharged together; the value of the threshold number depends on parameters, of course, but in general it can be much smaller than the total number of cells, even if much larger than one. What we did *not* consider at that time, however, was the possibility of electrical coupling between axons (Schmitz et al. 2001), which constitutes another pathway (besides excitatory chemical synapses) whereby action potentials might cross from neuron to neuron.

Because electrical coupling may well occur in neocortex between principal neurons (see APPENDIX B), and because of the heterogeneity of cell types in neocortex, it appears unlikely that an idea as simple as the "chain reaction" (described above) will suffice to capture exactly how synchronization takes place. Therefore what we shall attempt to do in the following is illustrate some examples of what can occur in the model, and make certain correlations with experimental observations. A more theoretical analysis must be deferred.

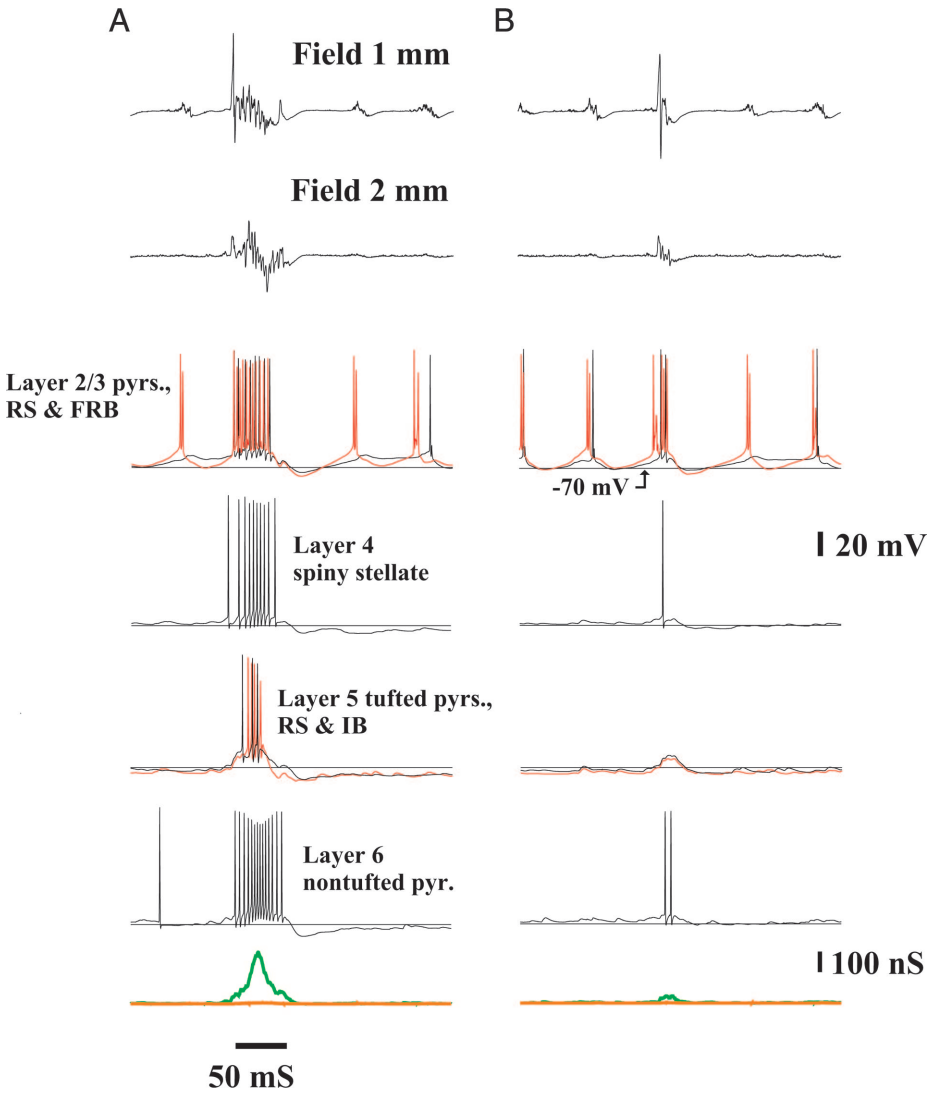

FIG. 6. Examples of synchronized epileptiform bursts that involve all cortical layers for about 50 ms (*A*), or that are attenuated and predominantly in superficial layers (*B*), from the same simulation. Note the superimposed very fast oscillation in the fields in *A* (about 300 Hz). Layer 2/3 pyramidal FRB and layer 5 tufted IB cell traces are in red. *Bottom traces*: total AMPA input (green) and $GABA_A$ input (orange) to the layer 6 nontufted pyramid just above. Thalamus disconnected and IPSC conductances × 0.1. Axonal gap junctions "open" between axons of superficial pyramids, spiny stellates and deep nontufted pyramids. Recurrent synaptic connections between spiny stellates have a "low" value (0.25 × baseline). Depolarizing bias currents of 0.1 nA to deep pyramids (tufted and nontufted).

SYNCHRONIZED AND PARTIALLY SYNCHRONIZED INTERICTAL BURSTS IN MODEL NEOCORTEX (THALAMUS DISCONNECTED), WITH INCOMPLETE DISINHIBITION, WEAK RECURRENT EXCITATION BETWEEN LAYER 4 SPINY STELLATES, AND ELECTRICAL COUPLING. Figure 6 illustrates varieties of "interictal" behavior when IPSCs are reduced (to 1/10 their baseline values), recurrent excitation between layer 4 spiny stellates is small (EPSCs at 0.25 × baseline; see APPENDIX B), and axonal gap junctions are "open" between superficial pyramids, between spiny stellates, and between layer 6 RS pyramids. (By "open" we mean that the gap junction has a high enough conductance that a spike can cross from axon to axon.) Figure 6*A* illustrates a "classical-appearing" interictal burst, which produces fields in superficial and deep layers and bursts in all cortical principal cell types. The *bottom traces* are the total AMPA conductance (green) and $GABA_A$ conductance (orange) developing in the layer 6 pyramid. Note the large "PDS" (paroxysmal depolarization shift) AMPA conductance, >100 nS (Matsumoto and Ajmone Marsan 1964; Prince 1968; Sawa et al. 1963). The inhibitory conductance during the PDS is small, even though inhibition is not completely blocked, and interneurons are firing robustly (not shown). Of additional note is the very fast oscillation (VFO) superimposed on the fields, especially at 1 mm (*topmost trace*), a topic to be considered further later on. Finally, there is a low-amplitude oscillation in the field at 1 mm (about 20 Hz), which results from the activity of the electrically and synaptically coupled superficial FRB pyramidal neurons.

In addition to the obvious synchronized burst in Fig. 6*A*, partially synchronized bursts can also occur; one of these is shown in Fig. 6*B*. The partially synchronized burst is most obvious (in terms of the fields and firing of individual neurons) in the more superficial layers, although a clear EPSC is seen in the illustrated layer 6 pyramid (*bottom trace*). Three layer 5 pyramids did not fire in the simulation of Fig. 6*B*, and the mean synaptically induced depolarization was 10 mV. The occurrence of partially synchronized bursts in the model is reminiscent of localized small-amplitude bursts during epileptogenesis in the cat in vivo (Steriade and Contreras 1998).

WITH STRONG RECURRENT EXCITATION BETWEEN LAYER 4 SPINY STELLATES, AND WITH EXTENSIVE ELECTRICAL COUPLING BETWEEN CORTICAL PRINCIPAL NEURONS, DISINHIBITION LEADS TO "POLYSPIKES." Figure 7 illustrates a series of simulations of the cortical portion of the model (thalamus disconnected), wherein recurrent synaptic connections between layer 4 spiny

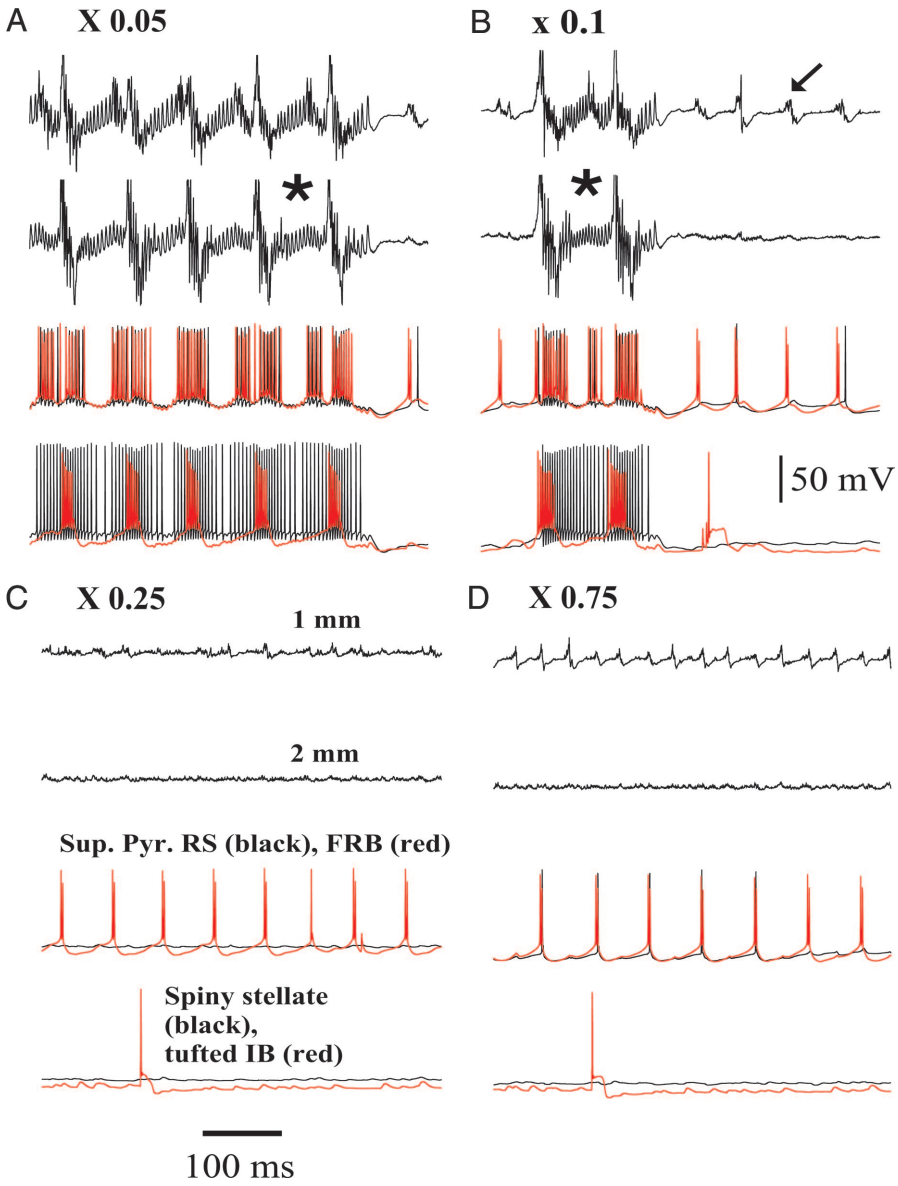

FIG. 7. Effects of disinhibition in model (cortex only, with thalamus disconnected), when there are open gap junctions between the axons of the respective principal cell populations (superficial pyramids, spiny stellates, layer 5 pyramids, layer 6 pyramids), and spiny stellates are strongly interconnected by AMPA receptors (conductance twice "baseline"; see APPENDIX B). In each panel, the *traces* are, respectively, field at 1 mm; field at 2 mm; superficial RS pyramid (black) and superficial FRB pyramid (red); spiny stellate (black) and layer 5 tufted IB cell (red). *A*: all IPSC values at 0.05 × baseline values (APPENDIX B). Runs of about 11-Hz epileptiform bursts occur, with superimposed very fast oscillation (VFO) (*). Note the almost continuous firing of the spiny stellate cell. *B*: all IPSC values at 0.1 × baseline. Figure shows a double burst with superimposed VFO (*). The spiny stellate cell fires almost continuously during the double burst, but pyramidal cells each fire 2 intense bursts (the superficial pyramids also fire some action potentials between the intense bursts). There is low-amplitude beta activity in the superficial layers (arrow) at about 17 Hz, driven by the superficial FRB pyramids. *C*: all IPSC values 0.25 × baseline. Superficial FRB pyramids are active, but there is little synchronized activity. *D*: all IPSC values 0.75 × baseline. There is a gamma oscillation (~30 Hz) in superficial layers, similar to Fig. 2.

stellates are "strong" (AMPA conductances at 2 × baseline value, peak conductance 1.47 nS); in addition, axonal gap junction conductances were "high" within the following neuronal populations: superficial pyramids; spiny stellates; layer 5 pyramids; layer 6 pyramids. Each panel shows the effects of scaling cortical IPSCs by some value (× 0.05 in Fig. 7*A*, × 0.1 in Fig. 7*B*, etc.).

In Fig. 7*A*, with $GABA_A$ conductances almost fully blocked (and recall that the model does not contain $GABA_B$ conductances), a "fast run" (Steriade et al. 1998a) occurs, at about 10 Hz, consisting of 17 burst complexes that terminate spontaneously; the last 5 of the bursts are shown in the panel. Of note is the continuous VFO in the fields (*), and the near continuous firing of the spiny stellate cell (*black trace* in *bottommost portion* of the panel); examination of the average behavior of spiny stellates (not shown) indicates that this near-continuous firing is typical. Even with such near-complete disinhibition, with the model parameters used, axonal coupling is necessary for epileptogenesis: when none of the cortical principal cells has such coupling, there is no synchronized bursting, after an initial transient (not shown). When layer 4 spiny stellates are the only principal cell population to be electrically coupled (parameters as in APPENDIX B), then a 4-burst polyspike occurs, complete with VFO (not shown). If layer 5 tufted IB pyramids were the only principal cells to be electrically coupled, a single synchronized burst occurred, with VFO much attentuated compared with Fig. 7*A*. When superficial pyramids were the only principal cells to be electrically coupled, then a 15-Hz oscillation occurred in superficial layers only, that appeared to be driven by the superficial FRB pyramidal cells (not shown). If, in this latter situation, IPSCs were suppressed completely, then a single synchronized burst did occur, but with attenuated VFO (not shown).

Thus recurrent synaptic connections and electrical coupling between layer 4 spiny stellates seem to be, in this model, critical factors in producing runs of synchronized bursts, and in generating VFO between, and superimposed on, the burst complexes.

When parameters are as in Fig. 7*A*, but IPSCs are somewhat larger (Fig. 7*B*), then double bursts occur, with a separation of

about 100 ms between bursts. Again there is VFO (*) between and on top of the bursts. The spiny stellate cell fires throughout the double burst (as do other spiny stellates; not shown), whereas layer 5 IB cells fire 2 separate bursts (*red trace* in *bottommost part* of the panel, Fig. 7*B*). Layer 5 tufted RS pyramids and layer 6 nontufted pyramids also fire in discrete bursts, in a pattern similar to that of layer 5 IB cells, both during the fast run of Fig. 7*A* and during the double burst in Fig. 7*B* (not shown).

A further increase in IPSC size (Fig. 7*C*) abolishes epileptiform activity, as well as population oscillations visible at the field level. A still further increase in IPSC size (Fig. 7*D*) returns the system to state in which there are gamma oscillations (~30 Hz) in superficial layers alone, a state similar to that illustrated in Fig. 2. Spiny stellates are mostly silent during the conditions of Fig. 7, *C* and *D*, as are deep pyramidal cells.

Epileptiform double bursts occur in rat auditory cortex in vitro, in kainate plus blockade of $GABA_A$ and $GABA_B$ receptors

Figure 8 shows (on the *left*) data from the simulation of Fig. 7*B*, in which $GABA_A$ conductances have been reduced by 90% and $GABA_B$ conductances are absent. The simulation illustrates a double burst in the field (*bottom trace*),with all cell types also exhibiting double bursts, with the exception of the spiny stellate, that fires almost continuously throughout the double burst. The *right side* of Fig. 8 illustrates experimental recordings (not simultaneous) from double bursts recorded in rat auditory cortex in vitro, in the presence of kainate (400 nM) and blockers of $GABA_A$ and $GABA_B$ receptors (picrotoxin, 40 μM, and CGP55845A,10 μM, respectively). The experimental interburst interval is somewhat longer than the simulated interburst interval. Again, in the experiment, all of the recorded cell types exhibited double bursts as well, approximately in

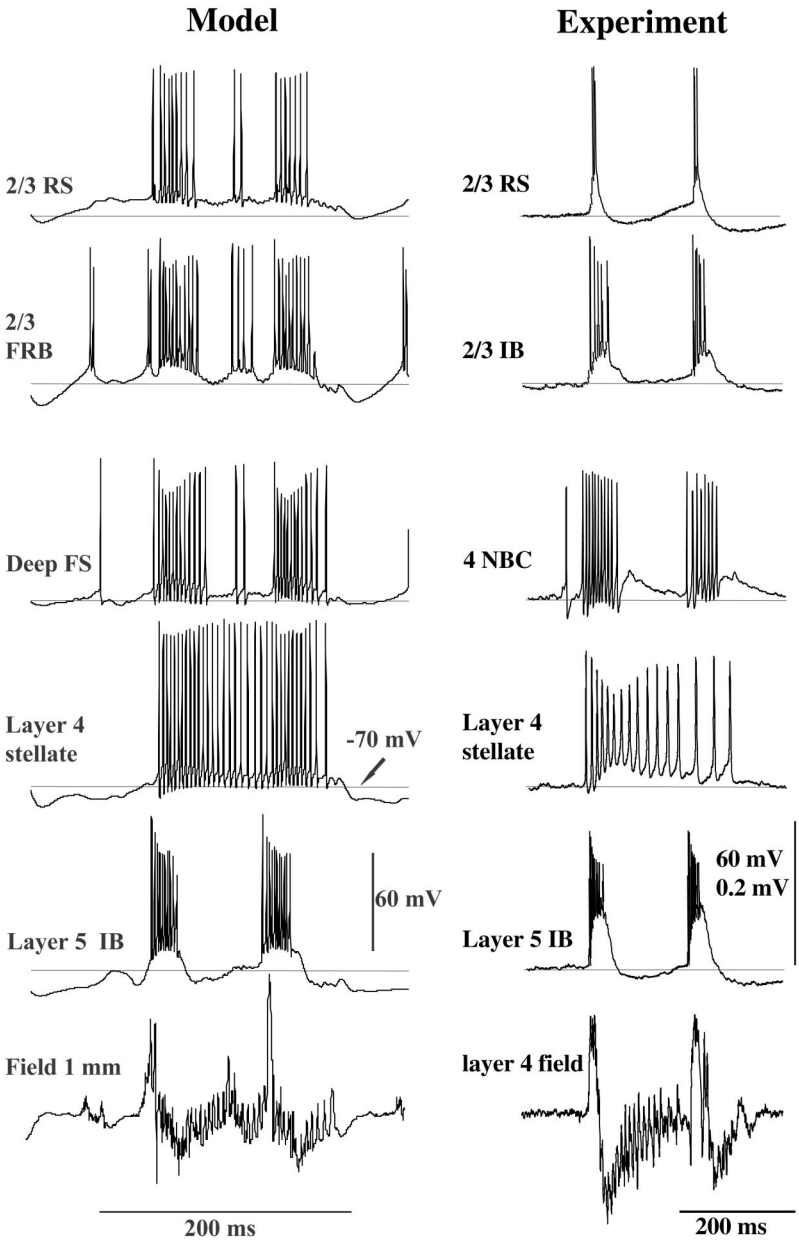

FIG. 8. Simulated double burst compared with a double burst recorded in vitro, in kainate together with block of $GABA_A$ and $GABA_B$ receptors. Model data are from the simulation used in Fig. 7*B*. Experimental data are from rat auditory cortex in vitro, bathed in kainate, picrotoxin, and CGP55845A. "NBC": nest basket cell (Wang et al. 2002). Experimental intracellular recordings were not obtained simultaneously: in the figure, they were aligned to the beginning of each concurrently recorded field potential burst.

phase with the major field deflections, with the exception of layer 4 neurons identified as spiny stellates. These cells fired throughout the double bursts ($n = 5$); one of the spiny stellates is shown in Fig. 8. However, this cell does show some degree of spike adaptation toward the end of its firing. Particularly striking in this Fig. 8 are the similar appearances of the fields in model and experiment, with prominent VFO in both.

The simulated layer 2/3 cells exhibit bursts that are less depolarized than the corresponding experimental bursts, perhaps a consequence (in part) of the incomplete disinhibition in the simulation. In addition, the simulated layer 2/3 cells generate a few action potentials between the larger bursts, unlike the experiment; this could be a result of the more intense firing of the model layer 4 stellate neurons than in the experiment, combined with the strong synaptic activation of superficial neurons by layer 4 neurons.

VOLTAGE-INDEPENDENT NMDA RECEPTORS AT BETWEEN-SPINY STELLATE CONNECTIONS, COMBINED WITH ELECTRICAL COUPLING, CAN ALSO LEAD TO EPILEPTIFORM BURSTS WITH PROLONGED SPINY STELLATE FIRING, AS WELL AS VFO. Fleidervish et al. (1998) described, in mouse somatosensory cortex in vitro (using tangentially cut slices to isolate barrels in layer 4), a system of recurrent excitatory connections between spiny stellates that was in large part mediated by NMDA receptors. This recurrent system was powerful, in that epileptiform activity could occur in disinhibited preparations even during blockade of AMPA/kainate receptors. Furthermore, perhaps because the NMDA receptors contained the NR2C subunit, NMDA-mediated currents were at least partially independent of membrane potential and of $[Mg^{2+}]_o$: NMDA EPSPs could be detected at or near resting potential without lowering $[Mg^{2+}]_o$. The observed NMDA conductances were brief, having time constants <20 ms.

We thus ran some simulations in which AMPA receptor conductances at between-spiny stellate connections were "low" (peak conductance 0.18 nS), whereas NMDA conductances were made completely voltage-independent (for the usual scheme of voltage-dependence of NMDA conductances, see APPENDIX B). Figure 9 illustrates an example simulation with spiny stellate NMDA conductance at 1.25 × baseline value, $\tau_{NMDA} = 15$ ms, and with complete disinhibition. The thalamic portion of the network was disconnected, and electrical coupling was present between the axons of superficial pyramids, of spiny stellates, and of layer 6 pyramids. Although a double burst does not occur, the synchronized burst is prolonged and has prominent VFO. Additionally, the firing of spiny stellate

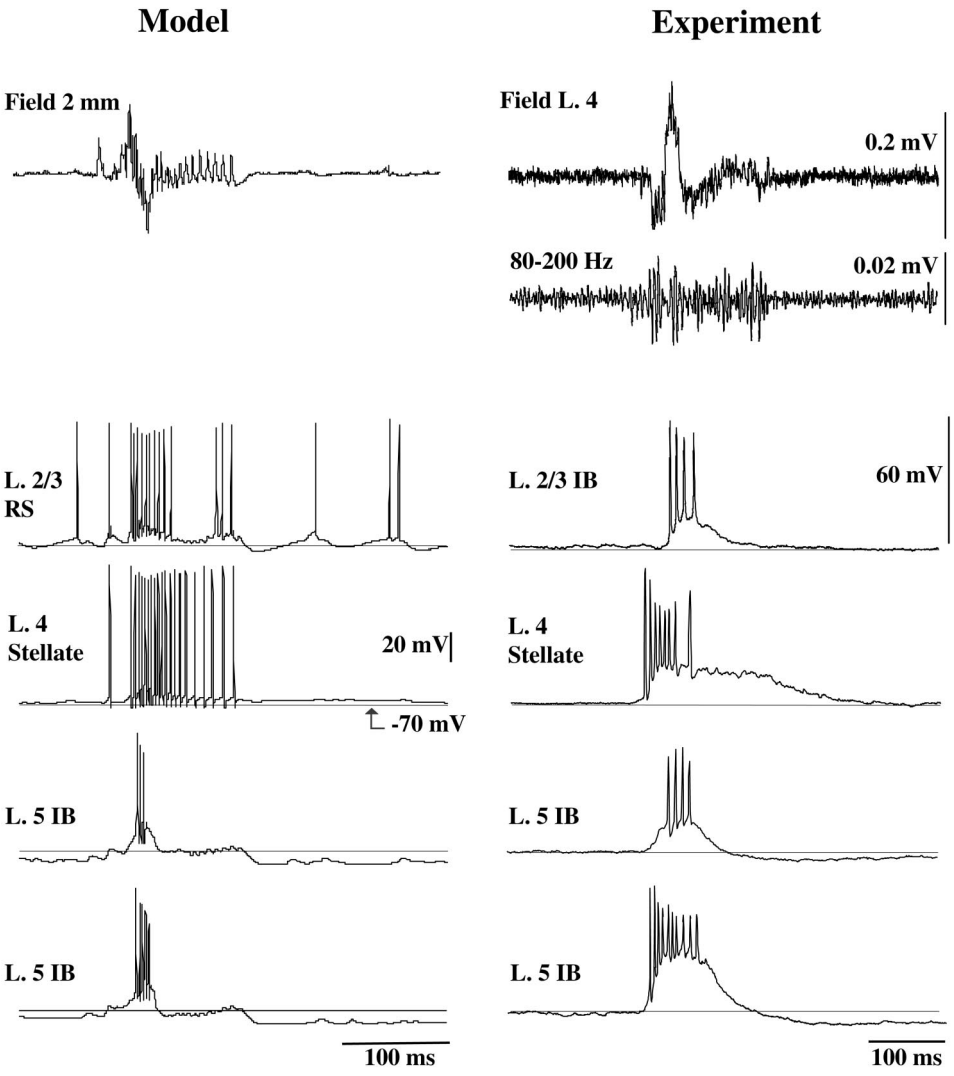

FIG. 9. An epileptiform burst with prolonged firing in spiny stellate cells, when layer 4 spiny stellate → spiny stellate connections use NMDA receptors that are voltage and $[Mg^{2+}]_o$ independent (cf. Fleidervish et al. 1998), although these authors claimed only relative voltage and magnesium independence of NMDA receptors at connections between spiny stellate cells in layer 4 of mouse barrel cortex). In the simulation shown here (*left column*), NMDA conductance between spiny stellates was 1.25 × baseline, and the decay time constant was 15 ms. AMPA conductances at these connections were 0.25 × baseline value. Cortical IPSCs were blocked and the thalamus disconnected. Bias currents were small (<0.1 nA). Axonal gap junctions were open between superficial pyramids, between spiny stellates, and between layer 6 pyramids, but not between layer 5 pyramids. *Right*: an experimental single burst shown for comparison. Experimental conditions were as in Fig. 7, but without CGP55845A in the bath (i.e., without block of $GABA_B$ receptors). A filtered version (80–200 Hz) of the *field trace* is shown to emphasize the occurrence of VFO in the field, as is obvious in the raw data for the simulated field.

neurons is prolonged compared with the firing of other principal cell types. An experimental epileptiform burst [rat auditory cortex bathed in kainate (400 nM) and picrotoxin (40 μM), but without block of $GABA_B$ receptors] is shown for comparison, in Fig. 9, to emphasize the similarity in cellular firing patterns, and in the occurrence of VFO in the field. [The precise experimental nature of the glutamate receptors at within-layer 4 spiny stellate connections in rat auditory cortex is (to our knowledge) not known, however.]

Thus sustained firing of layer 4 spiny stellate neurons, and layer 4 VFO, can occur in the model under at least 2 conditions: *1*) high-conductance AMPA receptors at connections between layer 4 spiny stellates (Figs. 7*B* and 8), or *2*) lower conductance AMPA receptors, together with rapid-time-course, relatively voltage-independent NMDA receptors, at connections between spiny stellate cells (Fig. 9). In both cases, there is strong phasic synaptic excitation between the spiny stellate neurons. As will be shown later, it is possible to "titrate" the number of bursts in a row by altering the amplitude of EPSCs at recurrent layer 4 spiny stellate synapse; in the model, these connections provide the essence of the transition between spike-wave and polyspike-wave.

Next, we shall consider 2 types of epileptogenesis in vivo: approximately 3-Hz spike-wave, and approximately 10-Hz fast runs.

THE CORTICAL NETWORK CAN GENERATE A SPIKE-WAVE-LIKE PATTERN IF—IN ADDITION TO PARTIAL DISINHIBITION AND ELECTRICAL COUPLING—LAYER 5 AND 6 PYRAMIDAL CELLS ARE DEPOLARIZED. Synchronized epileptiform bursts shown in simulations in the previous figures were sporadic (at least so far as could be determined in simulations that usually lasted 1.6 s, and at most 2.5 s), even with $GABA_A$ receptors largely blocked. In particular, we did not see synchronized bursts at frequencies >1 Hz when deep pyramidal cells were depolarized with small currents of <0.1 nA, even in disinhibited conditions. [The assumption that >2–3 Hz spike-wave patterns in vivo require some degree of cortical disinhibition seems reasonable for several reasons: *1*) there is an in vivo genetic rat model of spike-wave epilepsy in which intracortical inhibition is impaired (Luhmann et al. 1995). In addition, diffuse cortical application of a penicillin solution to cat cortex can elicit a spike-wave-like epileptic pattern (Avoli and Gloor 1982; Gloor et al. 1977). *2*) A spike-wave-like pattern (but at very low frequencies, about 0.1 Hz) has been observed in vitro during blockade of $GABA_A$ and $GABA_B$ receptors (Castro-Alamancos and Rigas 2002). The question is whether cortical disinhibition is *sufficient* for a spike-wave-like pattern.] We thus wondered whether simply depolarizing pyramidal cells, in addition to having electrical coupling and partial disinhibition present, could generate a spike-wave-like pattern at about 3 Hz.

Figure 10 demonstrates that, at least in our model (in this case with the thalamic portion disconnected), simply depolarizing deep (layers 5 and 6) pyramids is sufficient to speed up, and make more regular, the occurrence of synchronized bursts, so that a 3-Hz network oscillation can occur: the depolarizing currents serve to overcome the tendency of pyramidal cell AHPs to slow the burst frequency [deep pyramidal cells have an afterhyperpolarization (AHP) decay time constant of 1 s; see

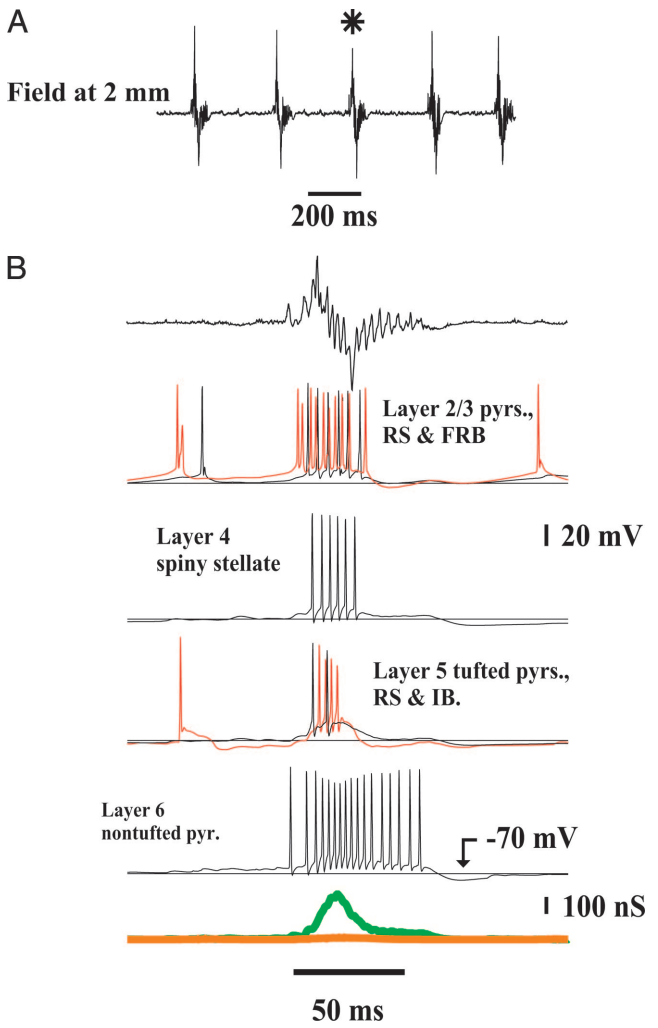

FIG. 10. Simulated spike-wavelike pattern (~3.2 Hz) in cortical portion of the model, with thalamus disconnected. Cortical IPSC values were 0.2 × baseline values, and layer 5 and layer 6 pyramids were depolarized with 0.35 to 0.45 nA depolarizing currents. Axonal gap junctions were open between superficial pyramids, between spiny stellates, and between layer 6 pyramids, but not between layer 5 pyramids. AMPA conductances at connections between spiny stellates were 0.25 × baseline. Burst marked with the * in *A* is expanded in *B*. *Traces* in *B* are (*from the top*): field at 2 mm (note superimposed VFO); layer 2/3 pyramids (black = RS, red = FRB); a layer 4 spiny stellate cell; layer 5 tufted pyramids (black = RS, red = IB); a layer 6 nontufted pyramid; total $GABA_A$ (orange) and AMPA (green) conductances in the illustrated layer 6 cell.

APPENDIX A]. In this figure, layer 5 and 6 pyramids were depolarized with 0.35–0.45 nA currents; whereas IPSC conductances were 0.2 × their baseline values; axonal gap junctions were open between superficial pyramids, between layer 4 spiny stellates, and between layer 6 pyramids; and AMPA receptors at connections between layer 4 spiny stellates had a "low" value (0.25 × baseline). The cellular firing patterns are similar to those previously illustrated, although spiny stellate bursting is brief (attributable to the limited recurrent excitation in layer 4), and layer 6 pyramidal cell bursting is more prolonged (attributable to the induced depolarization in this cell population). The only current in the neurons with time course appropriate for gating an oscillation at about 3 Hz is the slow calcium-mediated AHP current (compare Timofeev et al. 2004).

We emphasize once more the occurrence of VFO on the field potential signal in Fig. 10, a very specific prediction of our model. It is notable that VFO has indeed been observed superimposed on the "spike" component of spontaneous spike-wave seizures in ketamine–xylazine-anesthetized cats, seizures that originate in the depolarizing component of the slow rhythm of sleep [see, for example, Fig. 1 of Grenier et al. (2003), and also data below].

ORIGINS OF VFO IN THE SIMULATED FIELD. Figure 11*A* shows the power spectrum of somewhat over 1.6 s of simulated field data (at 2 mm), encompassing 6 "spikes" (same simulation as in Fig. 10). Of note is the peak near 100 Hz, quite similar to the in vivo cat data of Grenier et al. (2003; their Fig. 1). The spectrum in the model case, however, is more complex than the in vivo data, in that there are several additional regions of energy (e.g., around 200 Hz, and 300–400 Hz); the latter might correspond to what has been called "fast ripples" in some of the human epilepsy literature (Bragin et al. 1999; Staba et al. 2004).

We suggest that the complex spectrum of the field arises as follows. Principal cell electrical coupling in the model exists only between cells of defined populations, e.g., between superficial pyramids (RS and FRB together as one population), between spiny stellates, between layer 6 nontufted pyramids, and sometimes between layer 5 tufted pyramids (RS and IB together)—but not between pairs of cells, each of which lies in a different population. As a result, there is a clear correlation between spike firing times within populations, as seen in the average signals in Fig. 11*B*. The spiny stellates are especially correlated with each other (but note that, as described in APPENDIX B, spiny stellate transmembrane currents are not used in the estimation of extracellular fields because of the shape of the dendritic domain of these cells). There is some apparent correlation between average signals in a given cell population (see vertical lines in Fig. 11*B*), but in fact the field is influenced by transmembrane currents of all the cell populations, and interactions between the different cell populations arise by chemical synapses; that is, interactions that act slowly, relative to interactions mediated by gap junctions. Thus it is not surprising that the field spectrum is so complex and that it has peaks at very high frequencies. A significant point is that most of the field signal cannot be attributed directly to the activity of a particular subpopulation. A partial exception in our case is the tail of VFO in the field, which corresponds to the prolonged (and highly synchronized) firing of layer 6 nontufted pyramids (not shown).

IN VIVO RECORDINGS DURING EPILEPTOGENESIS: INTERICTAL BURSTS, SPIKE-WAVE, AND THE ASSOCIATION OF SPIKELETS WITH BURSTS. Intracellular recordings in vivo ($n = 8$), during spontaneous seizures in anesthetized rats (see METHODS), revealed a striking similarity with patterns previously reported in cats (Dichter and Spencer 1969; Matsumoto and Ajmone Marsan 1964; Prince 1968; Steriade and Contreras 1995; Steriade et al. 1998), and with the simulations and in vitro data presented above (but see following text), although the in vitro and simulated cells did not usually become depolarized enough to cause spike inactivation, and simulated neurons did not exhibit the long postburst depolarizing tails seen in vivo. Seizure activity was first detected as single large amplitude spikes (clearly paroxysmal) associated with sleep spindles.

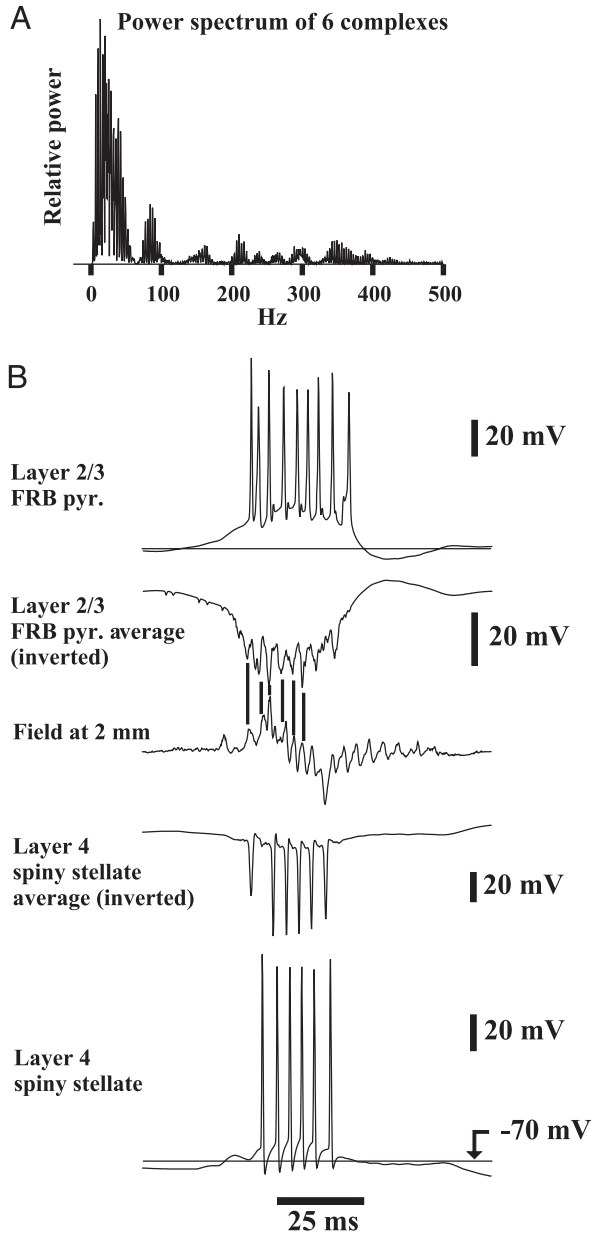

FIG. 11. There is high coherence among the cells in each electrically coupled subpopulation (data from same simulation as in Fig. 10). *A*: power spectrum of the 2-mm field, data encompassing 6 "spike" complexes. Note the peak near 100 Hz; compare Fig. 1 of Grenier et al. (2003). *B*: this part shows the average somatic voltages (inverted) for layer 2/3 FRB pyramids and layer 4 spiny stellates, along with sample cells of each type. Coherence within subpopulations does not, however, fully explain by itself the VFO in the field (*middle trace*) because the different subpopulations are not electrically coupled with each other. Note also that spiny stellate membrane currents are not used in the calculation of the extracellular field (APPENDIX B). The tail of VFO in the field corresponds to the sustained synchronized firing of layer 6 nontufted pyramids (cf. Fig. 10).

Spikes grew in amplitude and frequency and were followed by full-blown seizures characterized by a mixture of fast runs of spikes at 10–15 Hz, and spike-wave (SW) or polyspike-wave (PSW) activity at 1–4 Hz. Once established, seizures tended to recur every 1 to 3 min. Intracellularly, EEG spikes corresponded with large postsynaptic potentials similar to paroxysmal depolarizing shifts (PDS). Figure 12*A* shows an example of a PDS recorded from a fast spiking (FS) and a regular

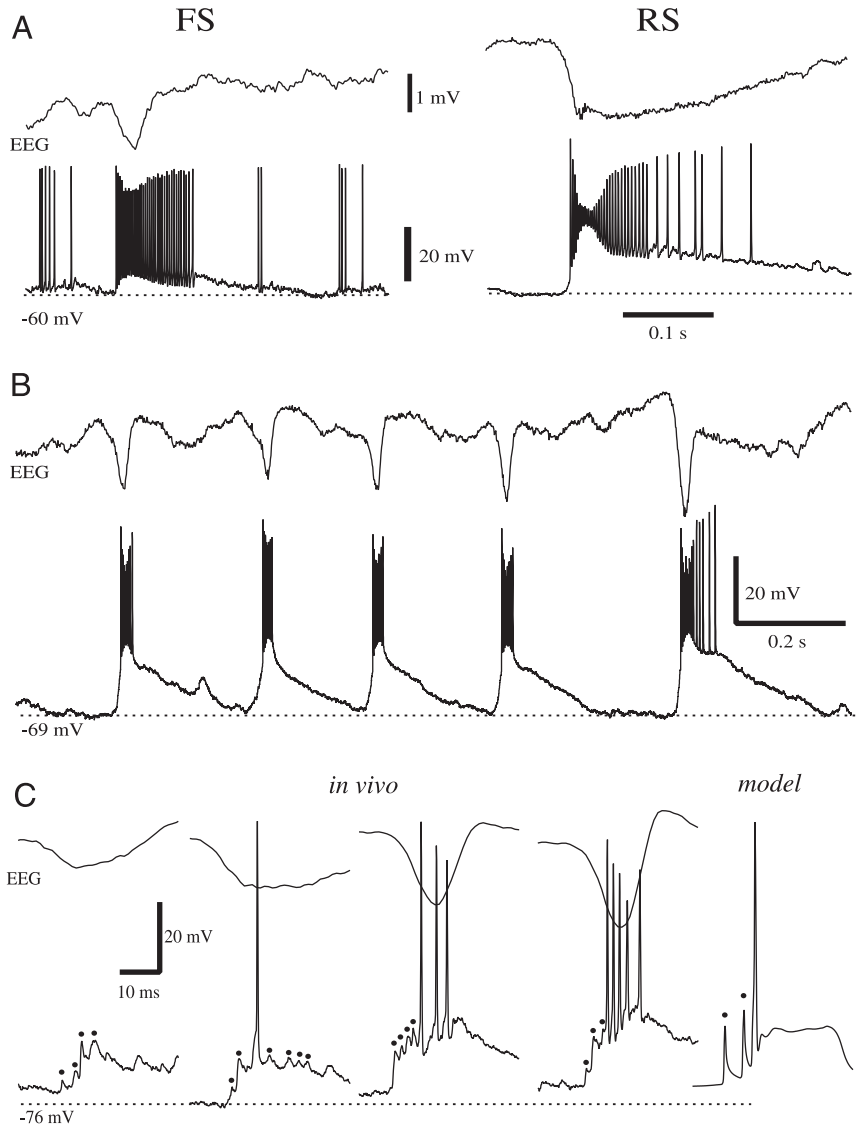

FIG. 12. Examples of seizure activity in cortex in vivo. *A*: FS cell and RS cell recorded intracellularly from rat neocortex in vivo each show a paroxysmal depolarization shift (PDS) during an interictal spike in the simultaneously recorded electroencephalogram (EEG) from the vicinity of the cell. *B*: stable epoch of large EEG spikes at 3–4 Hz resembling spike-wave, with simultaneous intracellular recording from the vicinity of the electrode, shows a PDS concomitant with each EEG spike. *C*: spikelets (indicated by dots) of 2–7 mV occurred in bursts associated with EEG spikes and often preceded bursts of action potentials (in vivo). Similar spikelets were observed in the model (*model*), where they represented antidromic spikes.

spiking (RS) neuron. The depolarization was larger than 20 mV in the RS cell and caused significant spike inactivation followed by a long depolarizing tail with similar time course as the negative (downward) wave in the EEG. (In vitro and simulated cells did not usually become depolarized enough to cause spike inactivation, and simulated neurons did not exhibit the long postburst depolarizing tails seen in vivo. The latter may reflect the omission in the model of metabotropic glutamate receptors and nonspecific cation currents.) Repetitive spikes at 1–4 Hz resembling SW seizures were associated with bursts of action potentials in all neurons recorded (Fig. 12*B*). In 5 cells the depolarization occurring during EEG spikes was preceded and crowned by bursts of short spikelets of 2–7 mV (Fig. 12*C*, in vivo) resembling the spikelets resulting from antidromic spikes in the model (Fig. 12*C*, model: same cell as the layer 5 tufted IB cell in Fig. 7*B*). Note that some of the action potentials in cells exhibiting spikelets (Fig. 12*C*) were inflected on the rising phase, suggesting an antidromic origin, as would be expected if some of the bursting activity involves an electrically coupled network of pyramidal cell axons (Cunningham et al. 2004a).

IN OUR MODEL OF SPIKE-WAVE, WITH THE THALAMUS CONNECTED, TCR FIRING IS LARGELY SUPPRESSED, AS REPORTED PREVIOUSLY IN VIVO AND IN A MODEL (LYTTON ET AL. 1997), CONSISTENT WITH A CORTICAL GENERATION OF SPIKE-WAVE WITHOUT ALTERATIONS IN SYNAPTIC CONDUCTANCES WITHIN THE THALAMUS. Steriade and Contreras (1995) reported that, during spike-wave seizures occurring spontaneously in ketamine–xylazine-anesthetized cats, and arising out of the slow (<1 Hz) rhythm, firing of TCR neurons is largely suppressed. In the Strasbourg rat model of spontaneous spike-wave epilepsy, Pinault et al. (1998) used both intracellular and extracellular recordings to show that TCR cells usually fired either one action potential or a burst concomitant with the EEG "spike" part of spike-wave.

Figure 13 shows the results when the simulation of Fig. 10 was repeated, but with the thalamic portion of the model now connected. The firing of cortical neurons is similar to what was seen before, although firing in layer 6 nontufted pyramids is not as prolonged. In addition, consistent with what has been reported in vivo, TCR neurons fire a single action potential per "EEG spike." [This was true for each of 3 TCR neurons (whose output was stored) in this simulation, for each of the "EEG

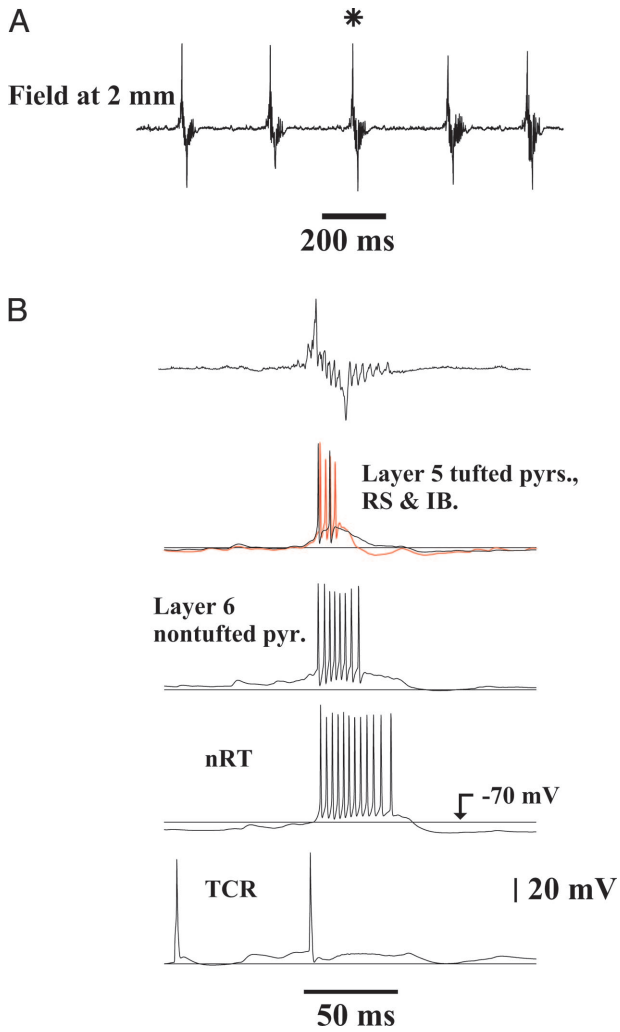

FIG. 13. During simulated spike-wave with the thalamus connected (same simulation as Fig. 10, except now the thalamic part of the model is included, with intrathalamic IPSCs at baseline values, whereas cortical IPSCs remain at 0.2 × baseline values), nRT neurons fire bursts and TCR neurons fire single spikes. Burst in *A* marked * is expanded in *B*, with the *top trace* the field at 2 mm. Note the bursting in the layer 6 cell, a representative of the population of pyramids that connects to nRT cells and TCR cells. nRT bursting and recurrent inhibition of TCR cells "wins" over the direct excitation of TCR cells, so that firing in TCR neurons is mostly suppressed. Compare Lytton et al. (1997). When this simulation was repeated with axonal gap junctions between cortical principal cells closed, then spike-wave did not occur (not shown).

spikes."] In contrast, nRT cells fire a burst of action potentials with each "EEG spike" [true for each of 3 nRT cells(whose output was stored) in each "EEG spike"], again in a pattern similar to that described by Steriade and Contreras (1995), Lytton et al. (1997), and Slaght et al. (2002).

Both Pinault et al. (1998) and Crunelli and Leresche (2002) reported prolonged hyperpolarizations in thalamic neurons during in vivo experimental spike-wave seizures. We did not observe such hyperpolarizations in our model, probably because the model did not include $GABA_B$ conductances.

IN THE MODEL, INCREASING RECURRENT SYNAPTIC EXCITATION BETWEEN LAYER 4 SPINY STELLATES CONVERTS A SPIKE-WAVE PATTERN INTO A POLYSPIKE-WAVE PATTERN. In the simulations of Figs. 10–13, the size of AMPA receptor conductances at spiny stellate → spiny stellate synaptic connections was at a "low" value (0.25 × baseline). Figure 14 shows the result of repeating the simulation of Fig. 13, but with this AMPA conductance instead at a "high" value (2 × baseline). Consistent with the results of earlier figures (e.g., Fig. 7), each "spike" now becomes a brief series of "spikes" at about 13 Hz: a polyspike. The frequency of polyspikes is about 1.6 to 2.5 Hz. Note that, as before, the spiny stellate cell fires almost continuously during a polyspike (Fig. 14*B*), whereas pyramids and nRT cells fire a burst of action potentials with each "spike" in the polyspike. Likewise, TCR neurons fire only a single action potential with each "spike" in the polyspike.

IN A SITUATION WHERE THE THALAMOCORTICAL MODEL GENERATES POLYSPIKE-WAVE, DISCONNECTION OF THE THALAMUS CAUSES THE MODEL TO GENERATE POLYSPIKE-WAVE AND A FAST RUN (ABOUT 12 HZ). The simulation of Fig. 14 was repeated, but with the thalamic portion of the model disconnected. The resulting

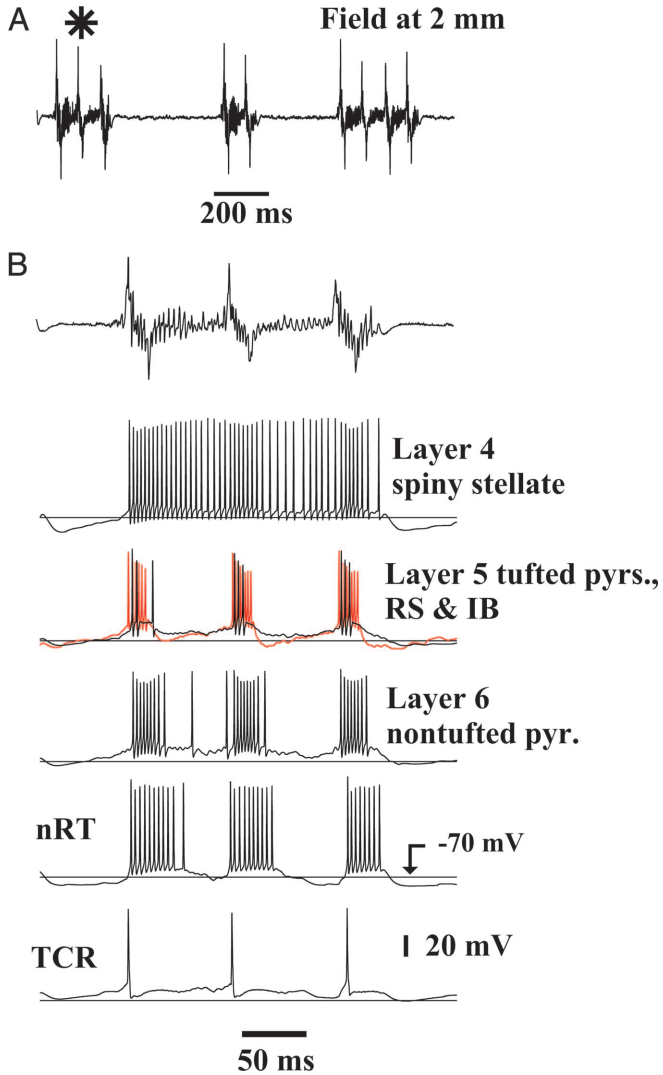

FIG. 14. Increasing recurrent chemical synaptic excitation between layer 4 spiny stellate neurons, in the model, converts spike-wave to polyspike-and-wave. Same simulation as Fig. 13, but here AMPA conductances at spiny stellate → spiny stellate synapses are 2 × baseline, rather than 0.25 × baseline. Triple burst at * in *A* is expanded in *B*, with the *topmost trace* in *B* the field at 2 mm. Note that the layer 4 spiny stellate cell fires throughout the triple burst, whereas layer 5/6 pyramids, and nRT cells, discharge in 3 distinct bursts. TCR neuron fires a single action potential with each "EEG spike." Note also the VFO throughout the triple burst (and also the other polyspikes).

signals began with spike-wave, but then transformed into a phenomenon resembling an in vivo "fast run" (Steriade et al. 1998a; see especially their Fig. 9), a collective highly synchronized oscillation in which pyramidal neurons depolarize and generate brief bursts together, at frequencies around 10 Hz. Note, however, that—not unexpectedly—spiny stellate cells (in the model) fire almost continuously throughout the fast run, a clear model prediction. Only part of the fast run is illustrated in Fig. 15; the fast run lasted for about 1.6 s.

The data in Fig. 15 indicate that the thalamus may, at least on occasion, exert a *restraining* effect on cortical epileptogenesis, in the sense that a fast run represents more neuronal action potentials per second than occurs just in polyspike-wave [compare also Topolnik et al. (2003)]; such a restraining effect could arise because of thalamic excitation of cortical interneurons, in a situation when spiny stellates are already firing near maximally (during EEG "spikes"), and are therefore not further excited by thalamic excitation themselves. Data of Castro-Alamancos (2000) support the idea that, in vivo, a fast run at 10 Hz can occur without the thalamus. It is also interesting that, in the generalized penicillin epilepsy model, in cats in vivo, tonic–clonic seizures occur (instead of the usual spike-wave), once thalamic electrical activity is suppressed by injection of hypertonic KCl (Avoli and Gloor 1981). Furthermore, in cat cortex in vivo, overlying a thalamectomy, fast runs can occur that go on for several minutes, far longer than what is usually seen (Steriade and Contreras 1998).

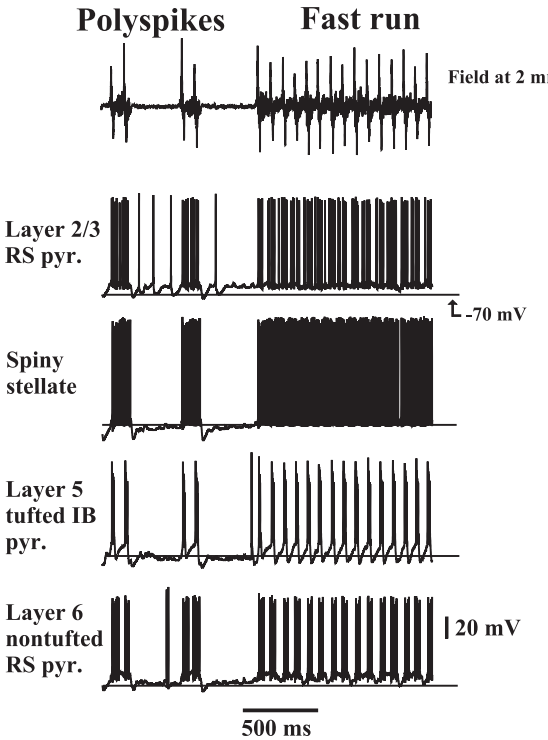

FIG. 15. Polyspike-and-wave simulation of Fig. 14 was repeated, but with the thalamus disconnected. Now, after a series of polyspikes, collective activity turns into a "fast run" (Steriade et al. 1998) at ~12 Hz. Only a portion of the ~1.6 s fast run is shown, for the sake of clarity. Note the almost continuous firing of the layer 4 spiny stellate neuron during the fast run, contrasted with the repeating bursts in other principal cortical neurons. We interpret this behavior to mean that the limited firing of TCR neurons during polyspikes may have more significant effects on the cortex by feedforward inhibition, than by direct excitation, under conditions of partial cortical disinhibition. This might also explain why undercutting cortex in vivo can lead to cortical hyperexcitability (Topolnik et al. 2003), and why feline cortex overlying a thalamectomy can exhibit sustained (minutes) fast runs (Steriade and Contreras 1998).

DISCUSSION

It is likely, in our opinion, that detailed modeling of extensive thalamocortical circuits will be one of many prerequisites for the understanding of any aspect of normal global brain function. Toward such an end, our present results represent an extremely preliminary first step—preliminary not only because of the relatively small number of cells (about 3,500) and limited number of cell types, but preliminary as well because (again, in our opinion) one cannot proceed directly from an initial network model to subtle aspects of brain function, such as learning or information processing. Rather, one must first calibrate the model against experimental preparations that exhibit relatively simplified network behaviors. Here, "relatively simplified" means "in comparison with physiological, normal, in vivo network behaviors." Network behaviors are simplified, relative to the normal case, when there is a high degree of correlation between the activities of different neurons, so that the network behavior can be defined by observations of a small number of cells, and of the extracellular field. We consider pharmacologically induced network oscillations, sleep spindles, and seizures, to be examples of such relatively simplified behaviors, and these are the examples we have chosen to study here. An inescapable conclusion of this preliminary work, we feel, is that global brain function can never be fully understood simply in terms of neuronal intrinsic properties and chemical synapses alone: electrical coupling between neurons is key as well, just as is the case with invertebrate central pattern generating circuits (Marder 1984). The model further indicates that the recurrent interactions between layer 4 spiny stellates may play a critical role in the patterning of seizure phenomenology.

TECHNICAL CONSIDERATIONS: INCREASING PROGRAM COMPLEXITY AS MORE CELL TYPES ARE ADDED. Before discussing scientific predictions of the model, we must first put the structural features of the model into context. The most important feature to understand is this: What exactly makes the model complicated? It is clear that, as more cell types are included, then more single-cell models must be built, and their behavior compared with the physiology of pharmacologically isolated, anatomically characterized single neurons. This model complexity added in this way grows linearly with the number of cell types: another cell, another model (unless one can assume that intrinsic properties of a new cell type are equivalent to the intrinsic properties of an existing cell type). Much more troubling for the modeler is that the complexity of code, arising from cellular *interactions*, grows as the *square* of the number of cell types. Thus for each ordered pair (*cell type 1*, *cell type 2*), one must decide on connectivity, where the connections go, and the properties of the connections. In addition, some piece of code must be devoted to calculating the synaptic conductances in the cells of *type 2* caused by activity in the cells of *type 1*, for every ordered pair of cell types. Any interested reader who examines the integration program will immediately see the consequences of this complexity, in terms of sheer length of code. This type of problem will, of course, only get worse—and rapidly so—as models start to include more types of neurons.

In addition, as the number of connectivity parameters goes up with the square of the number of cell types, it is easy to feel overwhelmed by the number of seemingly arbitrary choices that must be made. This is the main reason why, in our opinion, emergent properties of only the simplest kind have to be analyzed first, before the normal physiology can be studied properly.

Why then bother with such a detailed network model? Because it is useful. At least, we shall argue below that important experimental predictions can be made that would not have been made without the model.

The model also serves—as if it were necessary!—to encourage an extreme sense of humility in the face of the extraordinary richness of behavior that even a small number of neurons can generate.

We have used two well-studied collective oscillations, persistent gamma (Cunningham et al. 2004a) and thalamocortical spindles (Bal et al. 1995a,b; Steriade 2001 2003), as a form of calibration of the model (Figs. 2–4). The calibration cannot guarantee accuracy of all of the parameters, but does indicate, in our opinion, that the model "lives" in a reasonable region of its phase space.

The main predictions concern the existence of electrical coupling between principal cortical neurons (pyramidal cells and spiny stellate cells), and the contributions of spiny stellate connectivity to epileptogenesis.

AXONAL COUPLING BETWEEN PRINCIPAL CORTICAL NEURONS COULD EXPLAIN VERY FAST OSCILLATIONS DURING SEIZURES. The evidence for electrical coupling between the axons of cortical principal cells is only circumstantial, and is in part based on experimental data from hippocampus; even in the hippocampus, ultrastructural evidence is so far lacking. Because electrical coupling plays such an essential role in our model (except for spindles), we here briefly summarize the circumstantial evidence, so that the reader can make an independent decision on the rationale for including electrical axonal coupling in the manner we have done.

1) Spikelets can be induced in hippocampal pyramidal cells and dentate granule cells that are sensitive to gap junction blockers, follow ≤500 Hz stimuli without failure, propagate actively, and propagate antidromically (i.e., appear first in the axon, then the soma) (Schmitz et al. 2001; reviewed in Traub et al. 2002).

2) In 4 cases, CA1 pyramidal cells have been found to be dye-coupled between their axons, by light microscopic criteria (Schmitz et al. 2001).

3) Models based on sparse, strong axonal coupling can account for hippocampal VFO in calcium-free media (Draguhn et al. 1998; Traub et al. 1999), persistent gamma oscillations in the hippocampus (Traub et al. 2000), and in vivo sharp-wave ripples (Traub and Bibbig 2000).

4) Persistent gamma oscillations in superficial layers of rat auditory cortex in vitro have a similar appearance to hippocampal persistent gamma (Hormuzdi et al. 2001; Fisahn et al. 1998), and can also be accounted for with a model using axonal electrical coupling between superficial pyramidal cells (Cunningham et al. 2004a), provided FRB cells are included.

5) Spikelets are seen in cortical pyramidal cells (Cunningham et al. 2004a) and in entorhinal cortex neurons (Cunningham et al. 2004b).

6) A candidate set of gap junction forming proteins exists for putative axonal gap junctions, pannexins 1 and 2 (Bruzzone et al. 2003), and pannexin2 mRNA is found in cortical layers 2–6 (Cunningham et al. 2004a).

7) Dye coupling exists between cortical neurons, in deep and superficial layers, and in layer 4, between neurons both having their soma in the same layer (Gutnick and Prince 1981; Gutnick et al. 1985). Such coupling occurs between pyramidal cells and between stellate cells.

8) Surgically isolated stratum oriens, in the CA1 region in vitro, a preparation with few if any pyramidal cell somata, can generate VFO, as predicted by a model with axonal electrical coupling; in addition, interneuron EPSCs exhibit a very high-frequency superimposed oscillation, as expected from a coupled axonal plexus (Cunningham et al. 2004b; Traub et al. 2003b; Whittington and Traub 2003).

Finally, we are not aware of any other model (i.e., one *without* electrical coupling) that is able to account for the experimentally observed properties of VFO and persistent gamma oscillations, particularly the ability of isolated CA1 stratum oriens to generate approximately 100-Hz oscillations.

The effects, then, of including principal cell electrical coupling in the present model are these:

1) It allows persistent gamma oscillations to occur in superficial layers (Cunningham et al. 2004a).

2) It lowers the amount of recurrent synaptic excitation required for epileptiform synchronization to occur in partially disinhibited cortex. This happens because axonal coupling provides additional pathways by which action potentials in one excitatory axon might induce action potentials in another excitatory axon.

3) It introduces tight correlations in the firing times of cortical neurons, within specific subpopulations [e.g., among the spiny stellates, or among superficial pyramids (Fig. 11)]. These tight correlations then show up as observable VFO superimposed on EEG "spikes" and in the middle of polyspikes, as well as producing an approximately 100-Hz peak in the power spectrum of epileptiform events. This VFO and spectral peak are seen in experimental epilepsies (Grenier et al. 2003; Traub et al. 2001; this paper), and indeed a very high frequency peak shows up in the power spectrum of hippocampal persistent gamma as well (Traub et al. 2002).

We did not, however, observe in these simulations a clear epoch of low-amplitude VFO *before* the epileptiform burst. Such an epoch has been observed before epileptiform events in hippocampal slices and in children with seizures caused by a cortical dysplasia (Traub et al. 2001), and in anesthetized cats with spontaneous seizures (Grenier et al. 2003). The reason for the absence, in our model, of this early epoch of VFO is not clear. Our guess is that the reason has to do with the fact that we simulate only one column. Perhaps if we could model an array of columns, with heterogeneous conditions of disinhibition or axonal coupling, then low-amplitude VFO might be able to continue autonomously in one spot, and then induce seizure activity in another spot.

RECURRENT EXCITATORY INTERACTIONS—EITHER CHEMICAL SYNAPTIC OR GAP-JUNCTION-MEDIATED OR BOTH—BETWEEN LAYER 4 SPINY STELLATE CELLS APPEAR IMPORTANT FOR EPILEPTOGENESIS: ALLOWING EEG SPIKES TO OCCUR, AND ALLOWING EEG SPIKES TO BECOME POLYSPIKES. The excitatory interactions between layer 4 spiny stellate cells play a special role in epileptogenesis in our model. First, electrical coupling between spiny stellate

neurons favors the initial synchronization of bursting in excitatory neurons, in partially disinhibited cortex. Second, if recurrent synaptic excitation between spiny stellates is especially strong (either from large AMPA receptor currents, or from relatively voltage-independent NMDA receptors), then bursts become prolonged, or can even evolve into multiple bursts (polyspikes). Both in model and in experiment (Figs. 7, 8, 14, and 15), spiny stellate firing is nearly continuous during polyspikes. Of course, recurrent excitatory synaptic connections between pyramidal cells are critically important for epileptogenesis in our model (data not shown), as is the case in experimental epilepsy models (except for the hyperexcitability induced by low extracellular calcium concentration) (reviewed in Traub and Miles 1991).

Recurrent synaptic excitation between layer 4 spiny stellate cells (in visual and somatosensory cortices) has been proposed to enhance "responses to effect stimuli" coming into cortex from the thalamus (Miller et al. 2001). Whether this hypothesis is correct or incorrect, one assumes that Nature has emplaced the layer 4 recurrent excitatory system for a functional reason. Strong recurrent synaptic excitation between layer 4 neurons may be counterbalanced by the ability of the synapses to undergo long-term depression that is dependent on mGluR2 receptors (Egger et al. 1999): one wonders whether such LTD is ineffective in individuals predisposed to seizures containing polyspikes and/or fast runs. It is possible that a drug therapy aimed at preventing excessive recurrent excitation between spiny stellate neurons—possibly one that targets NR2C receptors (Fleidervish et al. 1998)—could have useful antiepileptic effects. A possible result of such targeting could be the prevention of polyspikes and fast runs, the characteristic interictal and ictal EEG abnormalities in certain epilepsies, including juvenile myoclonic epilepsy or Janz syndrome (Pedersen and Petersen 1998), and Lennox–Gastaut syndrome (Markand 2003; Steriade 2003).

ACKNOWLEDGMENTS

We thank Drs. Mircea Steriade, Hannah Monyer, Nancy Kopell, Vincenzo Crunelli, and Stuart Hughes for helpful discussions and encouragement. This work could not have been performed without the generous assistance of Dr. Robert Walkup of the IBM T. J. Watson Research Center.

GRANTS

This work was supported by the National Institute of Neurological Disorders and Stroke, the National Institutes of Health Bioengineering Research Partnership Grant R01NS-041811-01, the State University of New York Downstate Graduate Research Initiative Program, the Medical Research Council (United Kingdom), the Wellcome Trust, and Volkswagen Stiftung.

REFERENCES

Avoli M and Gloor P. The effects of transient functional depression of the thalamus on spindles and on bilateral synchronous epileptic discharges of feline generalized penicillin epilepsy. *Epilepsia* 22: 443–452, 1981.

Avoli M and Gloor P. Interaction of cortex and thalamus in spike and wave discharges of feline generalized penicillin epilepsy. *Exp Neurol* 76: 196–217, 1982.

Bal T, Debay D, and Destexhe A. Cortical feedback controls the frequency and synchrony of oscillations in the visual thalamus. *J Neurosci* 20: 7478–7488, 2000.

Bal T and McCormick DA. Mechanisms of oscillatory activity in guinea-pig nucleus reticularis thalami *in vitro*: a mammalian pacemaker. *J Physiol* 468: 669–691, 1993.

Bal T, von Krosigk M, and McCormick DA. Synaptic and membrane mechanisms underlying synchronized oscillations in the ferret lateral geniculate nucleus *in vitro. J Physiol* 483: 641–663, 1995a.

Bal T, von Krosigk M, and McCormick DA. Role of the ferret perigeniculate nucleus in the generation of synchronized oscillations *in vitro. J Physiol* 483: 665–685, 1995b.

Bazhenov M, Timofeev I, Steriade M, and Sejnowski TJ. Model of thalamocortical slow-wave sleep oscillations and transitions to activated states. *J Neurosci* 22: 8691–8704, 2002.

Bazhenov M, Timofeev I, Steriade M, and Sejnowski TJ. Potassium model for slow (2–3 Hz) in vivo neocortical paroxysmal oscillations. *J Neurophysiol* 92: 1116–1132, 2004.

Beierlein M, Fall CP, Rinzel J, and Yuste R. Thalamocortical bursts trigger recurrent activity in neocortical networks: layer 4 as a frequency-dependent gate. *J Neurosci* 22: 9885–9894, 2002.

Birtoli B and Ulrich D. Firing mode-dependent synaptic plasticity in rat neocortical pyramidal neurons. *J Neurosci* 24: 4935–4940, 2004.

Blatow M, Rozov A, Katona I, Hormuzdi SG, Meyer AH, Whittington MA, Caputi A, and Monyer H. A novel network of multipolar bursting interneurons generates theta frequency oscillations in neocortex. *Neuron* 38: 805–817, 2003.

Blethyn KL, Hughes SW, Cope DW, and Crunelli V. The role of ionic conductances underlying a slow (<1 Hz) oscillation in neurons of the thalamic reticular nucleus *in vitro. Soc Neurosci Abstr* 699.3, 2003.

Bragin A, Engel J Jr, Wilson CL, Fried I, and Mathern GW. Hippocampal and entorhinal cortex high-frequency oscillations (100–500 Hz) in human epileptic brain and in kainic acid-treated rats with chronic seizures. *Epilepsia* 40: 127–137, 1999.

Bruzzone R, Hormuzdi SG, Barbe MT, Herb A, and Monyer H. Pannexins, a family of gap junction proteins expressed in brain. *Proc Natl Acad Sci USA* 100: 13644–13649, 2003.

Buhl EH, Tamás G, and Fisahn A. Cholinergic activation and tonic excitation induce persistent gamma oscillations in mouse somatosensory cortex *in vitro. J Physiol* 513: 117–126, 1998.

Bush P and Sejnowski TJ. Inhibition synchronizes sparsely connected cortical neurons within and between columns in realistic network models. *J Comput Neurosci* 3: 91–110, 1996.

Castro-Alamancos MA. Origin of synchronized oscillations induced by neocortical disinhibition *in vivo. J Neurosci* 20: 9195–9206, 2000.

Castro-Alamancos MA and Rigas P. Synchronized oscillations caused by disinhibition in rodent neocortex are generated by recurrent synaptic activity mediated by AMPA receptors. *J Physiol* 542: 567–581, 2002.

Contreras D, Curró Dossi R, and Steriade M. Electrophysiological properties of cat reticular thalamic neurones *in vivo. J Physiol* 470: 273–294, 1993.

Contreras D, Destexhe A, Sejnowski TJ, and Steriade M. Control of spatiotemporal coherence of a thalamic oscillation by corticothalamic feedback. *Science* 274: 771–774, 1996.

Contreras D and Steriade M. Spindle oscillation in cats: the role of corticothalamic feedback in a thalamically generated rhythm. *J Physiol* 490: 159–179, 1996.

Crunelli V and Leresche N. Childhood absence epilepsy: genes, channels, neurons and networks. *Nat Rev Neurosci* 3: 371–382, 2002.

Cunningham MO, Halliday DM, Davies CH, Traub RD, Buhl EH, and Whittington MA. Coexistence of gamma and high-frequency oscillations in the medial entorhinal cortex *in vitro. J Physiol* 559: 347–353, 2004b.

Cunningham MO, Whittington MA, Bibbig A, Roopun A, LeBeau FEN, Vogt A, Monyer H, Buhl EH, and Traub RD. A role for fast rhythmic bursting neurons in cortical gamma oscillations in vitro. *Proc Natl Acad Sci USA* 101: 7152–7157, 2004a.

Deschênes M. Dendritic spikes induced in fast pyramidal tract neurons by thalamic stimulation. *Exp Brain Res* 43: 304–308, 1981.

Deschênes M, Paradis M, Roy JP, and Steriade M. Electrophysiology of neurons of lateral thalamic nuclei in cat: resting properties and burst discharges. *J Neurophysiol* 51: 1196–1219, 1984.

Destexhe A, Bal T, McCormick DA, and Sejnowski TJ. Ionic mechanisms underlying synchronized oscillations and propagating waves in a model of ferret thalamic slices. *J Neurophysiol* 76: 2049–2070, 1996.

Destexhe A, Contreras D, and Steriade M. Mechanisms underlying the synchronizing action of corticothalamic feedback through inhibition of thalamic relay cells. *J Neurophysiol* 79: 999–1016, 1998.

Destexhe A, Contreras D, and Steriade M. Cortically-induced coherence of a thalamic-generated oscillation. *Neuroscience* 92: 427–443, 1999.

Dichter M and Spencer WA. Penicillin-induced interictal discharges from the cat hippocampus. I. Characteristics and topographical features. *J Neurophysiol* 32: 649–662, 1969.

Douglas RJ and Martin KAC. A functional microcircuit for cat visual cortex. *J Physiol* 440: 735–769, 1991.

Egger V, Feldmeyer D, and Sakmann B. Coincidence detection and changes of synaptic efficacy in spiny stellate neurons in rat barrel cortex. *Nat Neurosci* 2: 1098–1105, 1999.

Feldmeyer D, Egger V, Lübke J, and Sakmann B. Reliable synaptic connections between pairs of excitatory layer 4 neurones within a single "barrel" of developing rat somatosensory cortex. *J Physiol* 521: 169–190, 1999.

Fisahn A, Pike FG, Buhl EH, and Paulsen O. Cholinergic induction of network oscillations at 40 Hz in the hippocampus *in vitro. Nature* 394: 186–189, 1998.

Fleidervish IA, Binshtok AM, and Gutnick MJ. Functionally distinct NMDA receptors mediate horizontal connectivity within layer 4 of mouse barrel cortex. *Neuron* 21: 1055–1065, 1998.

Fuentealba P, Crochet S, Timofeev I, Bazhenov M, Sejnowski TJ, and Steriade M. Experimental evidence and modeling studies support a synchronizing role for electrical coupling in the cat thalamic reticular nucleus in vivo. *Eur J Neurosci* 20: 111–119, 2004.

Gloor P, Quesney LF, and Zumstein H. Pathophysiology of generalized penicillin epilepsy in the cat: the role of cortical and subcortical structures. II. Topical application of penicillin to the cerebral cortex and to subcortical structures. *Electroenceph Clin Neurophysiol* 43: 79–94, 1977.

Golomb D and Amitai Y. Propagating neuronal discharges in neocortical slices: computational and experimental study. *J Neurophysiol* 78: 1199–1211, 1997.

Grenier F, Timofeev I, and Steriade M. Focal synchronization of ripples (80–200 Hz) in neocortex and their neuronal correlates. *J Neurophysiol* 86: 1884–1898, 2001.

Grenier F, Timofeev I, and Steriade M. Neocortical very fast oscillations (ripples, 80–200 Hz) during seizures: intracellular correlates. *J Neurophysiol* 89: 841–852, 2003.

Gutnick MJ, Connors BW, and Prince DA. Mechanisms of neocortical epileptogenesis in vitro. *J Neurophysiol* 48: 1321–1335, 1982.

Gutnick MJ, Lobel-Yaakov R, and Rimon G. Incidence of neuronal dye-coupling in neocortical slices depends on the plane of section. *Neuroscience* 15: 659–666, 1985.

Gutnick MJ and Prince DA. Dye coupling and possible electrotonic coupling in the guinea pig neocortical slice. *Science* 211: 67–70, 1981.

Hoffman SN, Salin PA, and Prince DA. Chronic neocortical epileptogenesis in vitro. *J Neurophysiol* 71: 1762–1773, 1994.

Hormuzdi SG, Pais I, LeBeau FEN, Towers SK, Rozov A, Buhl EH, Whittington MA, and Monyer H. Impaired electrical signaling disrupts gamma frequency oscillations in connexin 36-deficient mice. *Neuron* 31: 487–495, 2001.

Hughes SW, Blethyn KL, Cope DW, and Crunelli V. Properties and origin of spikelets in thalamocortical neurones *in vitro. Neuroscience* 110: 395–401, 2002a.

Hughes SW, Cope DW, Blethyn KL, and Crunelli V. Cellular mechanisms of the slow (<1 Hz) oscillation in thalamocortical neurons in vitro. *Neuron* 33: 947–958, 2002b.

Hughes SW, Lörincz M, Cope DW, Blethyn KL, Kékesi KA, Parri HR, Juhász G, and Crunelli V. Synchronized oscillations at α and θ frequencies in the lateral geniculate nucleus. *Neuron* 42: 1–20, 2004.

Jahnsen H and Llinás R. Electrophysiological properties of guinea-pig thalamic neurones: an *in vitro* study. *J Physiol* 349: 205–226, 1984a.

Jahnsen H and Llinás R. Ionic basis for the electroresponsiveness and oscillatory properties of guinea-pig thalamic neurones *in vitro. J Physiol* 349: 227–247, 1984b.

Jahromi SS, Wentlandt K, Piran S, and Carlen PL. Anticonvulsant actions of gap junctional blockers in an in vitro seizure model. *J Neurophysiol* 88: 1893–1902, 2002.

Jones MS and Barth DS. Spatiotemporal organization of fast (>200 Hz) electrical oscillations in rat vibrissa/barrel cortex. *J Neurophysiol* 82: 1599–1609, 1999.

Jones MS and Barth DS. Effects of bicuculline methiodide on fast (>200 Hz) electrical oscillations in rat somatosensory cortex. *J Neurophysiol* 88: 1016–1025, 2002.

Jones MS, MacDonald KD, Choi B, Dudek FE, and Barth DS. Intracellular correlates of fast (>200 Hz) electrical oscillations in rat somatosensory cortex. *J Neurophysiol* 84: 1505–1518, 2000.

Kawaguchi Y. Distinct firing patterns of neuronal subtypes in cortical synchronized activities. *J Neurosci* 21: 7261–7272, 2001.

Kim U and McCormick DA. Functional and ionic properties of a slow afterhyperpolarization in ferret perigeniculate neurons in vitro. *J Neurophysiol* 80: 1222–1235, 1998.

Köhling R, Gladwell SJ, Bracci E, Vreugdenhil M, and Jefferys JGR. Prolonged epileptiform bursting induced by 0-Mg^{2+} in rat hippocampal slices depends on gap junctional coupling. *Neuroscience* 105: 579–587, 2001.

Landisman CE, Long MA, Beierlein M, Deans MR, Paul DL, and Connors BW. Electrical synapses in the thalamic reticular nucleus. *J Neurosci* 22: 1002–1009, 2002.

Llinás R. The intrinsic electrophysiological properties of mammalian neurons: insights into central nervous system function. *Science* 242: 1654–1664, 1988.

Llinás RR, Grace AA, and Yarom Y. *In vitro* neurons in mammalian cortical layer 4 exhibit intrinsic oscillatory activity in the 10- to 50-Hz range. *Proc Natl Acad Sci USA* 88: 897–901, 1991.

Long MA, Landisman CE, and Connors BW. Small clusters of electrically coupled neurons generate synchronous rhythms in the thalamic reticular nucleus. *J Neurosci* 24: 341–349, 2004.

Luhmann HJ, Mittmann T, van Luijtelaar G, and Heinemann U. Impairment of intracortical GABAergic inhibition in a rat model of absence epilepsy. *Epilepsy Res* 22: 43–51, 1995.

Lüthi A and McCormick DA. Periodicity of thalamic synchronized oscillations: the role of Ca^{2+}-mediated upregulation of I_h. *Neuron* 20: 553–563, 1998.

Lytton WW, Contreras D, Destexhe A, and Steriade M. Dynamic interactions determine partial thalamic quiescence in a computer network model of spike-and-wave seizures. *J Neurophysiol* 77: 1679–1696, 1997.

Marder E. Roles for electrical coupling in neural circuits as revealed by selective neuronal deletions. *J Exp Biol* 112: 147–167, 1984.

Markand ON. Lennox–Gastaut syndrome (childhood epileptic encephalopathy). *J Clin Neurophysiol* 20: 426–441, 2003.

Matsumoto H and Ajmone Marsan C. Cortical cellular phenomena in experimental epilepsy: interictal manifestations. *Exp Neurol* 9: 286–304, 1964.

McCormick DA, Connors BW, Lighthall JW, and Prince DA. Comparative electrophysiology of pyramidal and sparsely spiny stellate neurons of the neocortex. *J Neurophysiol* 54: 782–806, 1982.

Metherate R and Cruikshank SJ. Thalamocortical inputs trigger a propagating envelope of gamma-band activity in auditory cortex in vitro. *Exp Brain Res* 126: 160–174, 1999.

Miles R and Wong RKS. Excitatory synaptic interactions between CA3 neurones in the guinea-pig hippocampus. *J Physiol* 373: 397–418, 1986.

Miles R and Wong RKS. Inhibitory control of local excitatory circuits in the guinea-pig hippocampus. *J Physiol* 388: 611–629, 1987.

Miller KD, Pinto DJ, and Simons DJ. Processing in layer 4 of the neocortical circuit: new insights from visual and somatosensory cortex. *Curr Opin Neurobiol* 11: 488–497, 2001.

Nowak LG, Azouz R, Sanchez-Vives MV, Gray CM, and McCormick DA. Electrophysiological classes of cat primary visual cortical neurons in vivo as revealed by quantitative analyses. *J Neurophysiol* 89: 1541–1566, 2003.

Nuñez A, Amzica F, and Steriade M. Voltage-dependent fast (20–40 Hz) oscillations in long-axoned neocortical neurons. *Neuroscience* 51: 7–10, 1992.

Pedersen SB and Petersen KA. Juvenile myoclonic epilepsy: clinical and EEG features. *Acta Neurol Scand* 97: 160–163, 1998.

Perez-Velazquez JL, Valiante TA, and Carlen PL. Modulation of gap junctional mechanisms during calcium-free induced field burst activity: a possible role for electrotonic coupling in epileptogenesis. *J Neurosci* 14: 4308–4317, 1994.

Pinault D and Deschênes M. Voltage-dependent 40-Hz oscillations in rat reticular thalamic neurons *in vivo. Neuroscience* 51: 245–258, 1992.

Pinault D, Leresche N, Charpier S, Deniau JM, Marescaux C, Vergnes M, and Crunelli V. Intracellular recordings in thalamic neurones during spontaneous spike and wave discharges in rats with absence epilepsy. *J Physiol* 509: 449–456, 1998.

Pinto DJ, Jones SR, Kaper TJ, and Kopell N. Analysis of state-dependent transitions in frequency and long-distance coordination in a model oscillatory cortical circuit. *J Comput Neurosci* 15: 283–298, 2003.

Porter JT, Johnson CK, and Agmon A. Diverse types of interneurons generate thalamus-evoked feedforward inhibition in the mouse barrel cortex. *J Neurosci* 21: 2699–2710, 2001.

Prince DA. The depolarization shift in "epileptic" neurons. *Exp Neurol* 21: 467–485, 1968.

Ross FM, Gwyn P, Spanswick D, and Davies SN. Carbenoxolone depresses spontaneous epileptiform activity in the CA1 region of rat hippocampal slices. *Neuroscience* 100: 789–796, 2000.

Sawa M, Maruyama N, and Kaji S. Intracellular potential during electrically induced seizures. *Electroenceph Clin Neurophysiol* 15: 209–220, 1963.
Schiller Y. Inter-ictal and ictal-like epileptic discharges in the dendritic tree of neocortical pyramidal neurons. *J Neurophysiol* 88: 2954–2962, 2002.
Schmitz D, Schuchmann S, Fisahn A, Draguhn A, Buhl EH, Petrasch-Parwez RE, Dermietzel R, Heinemann U, and Traub RD. Axo-axonal coupling: a novel mechanism for ultrafast neuronal communication. *Neuron* 31: 831–840, 2001.
Schweitzer JS, Wang H, Xiong ZQ, and Stringer JL. pH Sensitivity of non-synaptic field bursts in the dentate gyrus. *J Neurophysiol* 84: 927–933, 2000.
Slaght SJ, Leresche N, Deniau JM, Crunelli V, and Charpier S. Activity of thalamic reticular neurons during spontaneous genetically determined spike and wave discharges. *J Neurosci* 22: 2323–2334, 2002.
Snow RW and Dudek FE. Electrical fields directly contribute to action potential synchronization during convulsant-induced epileptiform bursts. *Brain Res* 323: 114–118, 1984.
Staba RJ, Wilson CL, Bragin A, Jhung D, Fried I, and Engel J Jr. High-frequency oscillations recorded in human medial temporal lobe during sleep. *Ann Neurol* 56: 108–115, 2004.
Steriade M. *The Intact and Sliced Brain.* Cambridge, MA: MIT Press, 2001.
Steriade M. *Neuronal Substrates of Sleep and Epilepsy.* Cambridge, UK: Cambridge Univ. Press, 2003.
Steriade M, Amzica F, and Contreras D. Synchronization of fast (30–40 Hz) spontaneous cortical rhythms during brain activation. *J Neurosci* 16: 392–417, 1996.
Steriade M, Amzica F, Neckelmann D, and Timofeev I. Spike-wave complexes and fast components of cortically generated seizures. II. Extra- and intracellular patterns. *J Neurophysiol* 80: 1456–1479, 1998a.
Steriade M and Contreras D. Relations between cortical and thalamic cellular events during transition from sleep patterns to paroxysmal activity. *J Neurosci* 15: 623–642, 1995.
Steriade M and Contreras D. Spike-wave complexes and fast components of cortically generated seizures. I. Role of neocortex and thalamus. *J Neurophysiol* 80: 1439–1455, 1998.
Steriade M, Contreras D, Amzica F, and Timofeev I. Synchronization of fast (30–40 Hz) spontaneous oscillations in intrathalamic and thalamocortical networks. *J Neurosci* 16: 2788–2808, 1996.
Steriade M, Curró Dossi R, and Contreras D. Electrophysiological properties of intralaminar thalamocortical cells discharging rhythmic (~40 Hz) spike-bursts at ~1000 Hz during waking and rapid eye movement sleep. *Neuroscience* 56: 1–9, 1993.
Steriade M, Domich L, Oakson G, and Deschênes M. The deafferented reticular thalamic nucleus generates spindle rhythmicity. *J Neurophysiol* 57: 260–273, 1987.
Steriade M, Nuñez A, and Amzica F. A novel slow (<1 Hz) oscillation of neocortical neurons *in vivo*: depolarizing and hyperpolarizing components. *J Neurosci* 13: 3266–3283, 1993.
Steriade M, Timofeev I, Dürmüller, and Grenier F. Dynamic properties of corticothalamic neurons and local cortical interneurons generating fast rhythmic (30–40 Hz) spike bursts. *J Neurophysiol* 79: 483–490, 1998b.
Swadlow HA. Fast-spike interneurons and feedforward inhibition in awake sensory neocortex. *Cereb Cortex* 13: 25–32, 2003.
Szente M, Gajda Z, Ali KS, and Hermesz E. Involvement of electrical coupling in the in vivo ictal epileptiform activity induced by 4-aminopyridine in the neocortex. *Neuroscience* 115: 1067–1078, 2002.
Thomson AM and Bannister AP. Electrical gap junctions involving somata and axons of neocortical and hippocampal pyramidal cells. *Abstr Soc Neurosci* 403: 13, 2004.
Timofeev I, Grenier F, and Steriade M. Spike-wave complexes and fast components of cortically generated seizures. IV. Paroxysmal fast runs in cortical and thalamic neurons. *J Neurophysiol* 80: 1495–1513, 1998.
Timofeev I, Grenier F, and Steriade M. Contribution of intrinsic neuronal factors in the generation of cortically driven electrographic seizures. *J Neurophysiol* 92: 1133–1143, 2004.
Timofeev I and Steriade M. Low-frequency rhythms in the thalamus of intact-cortex and decorticated cats. *J Neurophysiol* 76: 4152–4168, 1996.
Topolnik L, Steriade M, and Timofeev I. Partial cortical deafferentation promotes development of paroxysmal activity. *Cereb Cortex* 13: 883–893, 2003.
Traub RD and Bibbig A. A model of high-frequency ripples in the hippocampus, based on synaptic coupling plus axon-axon gap junctions between pyramidal neurons. *J Neurosci* 20: 2086–2093, 2000.
Traub RD, Bibbig A, Fisahn A, LeBeau FEN, Whittington MA, and Buhl EH. A model of gamma-frequency network oscillations induced in the rat CA3 region by carbachol *in vitro. Eur J Neurosci* 12: 4093–4106, 2000.
Traub RD, Buhl EH, Gloveli T, and Whittington MA. Fast rhythmic bursting can be induced in layer 2/3 cortical neurons by enhancing Na^+ conductance or by blocking BK channels. *J Neurophysiol* 89: 909–921, 2003c.
Traub RD, Cunningham MO, Gloveli T, LeBeau FEN, Bibbig A, Buhl EH, and Whittington MA. GABA-enhanced collective behavior in neuronal axons underlies persistent gamma-frequency oscillations. *Proc Natl Acad Sci USA* 100: 11047–11052, 2003b.
Traub RD, Draguhn A, Whittington MA, Baldeweg T, Bibbig A, Buhl EH, and Schmitz D. Axonal gap junctions between principal neurons: a novel source of network oscillations, and perhaps epileptogenesis. *Rev Neurosci* 13: 1–30, 2002.
Traub RD, Jefferys JGR, Miles R, Whittington MA, and Tóth K. A branching dendritic model of a rodent CA3 pyramidal neurone. *J Physiol* 481: 79–95, 1994.
Traub RD and Miles R. *Neuronal Networks of the Hippocampus.* Cambridge, UK: Cambridge Univ. Press, 1991.
Traub RD, Pais I, Bibbig A, LeBeau FEN, Buhl EH, Hormuzdi SG, Monyer H, and Whittington MA. Contrasting roles of axonal (pyramidal cell) and dendritic (interneuron) electrical coupling in the generation of gamma oscillations in the hippocampus in vitro. *Proc Natl Acad Sci USA* 100: 1370–1374, 2003a.
Traub RD, Schmitz D, Jefferys JGR, and Draguhn A. High-frequency population oscillations are predicted to occur in hippocampal pyramidal neuronal networks interconnected by axoaxonal gap junctions. *Neuroscience* 92: 407–426, 1999.
Traub RD, Whittington MA, Buhl EH, LeBeau FEN, Bibbig A, Boyd S, Cross H, and Baldeweg T. A possible role for gap junctions in generation of very fast EEG oscillations preceding the onset of, and perhaps initiating, seizures. *Epilepsia* 42: 153–170, 2001.
Traub RD and Wong RKS. Cellular mechanism of neuronal synchronization in epilepsy. *Science* 216: 745–747, 1982.
Ulrich D and Huguenard JR. $GABA_A$-receptor-mediated rebound burst firing and burst shunting in thalamus. *J Neurophysiol* 78: 1748–1751, 1997.
von Krosigk M, Bal T, and McCormick DA. Cellular mechanisms of a synchronized oscillation in the thalamus. *Science* 261: 361–364, 1993.
Wang XJ and Rinzel J. Spindle rhythmicity in the reticularis thalami nucleus: synchronization among mutually inhibitory neurons. *Neuroscience* 53: 899–904, 1993.
Wang Y, Gupta A, Toledo-Rodriguez M, Wu CZ, and Markram H. Anatomical, physiological, molecular and circuit properties of nest basket cells in the developing somatosensory cortex. *Cereb Cortex* 12: 395–410, 2002.
Whittington MA and Traub RD. Inhibitory interneurons and network oscillations in vitro. *Trends Neurosci* 26: 676–682, 2003.
Whittington MA, Traub RD, and Jefferys JGR. Synchronized oscillations in interneuron networks driven by metabotropic glutamate receptor activation. *Nature* 373: 612–615, 1995.
Williams SR, Stuart GJ. Mechanisms and consequences of action potential burst firing in rat neocortical pyramidal neurons. *J Physiol* 521: 467–482, 1999.
Ylinen A, Bragin A, Nádasdy Z, Jandó G, Szabó I, Sik A, and Buzsáki G. Sharp wave-associated high frequency oscillation (200 Hz) in the intact hippocampus: network and intracellular mechanisms. *J Neurosci* 15: 30–46, 1995.

APPENDIX A

Single-cell models

The network model used the following component model neurons (Fig. 1 of main text), each with a single-compartment soma, a 6-compartment branched axon, and multiple dendritic compartments:

1) superficial (layer 2/3) RS pyramidal cell, 74 compartments
2) superficial (layer 2/3) FRB pyramidal cell, 74 compartments
3) superficial basket cell, 59 compartments
4) superficial axoaxonic (chandelier) cell, 59 compartments
5) superficial LTS interneuron, 59 compartments
6) layer 4 spiny stellate cell, 59 compartments
7) layer 5 tufted IB pyramidal cell, 61 compartments

TABLE A1. *Membrane conductance densities for superficial RS pyramidal cells (mS/cm^2), by level in model structure*

Level	$g_{Na(F)}$	$g_{Na(P)}$	$g_{K(DR)}$	$g_{K(C)}$	$g_{K(A)}$	$g_{K(M)}$	g_{K2}	$g_{K(AHP)}$	$g_{Ca(L)}$	$g_{Ca(T)}$	g_{AR}
0	400	0	400	0	2	0	0.1	0	0	0	0
1	187.5	0.12	125	12	30	7.5	0.1	0.04	1	0.1	0.25
2	93.75	0.06	93.75	12	2	7.5	0.1	0.04	1	0.1	0.25
3	12.5	0.008	6.25	12	2	7.5	0.1	0.04	1	0.1	0.25
4	12.5	0.008	6.25	12	2	7.5	0.1	0.04	1	0.1	0.25
5	125	0.08	125	12	30	7.5	0.1	0.04	1	0.1	0.25
6	93.75	0.06	93.75	12	2	7.5	0.1	0.04	1	0.1	0.25
7	12.5	0.008	6.25	12	2	7.5	0.1	0.04	1	0.1	0.25
8	12.5	0.008	6.25	12	2	7.5	0.1	0.04	1	0.1	0.25
9	12.5	0.008	6.25	12	2	7.5	0.1	0.04	1	0.1	0.25
10	12.5	0.008	6.25	12	2	7.5	0.1	0.04	1	0.1	0.25
11	12.5	0.008	6.25	12	2	7.5	0.1	0.04	1	0.1	0.25
12	12.5	0.008	6.25	12	2	7.5	0.1	0.04	1	0.1	0.25

Explanation of levels: level 0 = axon; level 1 = soma; level 2 = proximal basal and oblique dendrites; level 3 = middle basal and oblique dendrites; level 4 = distal basal and oblique dendrites; levels 5–12 = progressively more distal apical dendrites.

8) layer 5 tufted RS pyramidal cell, 61 compartments
9) layer 6 nontufted RS pyramidal cell, 50 compartments
10) deep basket cell, 59 compartments
11) deep axoaxonic cell, 59 compartments
12) deep LTS interneuron, 59 compartments
13) thalamocortical relay (TCR) cell, 137 compartments
14) nucleus reticularis (nRT) cell, 59 compartments

The pyramids, spiny stellates, and TCR cells are glutamatergic, so that firing of their axons activates AMPA/kainate and NMDA receptors on postsynaptic cells. The cortical interneurons and nRT cells are GABAergic cells that activate $GABA_A$ receptors on postsynaptic cells. $GABA_B$ receptors were not simulated.

Different cortical layers exhibit far more diversity in neuronal morphology and connectivity than could be incorporated into this model; to cite one example, somatosensory layer 6 pyramids have different dendritic morphology and intracortical connectivity, depending on whether they connect to the thalamus (Zhang and Deschênes 1997). In addition, this (first version) of the model does not include interneurons within layer 4 itself (although such interneurons do exist; Tarczy-Hornoch et al. 1998), nor does it include layer 4 star pyramids, cells that have dendritic extensions into layer 2/3. Layer 4 pyramids seem to be the category of layer 4 excitatory neuron most likely to receive cortical excitatory inputs from outside layer 4 (Schubert et al. 2003); in our model, we placed such inputs onto the spiny stellates.

The neuron models incorporate a number of symmetries, thereby helping to reduce the very large number of parameters; note the following examples.

1) Several different cell types use identical compartmental topology (e.g., superficial RS and FRB pyramids, or all GABAergic cells and spiny stellates).

2) Within a given cell model, the compartments are lumped into a series of "levels," following earlier practice (Traub et al. 1994), and all compartments in a particular level have the same membrane conductance densities.

3) There is a standard repertoire of 11 active conductances used by all of the cells; however, the membrane density distributions, and perhaps details of kinetics, are adjusted for each type of cell. The conductances used were as described in Traub et al. 2003 and Cunningham et al. 2004: fast (transient) $g_{Na(F)}$, persistent $g_{Na(P)}$, delayed rectifier $g_{K(DR)}$, rapid voltage- and $[Ca^{2+}]_i$-dependent $g_{K(C)}$, transient inactivating $g_{K(A)}$, $g_{K(M)}$, g_{K2}, slow $[Ca^{2+}]_i$-dependent $g_{K(AHP)}$, high-threshold $g_{Ca(L)}$, low-threshold inactivating $g_{Ca(T)}$, and the anomolous rectifier or h-conductance g_{AR}. There were 2 sorts of g_{Na} kinetics, one for glutamatergic cells (other than spiny stellates) (as in Traub et al. 2003) and the other for spiny stellates and GABAergic cells (as described in the supplemental material for Cunningham et al. 2004). Both types of g_{Na} kinetics are based on quantitative data in Martina and Jonas (1997). Similarly, there were 2 sorts of $g_{K(DR)}$ kinetics, respectively $g_{Ca(T)}$ kinetics, one for glutamatergic cells other than spiny stellates (as in Traub et al. 2003), and one for spiny stellates and GABAergic cells (as in Cunningham et al. 2004). $g_{K(DR)}$ kinetics are based on data in Martina et al. (1998). $g_{Ca(T)}$ kinetics for glutamatergic cells (most important, TCR cells) used data in Destexhe et al. 1998; $g_{Ca(T)}$ kinetics for GABAergic cells (most important, nRT cells) used data in Destexhe et al. (1996).

TABLE A2. *Membrane conductance densities for superficial FRB pyramidal cells (mS/cm^2), by level in model structure*

Level	$g_{Na(F)}$	$g_{Na(P)}$	$g_{K(DR)}$	$g_{K(C)}$	$g_{K(A)}$	$g_{K(M)}$	g_{K2}	$g_{K(AHP)}$	$g_{Ca(L)}$	$g_{Ca(T)}$	g_{AR}
0	400	0	400	0	2	0	0.1	0	0	0	0
1	187.5	0.48	125	4.5	30	7.5	0.1	0.1	1	0.1	0.25
2	93.75	0.24	93.75	4.5	2	7.5	0.1	0.1	1	0.1	0.25
3	12.5	0.032	6.25	4.5	2	7.5	0.1	0.1	1	0.1	0.25
4	12.5	0.032	6.25	4.5	2	7.5	0.1	0.1	1	0.1	0.25
5	125	0.32	125	4.5	30	7.5	0.1	0.1	1	0.1	0.25
6	93.75	0.24	93.75	4.5	2	7.5	0.1	0.1	1	0.1	0.25
7	12.5	0.032	6.25	4.5	2	7.5	0.1	0.1	1	0.1	0.25
8	12.5	0.032	6.25	4.5	2	7.5	0.1	0.1	1	0.1	0.25
9	12.5	0.032	6.25	4.5	2	7.5	0.1	0.1	1	0.1	0.25
10	12.5	0.032	6.25	4.5	2	7.5	0.1	0.1	1	0.1	0.25
11	12.5	0.032	6.25	4.5	2	7.5	0.1	0.1	1	0.1	0.25
12	12.5	0.032	6.25	4.5	2	7.5	0.1	0.1	1	0.1	0.25

Explanation of levels: level 0 = axon; level 1 = soma; level 2 = proximal basal and oblique dendrites; level 3 = middle basal and oblique dendrites; level 4 = distal basal and oblique dendrites; levels 5–12 = progressively more distal apical dendrites.

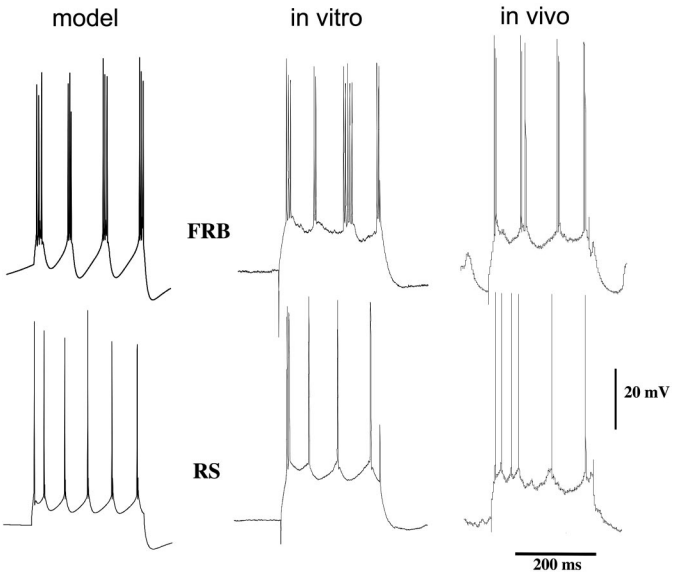

FIG. A1. RS and FRB firing behaviors in model layer 2/3 pyramidal neurons, in layer 2/3 putative pyramidal cells in rat auditory cortex in vitro, and in neurons in rat somatosensory cortex in vivo. Cells were injected with somatic depolarizing currents (0.4 and 0.75 nA for model, 0.5 nA for in vitro experiment). Model and in vitro data from Cunningham et al. (2004). In vivo RS cell was from layer 6, and the in vivo FRB cell from layer 4.

In our single-cell models, axonal and somatodendritic g_{Na} use the same kinetics, and axonal spike initiation is realized by an increased g_{Na} density in the axons (Mainen et al. 1995). It may be, however, that—as postulated in the historic model of Dodge and Cooley (1973)—axonal g_{Na} has a lower threshold than that of somatodendritic g_{Na}, at least in layer 5 pyramidal neurons (Colbert and Pan 2002), an effect we did not simulate.

Other sources of kinetic data

A-current and h-current kinetics were based on data in Huguenard and McCormick (1992). The K2 current followed Huguenard and McCormick (1992) and McCormick and Huguenard (1992), with some simplifications: only the faster component of inactivation was used, and the activation variable *m* was first order.

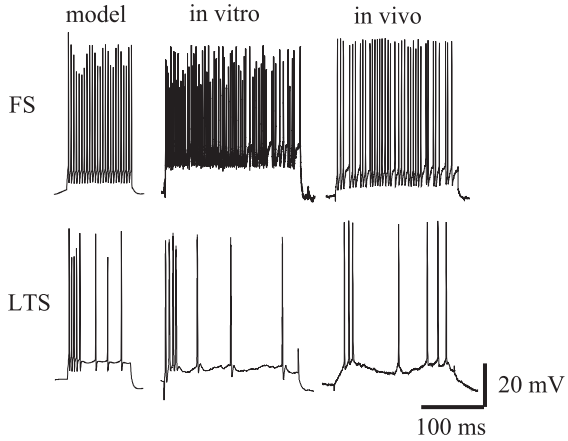

FIG. A2. FS and LTS firing behaviors in model neurons (0.4 nA depolarizing current pulses to somata), in neurons in layer 2/3 rat auditory cortex in vitro (0.5 nA current pulses), and in neurons from rat somatosensory cortex in vivo. Model and in vitro data from Cunningham et al. (2004). In vivo FS cell was from layer 5 and the in vivo LTS cell was from the layer 4/layer 5 border.

High-threshold calcium conductance kinetics came from Kay and Wong (1987). Persistent g_{Na} had rapid activation kinetics, but a lower activation threshold, than did transient g_{Na} (Kay et al. 1998); it did not inactivate.

Some electrotonic parameters

Soma/dendritic membrane resistivity was 50,000 Ω-cm^2 for cortical glutamatergic cells; 25,000 Ω-cm^2 for cortical GABAergic cells; 26,400 Ω-cm^2 for TCR cells; and 20,000 Ω-cm^2 for nRT cells. Soma/dendritic internal resistivity was 250 Ω-cm for cortical glutamatergic cells; 200 Ω-cm for cortical GABAergic cells and nRT cells; and 175 Ω-cm for TCR cells. Membrane capacitance density was 0.9 μF/cm^2 for all glutamatergic cells and 1.0 μF/cm^2 for all GABAergic cells. Axonal membrane and internal resistivities were smaller than for soma/dendrites: 1,000 Ω-cm^2 and 100 Ω-cm, respectively.

Reversal potentials

V_{Na} was +50 mV for all cell types. V_{Ca} was +125 mV for all types. V_L (the reversal potential for the leak conductance) was −65 mV for FS and LTS interneurons, and for spiny stellates; it was −75 mV for nRT cells; it was −70 mV for cortical pyramids and TCR neurons. V_{AR} (the reversal potential for the anomalous rectifier, or h conductance) was −40 mV for all GABAergic cells and spiny stellates; it was −35 mV for cortical pyramids and TCR cells. V_K was −100 mV for GABAergic neurons and for spiny stellates; it was −95 mV for cortical pyramids and TCR cells.

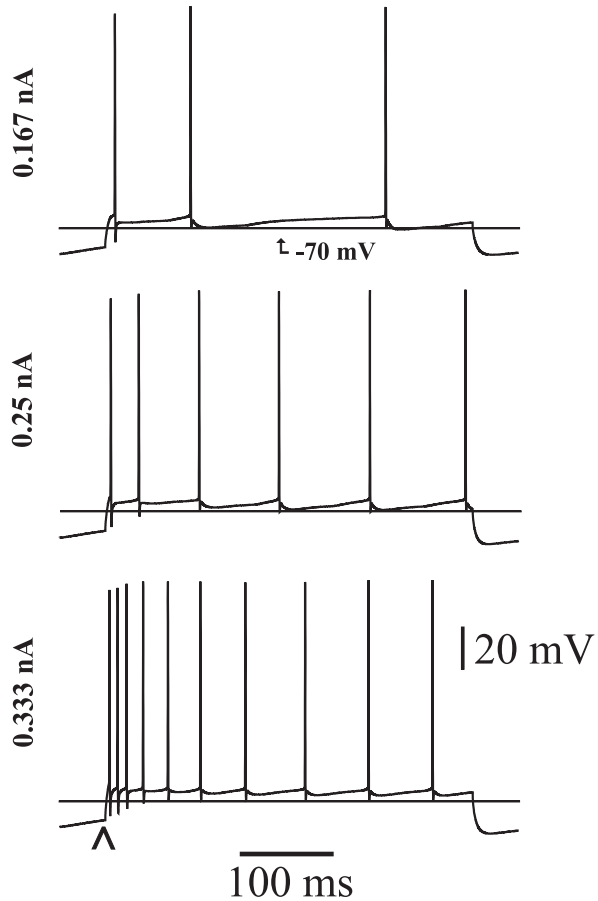

FIG. A3. Firing behavior of model spiny stellate cell in response to depolarizing current pulses, illustrating regular spiking (RS) behavior.

TABLE A3. *Membrane conductance densities for spiny stellate cells (mS/cm^2), by level in model structure*

Level	$g_{Na(F)}$	$g_{Na(P)}$	$g_{K(DR)}$	$g_{K(C)}$	$g_{K(A)}$	$g_{K(M)}$	g_{K2}	$g_{K(AHP)}$	$g_{Ca(L)}$	$g_{Ca(T)}$	g_{AR}
0	400	0.4	400	0	2	0	0.1	0	0	0	0
1	150	0.15	100	10	30	3.75	0.1	0.1	0.5	0.1	0.25
2	75	0.075	75	10	30	3.75	0.1	0.1	0.5	0.1	0.25
3	75	0.075	75	10	2	3.75	0.1	0.1	0.5	0.1	0.25
4	5	0.005	0	10	2	3.75	0.1	0.1	0.5	0.1	0.25
5	5	0.005	0	0	2	3.75	0.1	0.1	0.5	0.1	0.25
6	5	0.005	0	0	2	3.75	0.1	0.1	0.5	0.1	0.25
7	5	0.005	0	0	2	3.75	0.1	0.1	3	0.1	0.25
8	5	0.005	0	0	2	3.75	0.1	0.1	3	0.1	0.25
9	5	0.005	0	0	2	3.75	0.1	0.1	3	0.1	0.25

Explanation of levels: level 0 = axon; level 1 = soma; levels 2–9 = dendrites.

Calcium dynamics

[Ca^{2+}] was simulated in a thin shell beneath the soma-dendritic membrane. This variable was used to gate calcium-dependent K conductances. [Ca^{2+}] rises by the influx through high-threshold calcium channels, and then decays with first-order kinetics. The scaling constants for [Ca^{2+}] rise are specific to each integration subroutine and can be found in the code (variable "cafor"). The decay time constants for the (unitless) [Ca^{2+}] are different in soma and dendrites, and have the following values: for GABAergic neurons (FS, LTS, nRT), and for spiny stellates and TCR cells, the decay time constant was 50 ms in the soma and 20 ms in the dendrites; for superficial pyramids (RS and FRB) and for layer 6 nontufted pyramids, the time constants were 100 ms in the soma and 20 ms in the dendrites; for tufted pyramids (IB and RS), the time constants were 100 ms in the soma, 50 ms in the proximal dendrites, and 13.33 ms in all other dendrites.

Slow AHP time constants

The time constant for decay of the slow AHP conductance was 100 ms for superficial pyramidal cells (RS and FRB); for all other cells, it was 1 s.

Superficial RS pyramidal cell

The properties of this cell model are as described in Traub et al. (2003). Table A1 lists the conductance densities of the different regions of the cell, for comparison with other cell models. The cell architecture is shown in Fig. 1 of the main paper. In this model neuron, the distance from soma to the tip of the apical dendrites is 400 μm.

Layer 2/3 neurons are complicated in several ways: *1*) their dendrites are capable of producing calcium-dependent bursts during strong depolarization (Amitai et al.1993); *2*) their axons appear to generate more action potentials than somata (Traub et al. 2003); *3*) their intinsic firing properties are strongly dependent on the density of certain membrane conductances and on depolarization (Brumberg et al. 2000; Traub et al. 2003). In particular, RS behavior can be converted into FRB behavior by increasing $g_{Na(P)}$, or by decreasing $g_{K(C)}$, and FRB behavior is favored by strong membrane depolarization. FRB behavior does not appear to depend on calcium conductance(s). Firing of model and real (in vitro and in vivo) superficial RS pyramidal cells, in response to depolarizing current pulses, is shown in Fig. A1.

Superficial FRB pyramidal cell

FRB cells were included in the present model because—at least in superficial cortical layers—FRB neurons appear to be necessary for persistent gamma oscillations (Cunningham et al. 2004), an interesting type of collective behavior. In addition, FRB firing patterns have been suggested to be important for cortical gamma oscillations that appear transiently in visual cortex after visual stimulation (Gray and McCormick 1996). FRB cells were modeled, as were layer 2/3 RS pyramidal cells, following Traub et al. (2003). Compared with the RS layer 2/3 pyramidal cell described above, $g_{Na(P)}$ density has been increased and $g_{K(C)}$ has been decreased (Table A2). Figure A1 illustrates an FRB response to an injected depolarizing current pulse, in comparison with the FRB firing behavior of layer 2/3 putative pyramidal cells in vitro and in vivo. In most network simulations, FRB cells are held more depolarized than RS cells (0.25- to 0.35-nA bias current for FRB cells, vs. −0.025 to −0.02 nA for layer 2/3 RS cells).

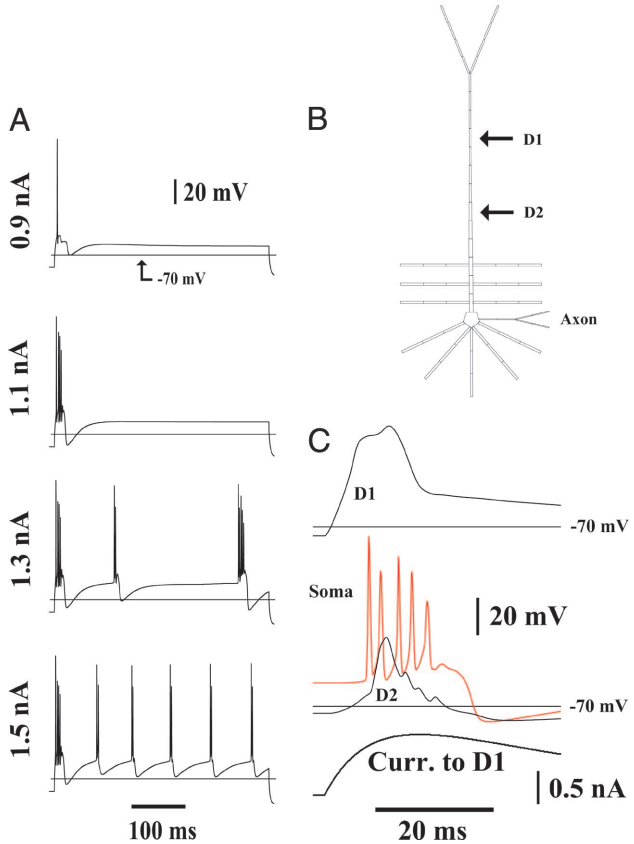

FIG. A4. Electrogenesis in the layer 5 tufted IB pyramidal cell model. *A*: cell soma was held with a −0.2 nA current, and then a depolarizing current pulse was applied. If the current was greater than about 1 nA, a burst would occur. Larger currents evoked repetitive bursting. *B*: compartmental structure of the model, indicating sites in the apical shaft referred to in *C*. *C*: calcium and sodium electrogenesis in the model. A depolarizing current (*bottom trace*) was injected into the distal apical trunk (D1). This led to a slow notched depolarization at D1 itself, in part produced by g_{Ca}, to a burst of action potentials at the soma (red), and to a slow depolarization at D2 with notches that reflect "backpropagating" somatic action potentials. Compare with Fig. 11 of Larkum et al. (2001).

TABLE A4. *Membrane conductance densities for tufted IB pyramidal cells (mS/cm^2), by level in model structure*

Level	$g_{Na(F)}$	$g_{Na(P)}$	$g_{K(DR)}$	$g_{K(C)}$	$g_{K(A)}$	$g_{K(M)}$	g_{K2}	$g_{K(AHP)}$	$g_{Ca(L)}$	$g_{Ca(T)}$	g_{AR}
0	450	0	450	0	0.6	42	0.5	0	0	0	0
1	200	0.16	170	16	20	11.9	0.5	0.2	4	0.1	0.1
2	75	0.06	75	16	8	19.04	0.5	0.2	4	0.1	0.1
3	15	0.012	0	0.5	0.6	19.04	0.5	0.2	4	0.1	0.1
4	15	0.012	0	0.5	0.6	19.04	0.5	0.2	4	0.1	0.1
5	150	0.12	120	16	8	19.04	0.5	0.2	4	0.1	0.1
6	75	0.06	75	16	8	19.04	0.5	0.2	4	0.1	0.1
7	15	0.012	0	0.5	0.6	19.04	0.5	0.2	4	0.1	0.1
8	15	0.012	0	0.5	0.6	19.04	0.5	0.2	4.5	0.1	0.1
9	15	0.012	0	0.5	0.6	19.04	0.5	0.2	4.5	0.1	0.1
10	15	0.012	0	0.5	0.6	19.04	0.5	0.2	4.5	0.1	0.1
11	15	0.012	0	0.5	0.6	19.04	0.5	0.2	4.5	0.1	0.1
12	15	0.012	0	0.5	0.6	19.04	0.5	0.2	4.5	0.1	0.1
13	15	0.012	0	0.5	0.6	19.04	0.5	0.2	4.5	0.1	0.1
14	15	0.012	0	0.5	0.6	19.04	0.5	0.2	4.5	0.1	0.1
15	3	0.0024	0	1.2	0.6	5.6	0.5	0.2	1	0.1	0.1
16	3	0.0024	0	1.2	0.6	5.6	0.5	0.2	1	0.1	0.1
17	3	0.0024	0	1.2	0.6	5.6	0.5	0.2	1	0.1	0.1
18 prox	3	0.0024	0	1.2	0.6	5.6	0.5	0.2	2.7	0.1	0.2
18 dist	3	0.0024	0	1.2	0.6	5.6	0.5	0.2	0.6	0.1	0.2

Explanation of levels: level 0 = axon; level 1 = soma; level 2 = proximal basal and oblique dendrites; level 3 = middle basal and oblique dendrites; level 4 = distal basal and oblique dendrites; levels 5–17 = progressively more distal apical dendritic shaft; level 18 = apical tuft.

BASKET AND AXOAXONIC INTERNEURONS. Both superficial and deep basket and axoaxonic cells had FS firing properties. The structure and conductance kinetics and densities are described in the supplemental material of Cunningham et al. (2004). Figure A2 illustrates firing behavior in the model neuron, in response to a depolarizing current pulse.

LTS INTERNEURONS. These cells (Kawaguchi 1995) were modeled as described in the supplemental material of Cunningham et al. (2004), and firing behavior is illustrated in Fig. A2. The initial burst is generated by low-threshold calcium channels (Goldberg et al. 2004). It was possible to convert the LTS model into an FRB interneuron (Steriade et al. 1998) by increasing $g_{Na(P)}$ density and $g_{K(M)}$ density, while slightly decreasing $g_{K(C)}$ density (data not shown), but FRB interneurons were not incorporated into the present network model. We were not able to convert FS interneurons into FRB interneurons by similar manipulations of conductance densities.

SPINY STELLATE NEURONS. These neurons are RS cells in our model (Beierlein et al. 2003), although we are aware that at least some spiny stellates can have IB properties (Connors and Gutnick 1990). Our spiny stellates were modeled (because of the small size of these neurons) as if they were interneurons, in terms of conductance kinetics and compartmental structure, but with the surface area of dendritic compartments doubled to allow for the spines (Major 1992), and with $g_{K(M)}$ and $g_{K(AHP)}$ adjusted so that firing rate adaptation would occur (Fig. A3, Table A3), i.e., so that the cells were "RS." Note that the spike AHPs are <10 mV, consistent with Fig. 2*C* of Porter et al. (2001), but the AHP in the model neuron does have a small, fast component that is not present in Fig. 2*A* of Porter et al. (2001). The fast AHP in this model neuron is attributed in part to A current and can be reduced by diminishing the density of the A type of conductance (not shown). We have also developed an alternative RS stellate neuron model that uses principal cell g_{Na} and $g_{K(DR)}$ kinetics; and that

TABLE A5. *Membrane conductance densities for tufted RS pyramidal cells (mS/cm^2), by level in model structure*

Level	$g_{Na(F)}$	$g_{Na(P)}$	$g_{K(DR)}$	$g_{K(C)}$	$g_{K(A)}$	$g_{K(M)}$	g_{K2}	$g_{K(AHP)}$	$g_{Ca(L)}$	$g_{Ca(T)}$	g_{AR}
0	450	0	450	0	0.6	30	0.5	0	0	0	0
1	200	0.16	170	28.8	20	8.5	0.5	0.2	1.6	0.1	0.1
2	75	0.06	75	28.8	8	13.6	0.5	0.2	1.6	0.1	0.1
3	15	0.012	0	0.9	0.6	13.6	0.5	0.2	1.6	0.1	0.1
4	15	0.012	0	0.9	0.6	13.6	0.5	0.2	1.6	0.1	0.1
5	150	0.12	120	28.8	8	13.6	0.5	0.2	1.6	0.1	0.1
6	75	0.06	75	28.8	8	13.6	0.5	0.2	1.6	0.1	0.1
7	15	0.012	0	0.9	0.6	13.6	0.5	0.2	1.6	0.1	0.1
8	15	0.012	0	0.9	0.6	13.6	0.5	0.2	0.4	0.1	0.1
9	15	0.012	0	0.9	0.6	13.6	0.5	0.2	0.4	0.1	0.1
10	15	0.012	0	0.9	0.6	13.6	0.5	0.2	0.4	0.1	0.1
11	15	0.012	0	0.9	0.6	13.6	0.5	0.2	0.4	0.1	0.1
12	15	0.012	0	0.9	0.6	13.6	0.5	0.2	0.4	0.1	0.1
13	15	0.012	0	0.9	0.6	13.6	0.5	0.2	0.4	0.1	0.1
14	15	0.012	0	0.9	0.6	13.6	0.5	0.2	0.4	0.1	0.1
15	3	0.0024	0	2.16	0.6	4	0.5	0.2	0.4	0.1	0.1
16	3	0.0024	0	2.16	0.6	4	0.5	0.2	0.4	0.1	0.1
17	3	0.0024	0	2.16	0.6	4	0.5	0.2	0.4	0.1	0.1
18 prox	3	0.0024	0	2.16	0.6	4	0.5	0.2	1.08	0.1	0.2
18 dist	3	0.0024	0	2.16	0.6	4	0.5	0.2	0.24	0.1	0.2

Explanation of levels: level 0 = axon; level 1 = soma; level 2 = proximal basal and oblique dendrites; level 3 = middle basal and oblique dendrites; level 4 = distal basal and oblique dendrites; levels 5–17 = progressively more distal apical dendritic shaft; level 18 = apical tuft.

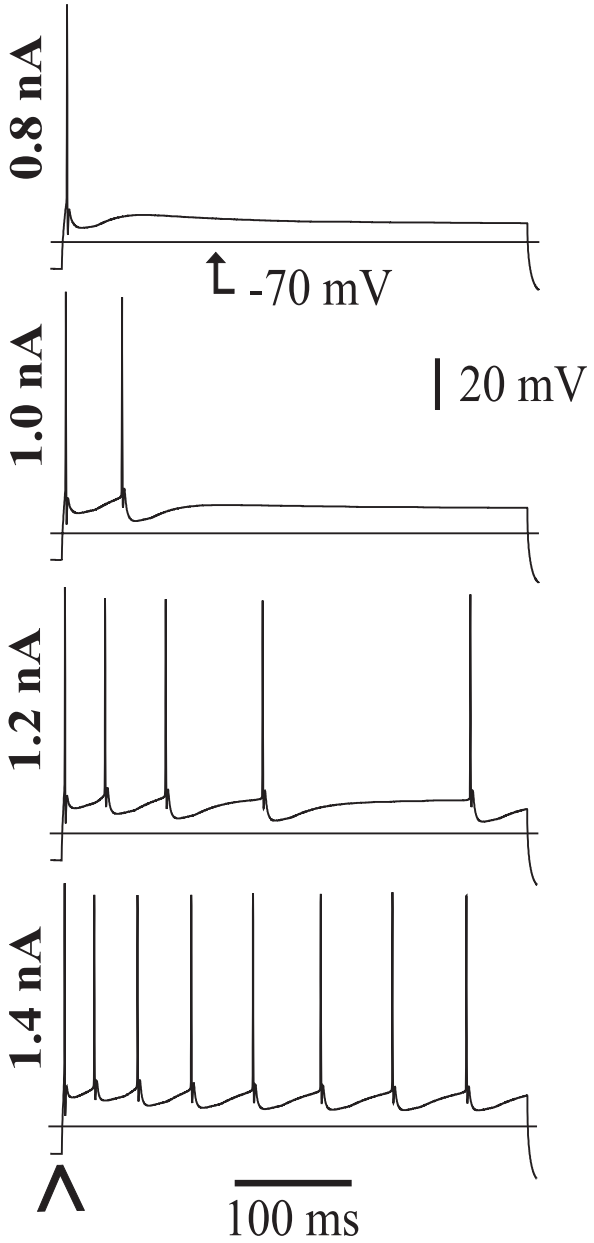

FIG. A5. RS firing behavior in another type of layer 5 tufted pyramidal neuron model used in our networks. Holding current was −0.4 nA.

uses comparable densitites of Na^+ channels between soma and axon, while shifting the axonal voltage-dependent rate functions on the voltage axis by 7 mV (Colbert and Pan 2002). The alternative model was not, however, used in the simulations reported here.

Layer 5 tufted IB pyramidal cell

Electrogenesis in these neurons is quite complex, in part attributed to the long tufted apical dendrite; to dendritic g_{Ca}, which permits slow depolarizations and dendritic bursts; and to complex voltage-dependent interactions along the length of the axonal/somatic/apical shaft/tuft axis (Kim and Connors 1993; Larkum and Zhu 2002; Larkum et al. 1999; Rhodes and Llinás 2001; Schiller et al. 1997; Stuart et al. 1997). Although bursting in these cells is g_{Ca}-dependent, the requisite calcium channels may be Ni^{2+} blockable, and thus high-threshold T channels (Williams and Stuart 1999); this possibility has also been suggested for high-threshold dendritic calcium spikes in TCR cells (Hughes et al. 2004). [In our model, however, dendritic bursting depends on high-threshold $g_{Ca(L)}$.] Sodium spikes in these cells favor apical dendritic bursts. Action potential amplitudes generally decrease during the course of the burst at soma, and each spike is initiated in the axon, in which there is no decrement of the amplitude (Williams and Stuart 1999). In our model as well, fast spikes are initiated in the axon (not shown). A burst of action potentials not only delivers more spikes to distal presynaptic terminals than does a single spike (Williams and Stuart 1999); in addition, a postsynaptic burst paired with a slightly delayed EPSP can unexpectedly lead to synaptic *depression*, as opposed to the potentiation that occurs when the EPSP is paired with a single spike (Birtoli and Ulrich 2004). Some of the complex physiology of calcium electrogenesis in the distal apical dendrite may be related to this phenomenon, along with the within-cell cooperativity between single somatic action potentials and apical EPSPs in eliciting slow dendritic calcium spikes.

The compartmental structure of the tufted pyramidal cell (also used for layer 5 RS pyramidal cells) is shown in Fig. A4. Dendritic lengths are as follows: soma to basal tips, 180 μm; apical shaft to apical

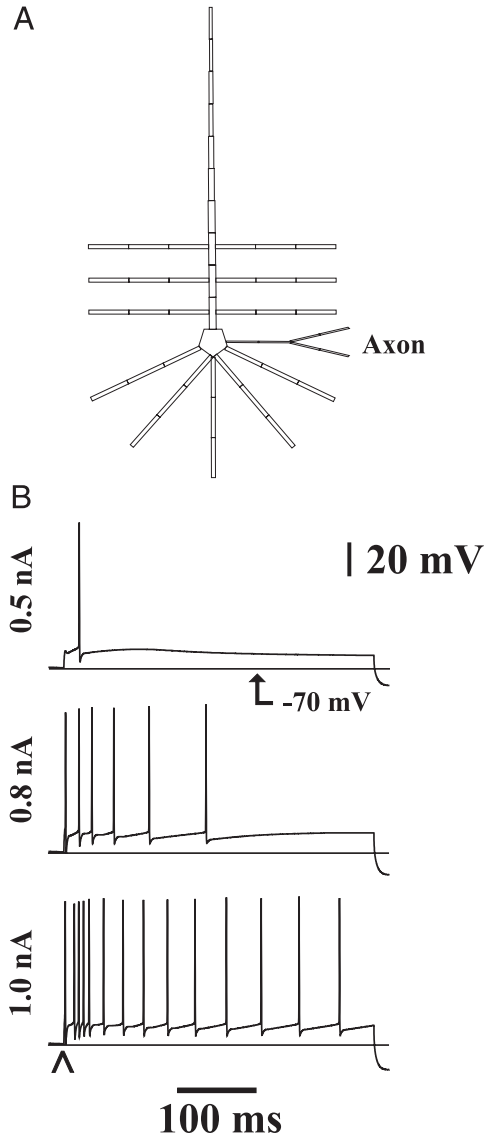

FIG. A6. Layer 6 nontufted pyramidal cell. *A*: compartmental architecture. *B*: RS firing behavior in response to depolarizing currents (onset at ^), holding current −0.25 nA. Note the tonic RS firing with 0.8-nA depolarizing current, and burst-tonic firing with 1.0-nA depolarizing current, firing patterns that have been described in rat layer 6 pyramidal cells (van Brederode and Snyder 1992).

TABLE A6. *Membrane conductance densities for nontufted RS pyramidal cells (mS/cm^2), by level in model structure*

Level	$g_{Na(F)}$	$g_{Na(P)}$	$g_{K(DR)}$	$g_{K(C)}$	$g_{K(A)}$	$g_{K(M)}$	g_{K2}	$g_{K(AHP)}$	$g_{Ca(L)}$	$g_{Ca(T)}$	g_{AR}
0	450	0	450	0	4	0	0.1	0	0	0	0
1	200	0.08	170	15	122.5	4.2	0.1	0.2	0.2	0.1	0.25
2	75	0.03	75	15	13.6	4.2	0.1	0.2	0.2	0.1	0.25
3	5	0.002	0	0	13.6	4.2	0.1	0.2	0.2	0.1	0.25
4	5	0.002	0	0	13.6	4.2	0.1	0.2	0.2	0.1	0.25
5	150	0.06	120	15	122.5	4.2	0.1	0.2	0.2	0.1	0.25
6	75	0.03	75	15	13.6	4.2	0.1	0.2	0.2	0.1	0.25
7	5	0.002	0	0	13.6	4.2	0.1	0.2	0.2	0.1	0.25
8	5	0.002	0	0	13.6	4.2	0.1	0.2	0.2	0.1	0.25
9	5	0.002	0	0	13.6	4.2	0.1	0.2	0.2	0.1	0.25
10	5	0.002	0	0	13.6	4.2	0.1	0.2	0.2	0.1	0.25
11	5	0.002	0	0	13.6	4.2	0.1	0.2	0.2	0.1	0.25
12	5	0.002	0	0	13.6	4.2	0.1	0.2	0.2	0.1	0.25
13	5	0.002	0	0	13.6	4.2	0.1	0.2	0.2	0.1	0.25
14	5	0.002	0	0	13.6	4.2	0.1	0.2	0.2	0.1	0.25

Explanation of levels: level 0 = axon; level 1 = soma; level 2 = proximal basal and oblique dendrites; level 3 = middle basal and oblique dendrites; level 4 = distal basal and oblique dendrites; levels 5–14 = progressively more distal apical dendrite.

oblique tips, 180 μm; apical trunk (soma to bifurcation at tuft), 975 μm; tuft bifurcation to tip of tuft, 240 μm.

Voltage-dependent conductance kinetics were as for superficial layer 2/3 pyramids, with the exception that $g_{K(A)}$ inactivation time constant, $\tau_h(V)$, was multiplied by 2.6. Conductance densities are listed in Table A4. That tufted IB cells have more apical calcium conductance than do tufted RS cells is consistent with data of Yuste et al. (1994).

As Fig.A4 shows, the model neuron can generate either single or multiple bursts in response to sufficiently large depolarizing current pulses. Sodium spikes attenuate with passage into the distal apical trunk, and slow calcium-dependent depolarizations can develop there. Figure A4 should be compared with Fig. 11 of Larkum et al. (2001). As a matter of detail, however, the potential at D2 peaks early and then declines with superimposed notches corresponding to somatic fast spikes, whereas in Larkum et al. (2001), the dendritic potential has a slowly rising envelope. Part of this difference in behavior may result from the fact that the somatic spikes in the model (unlike the experimental illustration) start to decline in amplitude after the first two.

Layer 5 tufted RS pyramidal cells

Not all tufted layer 5 pyramidal neurons are intrinsically bursting. Rather, at least some of them have RS firing properties (Markram et al. 1995; Williams and Stuart 1999). Our model used the same compartmental architecture as that for layer 5 tufted IB pyramids (see above), and usual $g_{K(A)}$ kinetics. The density of various conductances [particularly $g_{Ca(L)}$], however, was different between the 2 models (Table A5). RS firing behavior is shown in Fig. A5. The layer 5 tufted RS pyramidal neuron could be converted into an FRB neuron by increasing the density of $g_{Na(P)}$, and decreasing the density of $g_{K(C)}$ (not shown), but such models were not used in the present network.

Layer 6 nontufted RS pyramidal cell

Nontufted deep RS pyramidal cells have been electrophysiologically characterized and reconstructed by Mason and Larkman (1990) and Kang and Kayano (1994). In visual cortex, nontufted layer 5 RS pyramids include a subpopulation that projects through the corpus callosum, whereas the tufted IB pyramids projected to the superior colliculus (Kasper et al. 1994).

The structure of this type of model neuron is shown in Fig. A6, conductance densities are listed in Table A6, and RS firing is shown later in Fig. A6. Although our model uses such neurons in "layer 6," in fact there are many neurons of this sort in layer 5; our model is intended to resemble the structure of the cell in Fig. 4*B* of Mason and Larkman (1990). The basal dendrites extend 180 μm from the soma, the oblique dendrites 180 μm from the apical shaft, and the apical dendrite is 500 μm long. The kinetics of membrane conductances is as for layer 2/3 pyramidal cells (Traub et al. 2003).

This model neuron can be converted to one with FRB behavior by increasing the density of $g_{Na(P)}$, and blocking $g_{K(C)}$ (not shown). We did not use, in our network, deep FRB thalamus-projecting pyramidal cells, although such cells do exist in the cat (Steriade et al. 1998).

Thalamocortical relay (TCR) cell

These cells have multiple stubby dendrites and complex forms of electrogenesis, involving interactions between fast spikes, low-threshold calcium spikes (whose main conductance appears located in dendrites, but not distal dendrites; Destexhe et al. 1998; Williams and Stuart 2000), h current (hyperpolarization-activated current, or anomolous rectifier; McCormick and Pape 1990), and dendritic high-threshold calcium conductance (Hughes et al. 2004; Kammermeier and Jones 1997; Pedroarena and Llinás 1997). We included a dendritic high-threshold calcium conductance (Table A7), but did not explore particular firing behaviors dominated by

TABLE A7. *Membrane conductance densities for TCR cells (mS/cm^2), by level in model structure*

Level	$g_{Na(F)}$	$g_{Na(P)}$	$g_{K(DR)}$	$g_{K(C)}$	$g_{K(A)}$	$g_{K(M)}$	g_{K2}	$g_{K(AHP)}$	$g_{Ca(L)}$	$g_{Ca(T)}$	g_{AR}
0	400	0.8	180	0	1	0	0.5	0	0	0	0
1	100	0.2	33.75	12	6	0.5	2.0	0.05	0.5	0.5	0.25
2	100	0.2	22.5	12	6	0.5	2.0	0.05	0.5	5.0	0.50
3	5	0.01	0	20	0.2	0.5	2.0	0.05	0.25	3.0	0.3
4	5	0.01	0	20	0.2	0.5	2.0	0.05	0.25	0.5	0.3

Explanation of levels: level 0 = axon; level 1 = soma; levels 2–4 = progressively more distal dendrites.

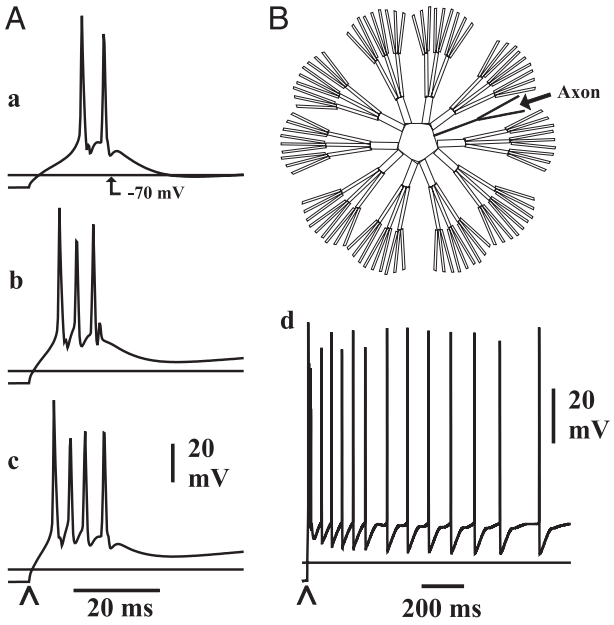

FIG. A7. Thalamocortical relay (TCR) cell. *A*: soma was held hyperpolarized with a −0.9 nA current. At ^, the current was switched to −0.3 nA (*a*), 0.1 nA (*b*), 0.3 nA (*c*), 0.5 nA (*d*; note different time scale). In *a*, *b*, and *c*, a low-threshold spike is evoked, with increasing numbers of superimposed fast action potentials. In *d*, a low-threshold spike occurs, followed by adapting tonic firing. Compare with Turner et al. (1997). *B*: compartmental structure. There are 10 stubby dendrites, each with 3 levels of branching.

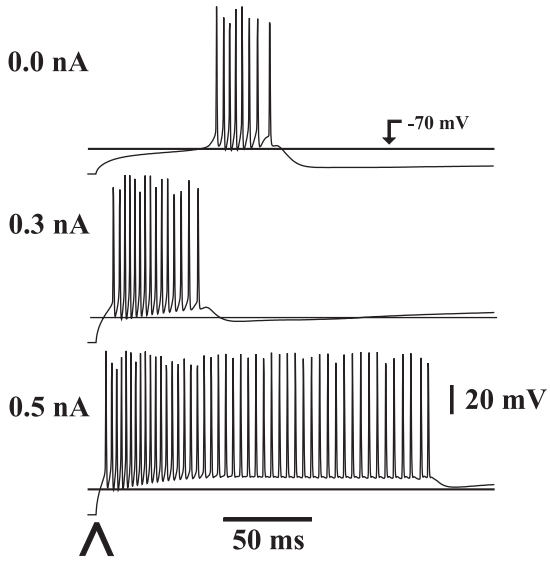

FIG. A8. Firing behavior of nucleus reticularis thalami (nRT) model cell. Cell was held with a −0.2 nA hyperpolarizing current, then stepped with the currents indicated. Broad low threshold spikes occur with superimposed fast action potentials. With 0.5 nA, there is a prolonged tail of tonic firing. Note the accelerando/decelerando pattern with steps to 0.0 and 0.3 nA. Compare Contreras et al. (1992).

it. For a review of some of the behavior of these cells see Steriade et al. (1997; chap. 5).

We used kinetics for the low-threshold calcium current (T current) derived from Destexhe et al. (1998), and for the h current derived from Huguenard and McCormick (1992).

The compartmental architecture and firing properties of the model TCR neuron are illustrated in Fig. A7. The model has 10 dendrites [compared with 11 in the study of Destexhe et al. (1998) in rat ventrobasal thalamus]. The length of one dendrite was 135 μm. [Compare firing properties with Turner et al. 1997, Fig. 9, as well as, for an in vivo study, Deschênes et al. (1984) and, for guinea pig in vitro, Jahnsen and Llinás (1984a,b).] The ability of model TCR and nRT neurons to participate in realistic-looking spindles is illustrated in the main text (Fig. 4).

Nucleus reticularis thalami (nRT) neuron

This cell model has the topological compartmental structure of an interneuron, but with longer dendrites than for FS and LTS cells (soma to distal dendritic tip = 600 μ). There are four primary dendrites. Interneuron rate functions are used for the kinetics of g_{Na}, $g_{K(DR)}$, and low-threshold $g_{Ca(T)}$. The rate functions for the latter are as in Destexhe et al. (1996; their p. 17)—motivated by the different kinetics, including slower inactivation—of this conductance in nRT cells compared with TCR cells (Huguenard and Prince 1992). We used

$$m_\infty = 1.0/\{1.0 + \exp[(-V - 52.0)/7.40]\}$$

$$h_\infty = 1.0/\{1.0 + \exp[(V + 80.0)/5.0]\}$$

$$\tau_m = 1.0 + 0.33/\{\exp[(V + 27.0)/10.0] + \exp[(-V - 102.0)/15.0]\}$$

$$\tau_h = 28.3 + 0.33/\{\exp[(V + 48.0)/4.0] + \exp[(-V - 407.0)/50.0]\}$$

The model nRT neuron does not exhibit intrinsic subthreshold 40 Hz (Pinault and Deschênes 1992), but does exhibit low-threshold bursts (with accelerando/decelerando pattern; Contreras et al. 1992, 1993), as well as tonic firing at depolarized membrane potentials (Fig. A8). It is interesting that the tonic firing in the model nRT neuron, in a state when T channels are relatively inactivated, resembles the tonic firing of Type II nRT cells (i.e., nonbursting nRT cells; cf. Fig. 2*B* of Contreras et al. 1992). Conductance densities are shown in Table A8.

TABLE A8. *Membrane conductance densities for nRT cells (mS/cm^2), by level in model structure*

Level	$g_{Na(F)}$	$g_{Na(P)}$	$g_{K(DR)}$	$g_{K(C)}$	$g_{K(A)}$	$g_{K(M)}$	g_{K2}	$g_{K(AHP)}$	$g_{Ca(L)}$	$g_{Ca(T)}$	g_{AR}
0	400	4.0	400	0	1	0	0.5	0	0	0	0
1	60	0.6	60	10	5	0.5	0.5	0.1	0.5	0.05	0.025
2	60	0.6	60	10	5	0.5	0.5	0.1	0.5	0.05	0.025
3	60	0.6	60	10	5	0.5	0.5	0.1	0.5	0.05	0.025
4	10	0.1	10	10	1	0.5	0.5	0.1	0.5	2	0.025
5	10	0.1	10	10	1	0.5	0.5	0.1	0.5	2	0.025
6	10	0.1	10	10	1	0.5	0.5	0.1	0.5	2	0.025
7	10	0.1	10	10	1	0.5	0.5	0.1	0.5	2	0.025
8	10	0.1	10	10	1	0.5	0.5	0.1	0.5	2	0.025
9	10	0.1	10	10	1	0.5	0.5	0.1	0.5	2	0.025

Explanation of levels: level 0 = axon; level 1 = soma; levels 2–9 = progressively more distal dendrites.

APPENDIX A REFERENCES

Amitai Y, Friedman A, Connors BW, and Gutnick MJ. Regenerative activity in apical dendrites of pyramidal cells in neocortex. *Cereb Cortex* 3: 26–38, 1993.

Bal T and McCormick DA. Mechanisms of oscillatory activity in guinea-pig nucleus reticularis thalami in vitro: a mammalian pacemaker. *J Physiol* 468: 669–691, 1993.

Beierlein M, Gibson JR, and Connors BW. Two dynamically distinct inhibitory networks in layer 4 of the neocortex. *J Neurophysiol* 90: 2987–3000, 2003.

Birtoli B and Ulrich D. Firing mode-dependent synaptic plasticity in rat neocortical pyramidal neurons. *J Neurosci* 24: 4935–4940, 2004.

Brumberg JC, Nowak LG, and McCormick DA. Ionic mechanisms underlying repetitive high-frequency burst firing in supragranular cortical neurons. *J Neurosci* 20: 4829–4843, 2000.

Colbert CM and Pan E. Ion channel properties underlying axonal action potential initiation in pyramidal neurons. *Nat Neurosci* 5: 533–538, 2002.

Connors BW and Gutnick MJ. Intrinsic firing patterns of diverse neocortical neurons. *Trends Neurosci* 13: 365–366, 1990.

Contreras D, Curró Dossi R, and Steriade M. Bursting and tonic discharges in two classes of reticular thalamic neurons. *J Neurophysiol* 68: 973–977, 1992.

Contreras D, Curró Dossi R, and Steriade M. Electrophysiological properties of cat reticular thalamic neurons in vivo. *J Physiol* 470: 273–294, 1993.

Cunningham MO, Whittington MA, Bibbig A, Roopun A, LeBeau FEN, Vogt A, Monyer H, Buhl EH, and Traub RD. A role for fast rhythmic bursting neurons in cortical gamma oscillations in vitro. *Proc Natl Acad Sci USA* 101: 7152–7157, 2004.

Deschênes M, Paradis M, Roy JP, and Steriade M. Electrophysiology of neurons of lateral thalamic nuclei in cat: resting properties and burst discharges. *J Neurophysiol* 51: 1196–1219, 1984.

Destexhe A, Contreras D, Steriade M, Sejnowski TJ, and Huguenard JR. In vivo, in vitro, and computational analysis of dendritic calcium currents in thalamic reticular neurons. *J Neurosci* 16: 169–185, 1996.

Destexhe A, Neubig M, Ulrich D, and Huguenard J. Dendritic low-threshold calcium currents in thalamic relay cells. *J Neurosci* 18: 3574–3588, 1998.

Dodge FA Jr and Cooley JW. Action potential of the motoneuron. *IBM J Res Dev* 17: 219–229, 1973.

Emri Z, Antal K, Tóth TI, Cope DW, and Crunelli V. Backpropagation of the δ oscillation and the retinal excitatory postsynaptic potential in a multi-compartment model of thalamocortical neurons. *Neuroscience* 98: 111–127, 2000.

French CR, Sah P, Buckett KJ, and Gage PW. A voltage-dependent persistent sodium current in mammalian hippocampal neurons. *J Gen Physiol* 95: 1139–1157, 1990.

Goldberg JH, Lacefield CO, and Yuste R. Global dendritic calcium spikes in mouse layer 5 low threshold spiking (LTS) interneurones: implications for control of pyramidal cell bursting. *J Physiol* 558: 465–478, 2004.

Gray CM and McCormick DA. Chattering cells: superficial pyramidal neurons contributing to the generation of synchronous oscillations in the visual cortex. *Science* 274: 109–113, 1996.

Hirsch JA. Synaptic integration in layer IV of the ferret striate cortex. *J Physiol* 483: 183–199, 1995.

Hughes SW, Lörincz M, Cope DW, Blethyn KL, Kékesi KA, Parri HR, Juhász G, and Crunelli V. Synchronized oscillations at α and θ frequencies in the lateral geniculate nucleus. *Neuron* 42: 1–20, 2004.

Huguenard JR, Coulter DA, and Prince DA. A fast transient potassium current in thalamic relay neurons: kinetics of activation and inactivation. *J Neurophysiol* 66: 1304–1315, 1991.

Huguenard JR and McCormick DA. Simulation of the currents involved in rhythmic oscillations in thalamic relay neurons. *J Neurophysiol* 68: 1373–1383, 1992.

Huguenard JR and Prince DA. A novel T-type current underlies prolonged Ca^{2+}-dependent burst firing in GABAergic neurons of rat thalamic reticular nucleus. *J Neurosci* 12: 3804–3817, 1992.

Jahnsen H and Llinás R. Electrophysiological properties of guinea-pig thalamic neurons: an in vitro study. *J Physiol* 349: 205–226, 1984a.

Jahnsen H and Llinás R. Ionic basis for the electroresponsiveness and oscillatory properties of guinea-pig thalamic neurons in vitro. *J Physiol* 349: 227–247, 1984b.

Kammermeier PJ and Jones SW. High-voltage-activated calcium currents in neurons acutely isolated from the ventrobasal nucleus of the rat thalamus. *J Neurophysiol* 77: 465–475, 1997.

Kang Y and Kayano F. Electrophysiological and morphological characteristics of layer VI pyramidal cells in the cat motor cortex. *J Neurophysiol* 72: 578–591, 1994.

Kasper EM, Larkman AU, Lübke J, and Blakemore C. Pyramidal neurons in layer 5 of the rat visual cortex. I. Correlation among cell morphology, intrinsic electrophysiological properties, and axon targets. *J Comp Neurol* 339: 459–474, 1994.

Kawaguchi Y. Physiological subgroups of nonpyramidal cells with specific morphological characteristics in layer II/III of rat frontal cortex. *J Neurosci* 15: 2638–2655, 1995.

Kay AR, Sugimori M, and Llinás R. Kinetic and stochastic properties of a persistent sodium current in mature guinea pig cerebellar Purkinje cells. *J Neurophysiol* 80: 1167–1179, 1998.

Kay AR and Wong RKS. Calcium current activation kinetics in pyramidal neurons of the CA1 region of the mature guinea pig hippocampus. *J Physiol* 392: 603–616, 1987.

Kim HG and Connors BW. Apical dendrites of the neocortex: correlation between sodium- and calcium-dependent spiking and pyramidal cell morphology. *J Neurosci* 13: 5301–5311, 1993.

Larkum ME, Kaiser KMM, and Sakmann B. Calcium electrogenesis in distal apical dendrites of layer 5 pyramidal cells at a critical frequency of back-propagating action potentials. *Proc Natl Acad Sci USA* 96: 14600–14604, 1999.

Larkum ME and Zhu JJ. Signaling of layer 1 and whisker-evoked Ca^{2+} and Na^{+} action potentials in distal and terminal dendrites of rat neocortical pyramidal neurons in vitro and in vivo. *J Neurosci* 22: 6691–7005, 2002.

Larkum ME, Zhu JJ, and Sakmann B. A new cellular mechanism for coupling inputs arriving at different cortical layers. *Nature* 398: 338–341, 1999.

Larkum ME, Zhu JJ, and Sakmann B. Dendritic mechanisms underlying the coupling of the dendritic with the axonal action potential initiation zone of adult rat layer 5 pyramidal neurons. *J Physiol* 533: 447–466, 2001.

Llinás RR, Grace AA, and Yarom Y. In vitro neurons in mammalian cortical layer 4 exhibit intrinsic oscillatory activity in the 10- to 50-Hz range. *Proc Natl Acad Sci USA* 88: 897–901, 1991.

Mainen ZE, Joerges J, Huguenard JR, and Sejnowski TJ. A model of spike initiation in neocortical pyramidal neurons. *Neuron* 15: 1427–1439, 1995.

Major G. *The Physiology, Morphology and Modeling of Cortical Pyramidal Neurons* (PhD thesis). Oxford, UK: Oxford Univ. Press, 1992.

Markram H., Helm PJ, and Sakmann B. Dendritic calcium transients evoked by single back-propagating action potentials in rat neocortical pyramidal neurons. *J Physiol* 485: 1–20, 1995.

Martina M and Jonas P. Functional differences in Na^{+} channel gating between fast-spiking interneurones and principal neurons of rat hippocampus. *J Physiol* 505: 593–603, 1997.

Martina M, Schultz JH, Ehmke H, Monyer H, and Jonas P. Functional and molecular differences between voltage-gated K^{+} channels of fast-spiking interneurons and pyramidal neurons of rat hippocampus. *J Neurosci* 18: 8111–8125, 1998.

Mason A and Larkman A. Correlations between morphology and electrophysiology of pyramidal neurons in slices of rat visual cortex. II. Electrophysiology. *J Neurosci* 10: 1415–1428, 1990.

McCormick DA, Connors BW, Lighthall JW, and Prince DA. Comparative electrophysiology of pyramidal and sparsely spiny stellate neurons of the neocortex. *J Neurophysiol* 54: 782–806, 1985.

McCormick DA and Huguenard JR. A model of the electrophysiological properties of thalamocortical relay neurons. *J Neurophysiol* 68: 1384–1400, 1992.

McCormick DA and Pape H-C. Properties of a hyperpolarization-activated cation current and its role in rhythmic oscillation in thalamic relay neurons. *J Physiol* 431: 291–318, 1990.

Mittman T, Linton SM, Schwindt P, and Crill W. Evidence for persistent Na^{+} current in apical dendrites of rat neocortical neurons from imaging of Na^{+}-sensitive dye. *J Neurophysiol* 78: 1188–1192, 1997.

Paré D and Lang EJ. Calcium electrogenesis in neocortical pyramidal neurons in vivo. *Eur J Neurosci* 10: 3164–3170, 1998.

Pedroarena C and Llinás R. Dendritic calcium conductances generate high-frequency oscillation in thalamocortical neurons. *Proc Natl Acad Sci USA* 94: 724–728, 1997.

Pinault D and Deschênes M. Voltage-dependent 40-Hz oscillations in rat reticular thalamic neurons in vivo. *Neuroscience* 51: 245–258, 1992.

Porter JT, Johnson CK, and Agmon A. Diverse types of interneurons generate thalamus-evoked feedforward inhibition in the mouse barrel cortex. *J Neurosci* 21: 2699–2710, 2001.

Rhodes PA and Llinás RR. Apical tuft input efficacy in layer 5 pyramidal cells from rat visual cortex. *J Physiol* 536: 167–187, 2001.

Schiller J, Schiller Y, Stuart G, and Sakmann B. Calcium action potentials restricted to distal apical dendrites of rat neocortical pyramidal neurons. *J Physiol* 505: 605–616, 1997.

Schubert D, Kötter R, Zilles K, Luhmann HJ, and Staiger JF. Cell type-specific circuits of cortical layer IV spiny neurons. *J Neurosci* 23: 2961–2970, 2003.

Steriade M, Jones EG, and McCormick DA. *Thalamus*. Amsterdam: Elsevier, 1997.

Steriade M, Timofeev I, Dürmüller N, and Grenier F. Dynamic properties of corticothalamic neurons and local cortical interneurons generating fast rhythmic (30–40 Hz) spike bursts. *J Neurophysiol* 79: 483–490, 1998.

Stuart G, Schiller J, and Sakmann B. Action potential initiation and propagation in rat neocortical pyramidal neurons. *J Physiol* 505: 617–632, 1997.

Tarczy-Hornoch K, Martin KA, Jack JJ, and Stratford KJ. Synaptic interactions between smooth and spiny neurons in layer 4 of cat visual cortex in vitro. *J Physiol* 508: 351–363, 1998.

Traub RD, Buhl EH, Gloveli T, and Whittington MA. Fast rhythmic bursting can be induced in layer 2/3 cortical neurons by enhancing Na^+ conductance or by blocking BK channels. *J Neurophysiol* 89: 909–921, 2003.

Turner JP, Anderson CM, Williams SR, and Crunelli V. Morphology and membrane properties of neurons in the cat ventrobasal thalamus in vitro. *J Physiol* 505: 707–726, 1997.

van Brederode JF and Snyder GL. A comparison of the electrophysiological properties of morphologically identified cells in layers 5B and 6 of the rat neocortex. *Neuroscience* 50: 315–357, 1992.

Williams SR and Stuart GJ. Mechanisms and consequences of action potential burst firing in rat neocortical pyramidal neurons. *J Physiol* 521: 467–482, 1999.

Williams SR and Stuart GJ. Action potential backpropagation and somatodendritic distribution of ion channels in thalamocortical neurons. *J Neurosci* 20: 1307–1317, 2000.

Yuste R, Gutnick MJ, Saar D, Delaney KR, and Tank DW. Ca^{2+} accumulations in dendrites of neocortical pyramidal neurons: an apical band and evidence for two functional compartments. *Neuron* 13: 23–43, 1994.

Zhang ZW and Deschênes M. Intracortical axonal projections of lamina VI cells of the primary somatosensory cortex in the rat: a single-cell labeling study. *J Neurosci* 17: 6356–6379, 1997.

APPENDIX B

Synaptic and gap junctional mechanisms and connectivity

The network model consisted of the following cell subpopulations: 1,000 superficial RS pyramids, 50 superficial FRB pyramids, 90 superficial basket cells, 90 superficial axoaxonic cells (Freund et al. 1983), 90 superficial LTS interneurons (Thomson and Deuchars 1997), 240 spiny stellates, 800 layer 5 tufted IB pyramids, 200 layer 5 tufted RS pyramids, 500 nontufted deep RS pyramids, 100 deep basket cells, 100 deep axoaxonic cells, 100 deep LTS interneurons, 100 TCR cells, and 100 nRT cells: 3,560 neurons in all. Of the model cortical neurons 19% are GABAergic, compared with the 21% figure given by Gabbott and Somogyi (1986) and 15% by Beaulieu (1993). O'Kusky and Colonnier (1982) reported approximately equal numbers of neurons in layers 1–3 as compared with layers 5–6, in monkey area 17; our model has somewhat more total neurons in layers 5–6 (1,800 neurons) than in layers 2–3 (1,320 neurons), although we used a far smaller proportion of layer 4 cells than are found in the highly specialized visual cortex (O'Kusky and Colonnier 1982).

Herein we describe the chemical synaptic and gap junctional communications within and between these subpopulations.

Reversal potentials for synaptic conductances

The reversal potential for AMPA and NMDA receptor-mediated conductances was 0 mV. We did not consider kainate receptor-mediated conductances separately because their time course—at least in some cortical neurons—is similar to the time course of AMPA conductances (Ali 2003), so that AMPA and kainate conductances could be lumped together. The $GABA_A$ reversal potential depended on cell type: it was −75 mV for GABAergic cells (Sanchez-Vives et al. 1997), spiny stellates, and deep pyramids; it was −81 mV for superficial pyramids and TCR neurons [the latter value being close to the −83 mV reported by Sanchez-Vives and McCormick (1997)].

Synaptic connectivity patterns

Here we list, for any particular cell type, the numbers of neurons of the cell type that provide synaptic input to neurons of that and of any other cell type. Synaptic connections are formed randomly, subject to the constraint that the number of synaptic inputs that a cell of type "*post*" receives from a cell of type "*pre*" is equal to the value given in the text below. From the number of inputs n that a cell of type *post* receives from a cell of type *pre*, one can calculate the connection probability P, for the *pre-to-post* connections: the total number of connections from the *pre* population to the *post* population = $n \times$ # *post cells.* The probability of a connection is then this total divided by the number of possible connections, which is # *pre cells* × # *post cells.* Thus $P = n/$# *pre cells.* [Actually, this provides only an estimate of P, because the above calculation assumes that the connections made onto a neuron are all from different cells, whereas the connection algorithm used in the simulation program does not follow this constraint; instead, it just picks presynaptic cells randomly, one by one, without checking to see whether the same cell has been picked more than once.]

INPUTS FROM SUPERFICIAL RS PYRAMIDS. A superficial RS pyramidal neuron receives synaptic input from 50 *superficial RS pyramidal neurons* (i.e., a 1/20 connection probability); a superficial FRB pyramidal neuron receives input from 50 superficial RS pyramidal neurons; a superficial basket cell, a superficial axoaxonic cell, and a superficial LTS interneuron each receive input from 90 superficial RS pyramidal neurons (about 1/11 connection probability); a spiny stellate cell receives input from 3 superficial RS pyramidal neurons [a small number according to Thomson and Bannister (2003) and Gottlieb and Keller (1997)]; a tufted IB pyramid and a tufted RS pyramid each receive input from 60 superficial RS pyramids (about 1/16 connection probability); deep basket, axoaxonic, and LTS interneurons each receive input from 30 superficial RS pyramids; each nontufted RS pyramid receives input from 3 superficial RS pyramids. TCR and nRT cells are not contacted by superficial RS pyramids. Thomson and Deuchars (1997) found a connection probability of 1/4 to 1/21 for layer 2/3 → layer 2/3 pyramidal cell connections, and between 1/4 and 1/11 for layer 2/3 → layer 5 pyramidal cell connections; the connection probability, within-layer, for pyramidal → interneuron connections, was between 1/3 and 1/10.

INPUTS FROM SUPERFICIAL FRB PYRAMIDS. A superficial RS pyramidal neuron receives synaptic input from 5 *superficial FRB pyramidal neurons*; a superficial FRB pyramidal neuron receives input from 5 superficial FRB pyramidal neurons; a superficial basket cell, a superficial axoaxonic cell, and a superficial LTS interneuron each receive input from 5 superficial FRB pyramidal neurons; a spiny stellate cell receives input from one superficial FRB pyramidal neuron [a small number according to Thomson and Bannister (2003)]; a tufted IB pyramid and a tufted RS pyramid each receive input from 3 superficial FRB pyramids; deep basket, axoaxonic, and LTS interneurons each receive input from 3 superficial FRB pyramids; each nontufted RS pyramid receives input from one superficial FRB pyramid. TCR and nRT cells are not contacted by superficial FRB pyramids.

INPUTS FROM SUPERFICIAL BASKET CELLS. A superficial RS pyramid or FRB pyramid receives input from 20 superficial baskets (about 1/5 connection probability); superficial basket, axoaxonic, and LTS

interneurons each receive input from 20 superficial baskets; a spiny stellate cell receives input from 20 superficial baskets. [According to Tamás et al. (1997), almost all boutons of layer 2/3 basket cells, in visual cortex, lie in layer 2/3. These authors estimated that, in vitro, 23–40 basket cells converge on a layer 2/3 pyramidal cell.] Thomson and Deuchars (1997) found, for local within-layer interneuron → pyramidal cell connections, a probability of 1/2.5 to 1/5.

INPUTS FROM SUPERFICIAL AXOAXONIC CELLS. A superficial RS pyramid or FRB pyramid receives input from 20 superficial axoaxonic cells; a spiny stellate cell receives input from 5 superficial axoaxonic cells; tufted IB and RS pyramids, and nontufted RS pyramids, each receive input from 5 superficial axoaxonic cells (Somogyi et al. 1982). Note that axoaxonic cells do not contact interneurons (Buhl et al. 1994), and that axoaxonic cells do contact at least some spiny stellate cells (Saint Marie and Peters 1985).

INPUTS FROM SUPERFICIAL LTS INTERNEURONS. Each of the following sorts of cell receives input from 20 LTS interneurons: all cortical glutamatergic cells and all cortical GABAergic cells. Salin and Prince (1996b) provide functional evidence for cross-laminar projections of at least some interneurons, probably including dendrite-contacting interneurons: IPSCs evoked by stimulation at a distance from the soma (e.g., in layer 1) were often slower than IPSCs evoked by near-soma stimulation. Kim et al. (1995) provide evidence that layer 2/3 interneurons (not necessarily LTS interneurons) contact the dendrites of layer 5 pyramidal cells.

INPUTS FROM LAYER 4 SPINY STELLATE CELLS. Each spiny stellate cell receives input from 30 spiny stellate cells, giving a connection probability of 1/8. [Fleidervish et al. (1998) estimated a connection probability of 3.75% for spiny stellate/spiny stellate connections, in mouse barrel cortex, whereas Lübke et al. (2003) estimated that—in juvenile rat barrel cortex in vivo—a single layer 4 spiny stellate receives input from about 200 other layer 4 spiny stellates. Beierlein et al. (2003) reported a connection probability of 6% between layer 4 RS cells in rat barrel cortex in vitro.] All other cortical glutamatergic cells, and all cortical GABAergic cells, each receive input from 20 spiny stellates. [Note that the axons of layer 4 glutamatergic cells extend through all cortical layers, within a given column (Lübke et al. 2000). In addition, Lübke et al. (2003) estimate that—again, in juvenile rat barrel cortex in vivo—a single layer 2/3 pyramid receives input from 300 to 400 layer 4 spiny stellates. The discrepancies between model parameters and in vivo data result in part from the relatively small total number of spiny stellates in the model.]

INPUTS FROM TUFTED IB PYRAMIDS. Superficial pyramids (RS, FRB) each receive input from 2 tufted IB pyramids. Each tufted IB pyramid receives input from 50 tufted IB pyramids. [Thus the connection probability between tufted IB pyramids was 6.25%; the connection probability for pairs of tufted layer 5 pyramids (whether IB or RS was not stated), within 50 μm of each other, was 10% in the study of Markram et al. (1997).] Each tufted RS pyramid, each spiny stellate cell, and each nontufted RS pyramid receives input from 20 tufted IB pyramids. All cortical GABAergic cells receive input from 20 tufted IB pyramids.

INPUTS FROM TUFTED RS PYRAMIDS. Superficial pyramids (RS, FRB) each receive input from 2 tufted RS pyramids. Each tufted RS pyramid receives input from 10 tufted RS pyramids. Spiny stellates, tufted IB pyramids, and nontufted RS pyramids each receive input from 20 tufted RS pyramids. All cortical GABAergic cells receive input from 20 tufted RS pyramids.

INPUTS FROM NONTUFTED RS PYRAMIDS. The following cells each receive 10 inputs from nontufted RS pyramids: superficial pyramids (RS, FRB); tufted pyramids (RS, IB); spiny stellates (according to Tarczy-Hornoch et al. 1999); all cortical GABAergic neurons. The following cells each receive 20 inputs from nontufted RS pyramids: nontufted RS pyramids, TCR cells, nRT cells (Gentet and Ulrich 2004).

INPUTS FROM DEEP BASKET CELLS. The following cells each receive input from 20 deep basket cells: spiny stellates, tufted pyramids (RS, IB), deep nontufted RS pyramids, deep interneurons (basket, axoaxonic, LTS). [Note that White et al. (1994) found, with ultrastructural methods, that layer 5 IB and RS cells had similar perisomatic synaptology.]

INPUTS FROM DEEP AXOAXONIC CELLS. All cortical glutamatergic cells receive inputs from 5 deep axoaxonic cells (Somogyi et al. 1982).

INPUTS FROM DEEP LTS INTERNEURONS. Each superficial pyramid (RS and FRB) and superficial GABAergic cell (basket, axoaxonic, LTS interneuron) receives input from 10 deep LTS interneurons. Spiny stellates, tufted pyramids (RS, IB), nontufted RS pyramids, and deep GABAergic cells (basket, axoaxonic, LTS interneuron) receive input from 20 deep LTS interneurons.

INPUTS FROM THALAMOCORTICAL RELAY (TCR) CELLS. Each nRT cell receives input from 40 TCR cells. The following cells each receive input from 10 TCR cells: superficial pyramids (RS, FRB), superficial basket and axoaxonic cells, tufted pyramids (RS, IB), nontufted RS pyramids, deep axoaxonic cells. [Note that there is direct evidence that lateral geniculate neurons synapse onto spiny layer 6 neurons (Bannister et al. 2002). In addition, it is the case that in rat barrel cortex, the TCR → axoaxonic (chandelier) pathway is actually rather weak (Zhu et al. 2004).] Each of the following cells receives input from 20 TCR cells: spiny stellates, deep baskets. LTS interneurons do not receive input from TCR cells (Gibson et al. 1999). [Note that, in vivo in mouse barrel cortex, a spiny stellate cell was estimated to have 43 thalamocortical synapses (Segev et al. 1995). In addition, the model has more spiny stellate inputs—to a given spiny stellate cell—than it has TCR inputs (Stratford et al. 1996).]

INPUTS FROM NUCLEUS RETICULARIS (NRT) CELLS. TCR cells each receive input from 30 nRT cells; nRT cells each receive input from 10 nRT cells. Nucleus reticularis synaptic interconnections are axodendritic; we did not include dendrodendritic synaptic interactions (Pinault et al. 1997). Liu and Jones (1999) did not observe such synapses in rat nucleus reticularis.

Regions of neurons synaptically contacted by the various presynaptic neurons

The postsynaptic compartments where synaptic connections may form are shown in Figs. B1 to B10. Each synaptic connection, from *cell 1* (of whatever type) to *cell 2* (of whatever type), involves exactly one postsynaptic compartment. Connections made by axoaxonic interneurons must go to principal cell initial segments. For other sorts of connections (e.g., for connections between subpopulation A and subpopulation B) additional postsynaptic compartments can be forced into the network, if necessary, by increasing the density of the appropriate connections from A-cells to B-cells, and by making corresponding reductions in the appropriate unitary synaptic conductances.

[*Comparisons with data*: we did not include tufted pyramid connections to the tufts of other tufted pyramids, although such connections seem to exist (Feldmeyer and Sakmann 2000). We placed connections from superficial pyramids to layer 5 cells on the apical shaft, as in Reyes and Sakmann (1999), although we did not include the connections onto oblique layer 5 cell dendrites that were described in that paper.]

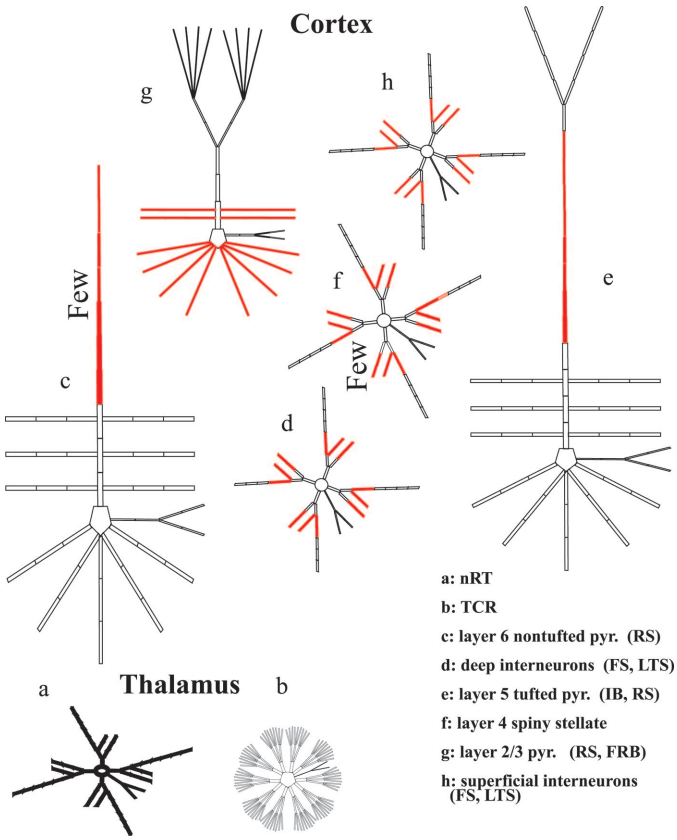

FIG. B1. Cells and membrane regions thereof to which superficial (layer 2/3) pyramidal cells (RS and FRB) deliver synaptic excitation. Contacted regions are shown in red. Note that superficial pyramids contact the basal and oblique dendrites of each other, and that there are few connections to spiny stellates and to layer 6 pyramids. There is, however, a projection to the apical trunks of layer 5 tufted pyramids.

Kinetics of unitary synaptic conductances, baseline conductance scaling constants, and rescaling in particular simulations

First, we shall consider the general form of unitary synaptic conductances. Following that, we shall list the values of the scaling conductance constants.

AMPA conductances have the time course: $c \times t \times e^{-t/\tau(\mathrm{AMPA})}$, where c is the conductance scaling constant, t is time in ms after arrival of a presynaptic spike at the terminal, and τ(AMPA) is a parameter. The program actually constructs c as a product of 2 terms; we shall explain how this is done, so that people looking into the actual code will be able to make sense of it. First, the program constructs a table of "baseline" conductance scaling constants. Later, some or all of the baseline constants are multiplied by an additional factor. This device makes it easier to "rescale" groups of scaling constants together: for example, one might want to reduce all $GABA_A$ conductances by a fixed factor, or scale all the thalamocortical conductances together. It will therefore be necessary to list all the baseline conductance scaling constants, along with at least some of the usual additional scaling factors. Note also, that the AMPA conductance is maximum when $t = \tau$(AMPA), and therefore the peak AMPA conductance takes a value of $c \times \tau$(AMPA)/e.

τ(AMPA) takes on the following values:

- 0.8 ms for pyramidal cell → FS cell, and spiny stellate → FS cell connections.
- 1.0 ms for pyramidal cell → LTS cell, and TCR cell → FS cell connections. [Note that TCR cells do not connect to LTS interneurons (Gibson et al. 1999).]
- 2.0 ms for pyramidal cell → pyramidal cell, pyramidal cell → spiny stellate, spiny stellate → pyramidal cell, spiny stellate → spiny stellate; TCR cell → pyramidal cell, spiny stellate, and nRT cell; layer 6 pyramidal cells → TCR cells. [Note that, at least in hippocampus, AMPA conductances have a faster time course in interneurons than in pyramidal cells (Geiger et al. 1997), and we have followed that principle here.]

NMDA conductances have the time course: $c \times g(V, [Mg^{2+}]) \times S(t)$; here, c is a conductance scaling constant, as above; g is a function of membrane potential V, and $[Mg^{2+}]_o$, taking values between 0 and 1, and corresponding to the voltage and magnesium dependence of the NMDA conductance (Jahr and Stevens 1990) (without, however, taking into account the kinetics of this dependency; the dependency is assumed to be instantaneous); and $S(t)$ is the time-dependent portion of the ligand-gated conductance. This general scheme is the same as was used in an earlier publication (Traub et al. 1994). The form of the function g, for various values of $[Mg^{2+}]_o$, is shown in Fig. B11. $S(t)$ rises linearly with time, from 0 to 1, over the time interval 0 to 5 ms; $S(t)$ then decays exponentially with time constant τ_{NMDA}. In a few simulations, we set $g \equiv 1$; that is, we removed the voltage and magnesium dependence of the NMDA conductance.

τ_{NMDA} takes on the following values as defaults:

- 150 ms for TCR → nRT connections.
- 130 ms for pyramidal → pyramidal (Flint et al. 1997), pyramidal → spiny stellate, spiny stellate → pyramidal, spiny stellate → spiny stellate (with some exceptions), TCR → pyramidal, TCR → spiny stellate, layer 6 pyramids → TCR connections.
- 100 ms for pyramidal and spiny stellates → FS and LTS interneurons; and TCR cells → FS interneurons. [At least in hippocampus, NMDA conductances are briefer in interneurons than in pyramidal cells (Perouansky and Yaari 1993).]

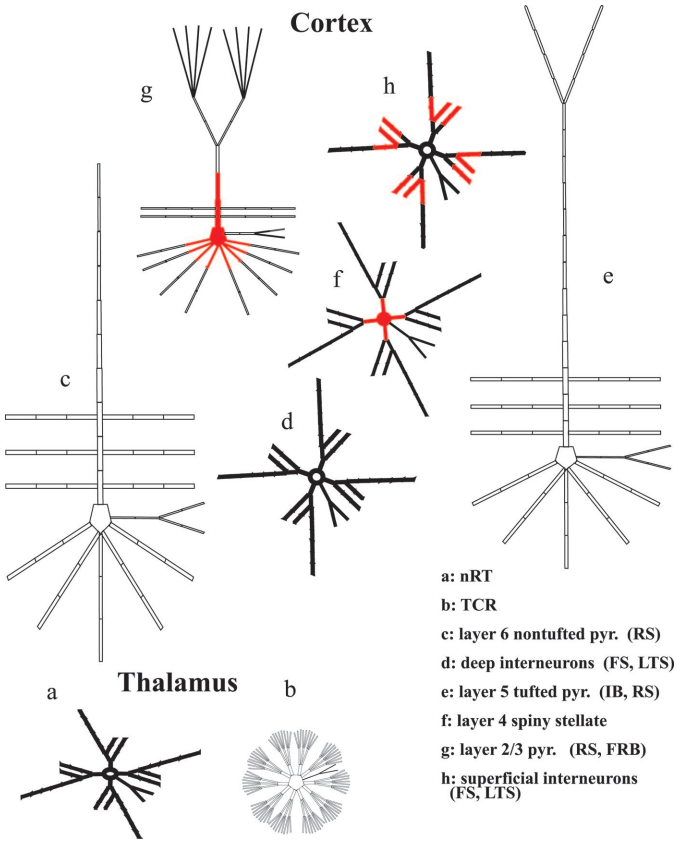

FIG. B2. Cells and membrane regions thereof to which superficial basket cells connect. All connections are to superficial pyramids and interneurons, and to spiny stellates. Contacted regions are shown in red.

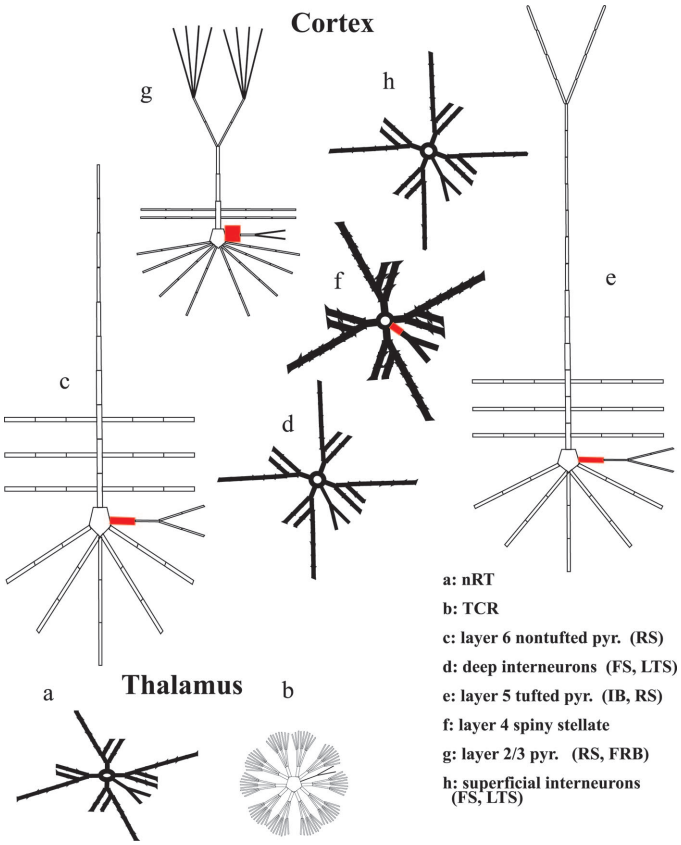

FIG. B3. Cells and membrane regions to which superficial and deep axoaxonic (chandelier) interneurons connect. These interneurons contact the axon initial segment of all cortical principal (glutamatergic) cell types (i.e., pyramidal cells and spiny stellates), but do not contact interneurons. Contact regions are shown in red. Connection probabilities for superficial and deep axoaxonic interneurons are different (see APPENDIX B text).

$GABA_A$ conductances have the time course $c \times e^{-t/\tau(\mathrm{GABA})}$ for all inhibitory connections except those made by nRT neurons. These latter have 2 decay time constants, so that the time course is $c_1 \times e^{-t/\tau(\mathrm{GABA\text{-}fast})} + c_2 \times e^{-t/\tau(\mathrm{GABA\text{-}slow})}$. τ_{GABA} takes on the following values:

- 6 ms for FS → pyramidal cell or spiny stellate connections.
- 3 ms for basket cell → cortical interneuron connections (note that axoaxonic cells do not contact interneurons) [in fact, in the dentate gyrus, GABA conductances in interneurons can relax with a time constant as short as 1.8 ms (Bartos et al. 2001)].
- 20 ms for LTS interneuron → all cortical cells. [Here, we are assuming that dendritic IPSCs have a longer time course than do perisomatic IPSCs, as is the case in hippocampus (Miles et al. 1996).]

Note that Salin and Prince (1996) estimated a value of τ_{GABA} of 8 ms for principal cells in somatosensory cortex slices, at a holding potential of 0 mV; but they also found τ_{GABA} to be voltage-dependent, increasing with depolarization. Xiang et al. (2002) found equivalent decay time constants for LTS and FS cell-induced IPSCs in layer 5 visual cortex pyramids, but these data may be difficult to interpret, based as they are on voltage-clamp experiments in very large neurons. We used a slower time constant for dendritic IPSC decay than for perisomatic IPSC decay, following observations in piriform cortex pyramidal cells (Kapur et al. 1997).

- $\tau_{\mathrm{GABA(fast)}}$ is 3.3 ms at nRT → TCR connections, and 9 ms at nRT → nRT connections.
- $\tau_{\mathrm{GABA(slow)}}$ is 10 ms at nRT → TCR connections, and 44.5 ms at nRT → nRT connections (Huntsman and Huguenard 2000).

Values of "baseline" synaptic conductance scaling factors (nS)

Conductances for most of the possible synaptic connections are not known experimentally. We generally chose initial values in the range 0.25 to 3.0 nS, and then made adjustments after observing firing patterns in initial simulations. It is also the case that synaptic conductances vary under particular experimental conditions, and possibly in different behavioral states, under the influence of neuromodulators. For example, connections between pyramidal cells can be quite powerful in vitro in physiological bathing media, but population EPSPs during kainate-induced gamma oscillations tend to be small in pyramidal cells (Cunningham et al. 2004a). Synaptic conductances are also time-varying and heterogeneous over different connections, but we used time-invariant and nonheterogeneous values (for the most part).

For AMPA

- Connections made by superficial (layer 2/3) pyramids (RS and FRB): to other superficial pyramids (RS and FRB), 0.25 nS; to superficial FS cells, 3 nS; to superficial LTS cells, 2 nS; to spiny stellates, 0.1 nS; to tufted pyramids (layer 5, RS and IB), 0.1 nS; to deep interneurons (FS and LTS), 1.0 nS; to layer 6 nontufted pyramids, 0.5 nS.
- Connections made by layer 4 spiny stellates: to superficial pyramids, 1.0 nS; to superficial interneurons, 1.0 nS; to other spiny stellates, 1.0 nS; to deep pyramids and interneurons, 1.0 nS.

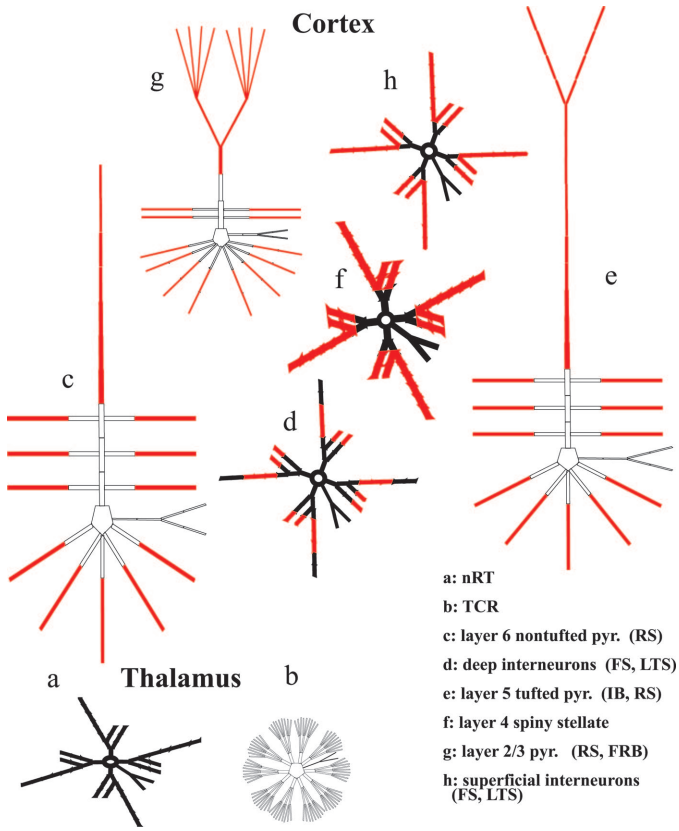

FIG. B4. Cells and membrane regions thereof to which superficial and deep LTS interneurons connect (shown in red). These interneurons contact dendritic regions of cortical principal cells and interneurons [although LTS/LTS connections have been reported to be rare, at least in layer 4 (Beierlein et al. 2003)].

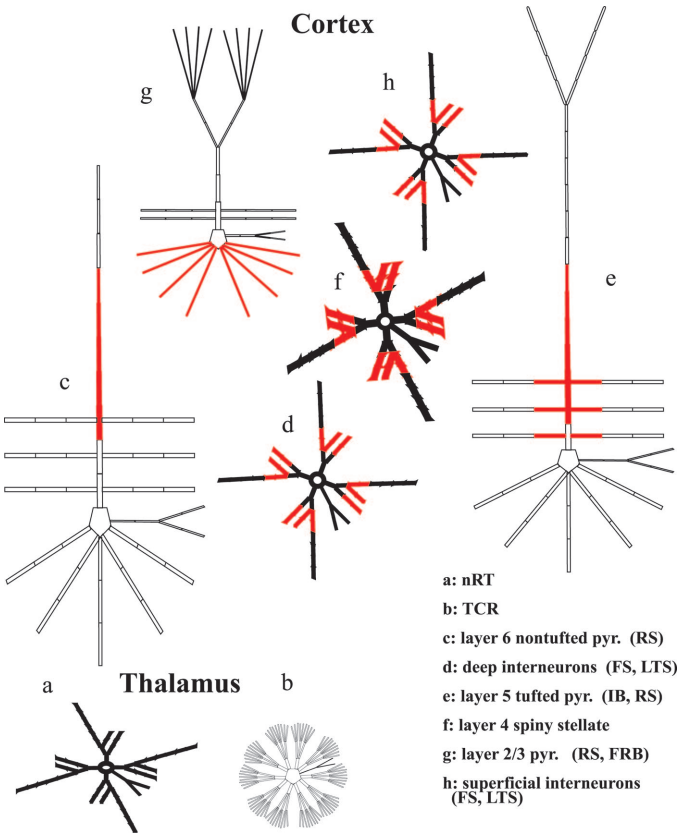

FIG. B5. Cells and membrane regions thereof to which layer 4 spiny stellate cells connect. These cells contact all types of cortical neurons, including each other. Connections to layer 2/3 pyramids are on basal dendrites (Feldmeyer et al. 2002).

Many of these conductances are then "rescaled" (see following text).

- Connections made by layer 5 tufted IB cells: to superficial pyramids, 0.5 nS; to superficial interneurons, 1.0 nS; to spiny stellates, 0.5 nS; to other tufted cells (IB and RS), 2.0 nS; to deep FS cells, 3 nS; to deep LTS cells, 2.0 nS; to layer 6 nontufted pyramids, 2 nS. [Markram et al. (1997) estimated a mean conductance of 3 nS for connections between nearby tufted layer 5 pyramids in 14- to 16-day- old rat somatosensory cortex. Notably, EPSP size at these mutual interconnections was quite variable, 0.15 to 5.5 mV, and estimated quantal peak conductance was 1.5 to 5.5 nS; however, we used a constant value of conductance for pyramid → pyramid connections.]
- Connections made by layer 5 tufted RS cells: to superficial pyramids, 0.5 nS; to superficial interneurons, 1.0 nS; to spiny stellates, 0.5 nS; to layer 5 tufted pyramids (RS and IB), 1.0 nS; to deep FS cells, 3.0 nS; to deep LTS cells, 2.0 nS; to layer 6 nontufted pyramids, 1.0 nS.
- Connections made by layer 6 nontufted RS pyramids: to superficial pyramids, 0.5 nS; to superficial FS cells, 1.0 nS; to spiny stellates, 0.5 nS; to tufted layer 5 pyramids (IB and RS), 1.0 nS; to deep FS cells, 3.0 nS; to deep LTS cells, 2.0 nS; to other layer 6 nontufted pyramids, 1.0 nS; to TCR cells, 0.75 nS; to nRT cells, 0.5 nS. [Note, however, that nRT model cells have a higher input resistance (71 MΩ, measured with all active conductances blocked) than do model TCR cells (59 MΩ). Nevertheless, physiological measurements indicate a greater disparity than in the model for nRT cortically evoked EPSPs, as compared with TCR cortically evoked EPSPs, the nRT EPSPs being significantly larger (Golshani et al. 2001).]
- Connections made by TCR cells: to superficial pyramids, 0.5 nS; to superficial FS cells, 0.1 nS; to spiny stellates, 1.0 nS; to layer 5 tufted pyramids (IB and RS), 1.5 nS; to deep basket cells, 1.5 nS; to deep axoaxonic cells, 1.0 nS; to layer 6 nontufted pyramids, 1.0 nS; to nRT cells, 0.75 nS (a large value for these "tight" cells; Gentet and Ulrich 2003). Note that the major pathway for feedforward inhibition from the thalamus is by deep FS cells, which in the present model includes the population of layer 4 FS cells. [Note that the unitary TCR/spiny stellate conductance has been estimated to be 0.5 nS peak (Segev et al. 1995), smaller than we used.]

For NMDA

- Connections made by superficial (layer 2/3) RS pyramids: to superficial pyramids (RS and FRB), 0.025 nS; to superficial interneurons, 0.15 nS; to spiny stellates, 0.01 nS; to deep tufted pyramids, 0.01 nS; to deep FS cells, 0.1 nS; to deep LTS interneurons, 0.15 nS; to deep nontufted RS pyramids, 0.05 nS. (However, note the significant rescaling of most NMDA conductances below.)
- Connections made by superficial (layer 2/3) FRB pyramids: to superficial pyramids (RS and FRB), 0.025 nS; to superficial interneurons, 0.1 nS; to spiny stellates, 0.01 nS; to tufted deep pyramids, 0.01 nS; to deep interneurons, 0.1 nS; to deep nontufted pyramids, 0.05 nS.
- Connections made by spiny stellates: to superficial pyramids (RS and FRB), 0.1 nS; to superficial interneurons, 0.15 nS; to other spiny stellates, 0.1 nS; to deep pyramids (tufted and nontufted), 0.1 nS; to deep interneurons, 0.15 nS.
- Connections made by layer 5 tufted IB pyramids: to superficial pyramids (RS and FRB), 0.05 nS; to superficial interneurons,

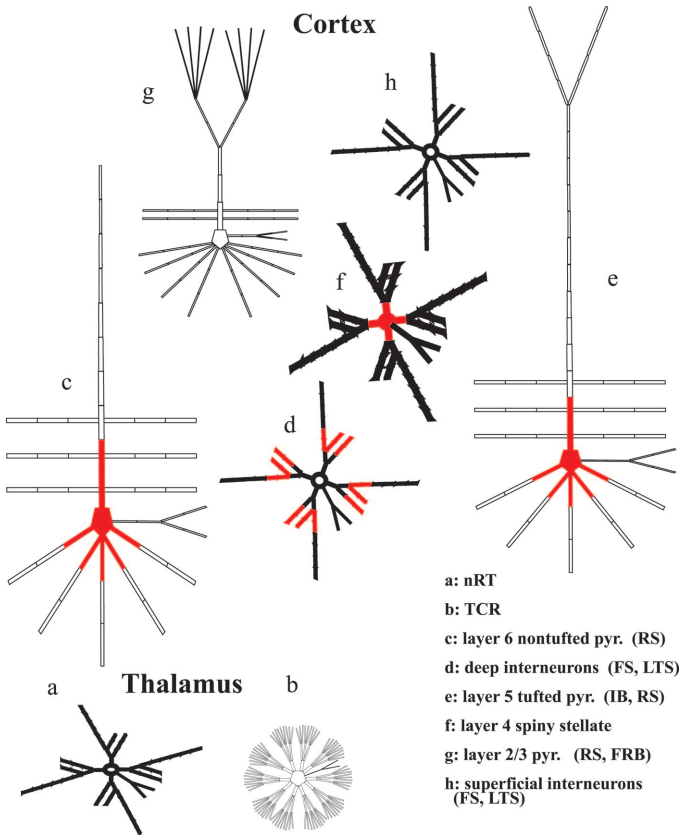

FIG. B6. Cells and membrane regions thereof to which deep basket cells connect. These cells contact perisomatic regions of deep pyramidal neurons and spiny stellates, as well as deep interneurons.

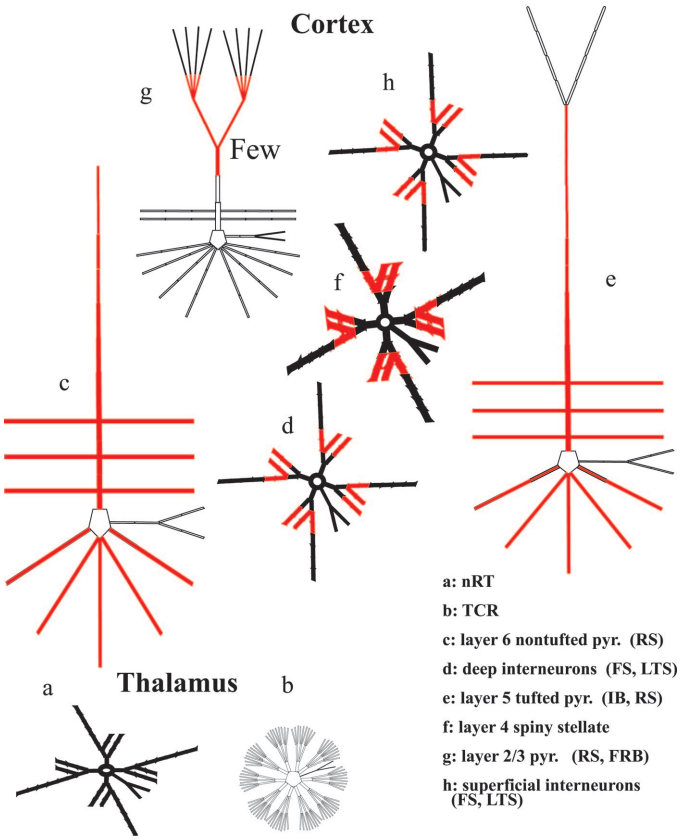

FIG. B7. Cells and membrane regions thereof to which deep (layer 5) tufted pyramidal cells (IB and RS) connect. These cells contact dendrites of each other and of layer 6 nontufted pyramids, dendrites of spiny stellates and deep and superficial interneurons, a few superficial pyramids.

0.15 nS; to spiny stellates, 0.05 nS; to deep pyramids (tufted and nontufted), 0.2 nS; to deep interneurons, 0.15 nS.

- Connections made by layer 5 tufted RS pyramids: to superficial pyramids (RS and FRB), 0.05 nS; to superficial interneurons, 0.15 nS; to spiny stellates, 0.05 nS; to deep pyramids (tufted and nontufted), 0.1 nS; to deep interneurons, 0.1 nS.
- Connections made by layer 6 nontufted pyramids: to superficial pyramids (RS and FRB), 0.05 nS; to superficial baskets, 0.1 nS; to spiny stellates, 0.05 nS; to tufted and nontufted pyramids, 0.1 nS; to deep interneurons, 0.1 nS; to TCR cells, 0.075 nS; to nRT cells, 0.05 nS.
- Connections made by TCR cells: to superficial pyramids (RS and FRB), 0.05 nS; to superficial FS cells, 0.01 nS; to spiny stellates, 0.1 nS; to layer 5 tufted pyramids (RS and IB), 0.15 nS; to deep FS cells, 0.1 nS; to layer 6 nontufted pyramids, 0.1 nS; to nRT cells, 0.15 nS.

For $GABA_A$

- Connections made by superficial basket cells: to superficial (layer 2/3) pyramids, 1.2 nS; to other superficial basket cells, 0.2 nS; to superficial axoaxonic cells, 0.2 nS; to superficial LTS interneurons, 0.5 nS; to spiny stellates, 0.1 nS. [It is possible that the IPSC conductance in LTS interneurons should have been smaller than in basket cells, rather than the reverse (Bacci et al. 2003). Salin and Prince (1996a) observed spontaneous IPSC amplitudes of about 0.5 nS in principal somatosensory cortex neurons, a smaller value than we used for unitary connections.]
- Connections made by superficial axoaxonic cells: to superficial-(layer 2/3) pyramids, 1.2 nS; to spiny stellates, 0.1 nS; to deep pyramids (tufted and nontufted), 1.0 nS.
- Connections made by superficial LTS interneurons: to superficial pyramids, 0.01 nS; to superficial FS cells, 0.01 nS; to superficial LTS cells, 0.05 nS; to spiny stellates, 0.01 nS; to tufted pyramids, 0.02 nS; to deep FS cells, 0.01 nS; to deep LTS cells, 0.05 nS; to nontufted deep pyramids, 0.01 nS.
- Connections made by deep basket cells: to spiny stellates, 1.5 nS; to tufted pyramids, 0.7 nS; to deep FS cells, 0.2 nS; to deep LTS cells, 0.7 nS; to deep nontufted pyramids, 0.7 nS.
- Connections made by deep axoaxonic cells: to superficial pyramids, 1.0 nS; to spiny stellates, 1.5 nS, to deep pyramids (tufted and nontufted), 1.0 nS.
- Connections made by deep LTS cells: to superficial pyramids, 0.01 nS; to superficial FS cells, 0.01 nS; to superficial LTS cells, 0.05 nS; to spiny stellates, 0.01 nS; to tufted IB pyramids, 0.05 nS; to tufted RS pyramids, 0.02 nS; to deep FS cells, 0.01 nS; to deep LTS cells, 0.05 nS; to deep nontufted pyramids, 0.01 nS.
- Connections made by nRT cells: to TCR cells, 0.7 to 2.1 nS (uniformly, randomly distributed); to nRT cells, 0.3 nS. The heterogeneity in nRT → TCR connections follows Cox et al. (1997).

"Rescaling" of baseline synaptic conductances

As mentioned above, the program first constructs tables of the baseline synaptic conductance constants (as just listed), but then—depending on the simulation—the program multiplies subsets of the conductance factors by "rescaling" factors. Thus for example, the thalamic portion of the network can be disconnected from the cortex by setting all AMPA and NMDA conductances in thalamocortical connections to 0. Picrotoxin is simulated by multiplicative scaling of

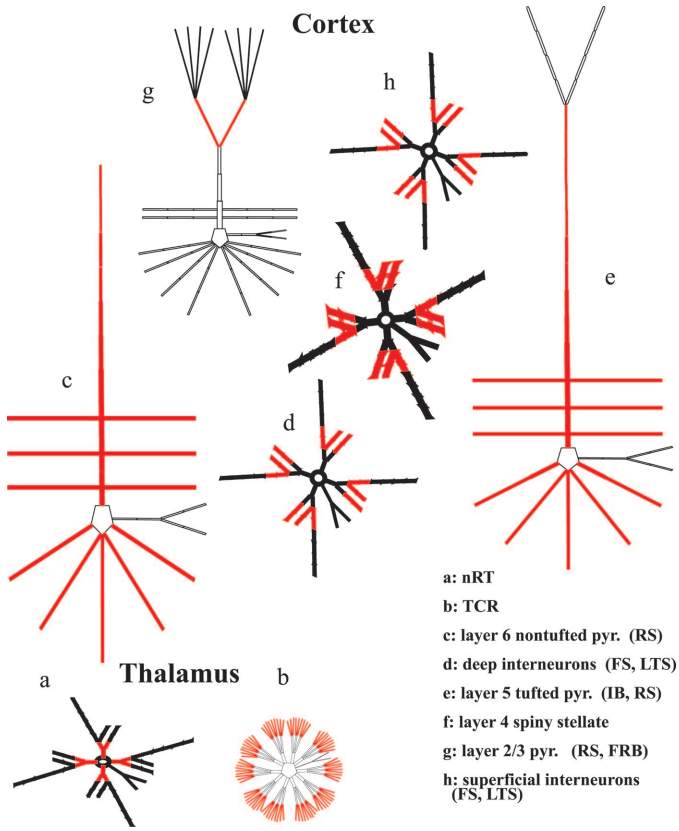

FIG. B8. Cells and membrane regions thereof to which layer 6 nontufted pyramids connect. These cells contact similar portions of cortical neurons as do layer 5 tufted pyramids, and portions of the apical dendrites of layer 2/3 pyramids. In addition, layer 6 nontufted pyramids contact the proximal dendrites of nRT neurons and the distal dendrites of TCR neurons.

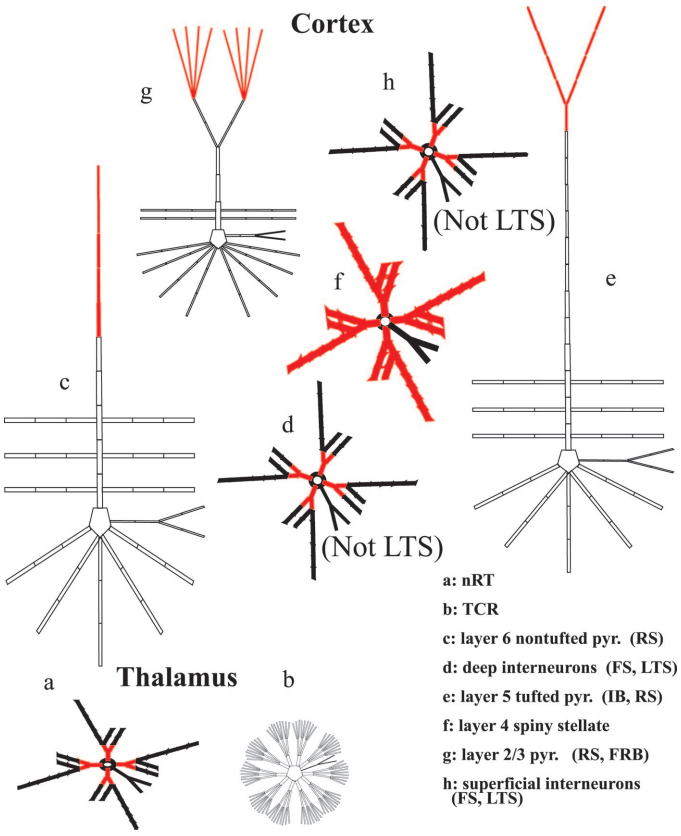

FIG. B9. Cells and membrane regions thereof to which TCR neurons connect. These cells contact primarily the proximal dendrites of nRT neurons and the dendrites of layer 4 spiny stellate neurons. In addition, they contact cortical FS neurons [although there is evidence in barrel cortex that thalamic afferents do not contact axoaxonic interneurons (Beierlein et al. 2003)], and they contact distal dendrites of cortical pyramids, including the tufts of layer 5 tufted pyramids.

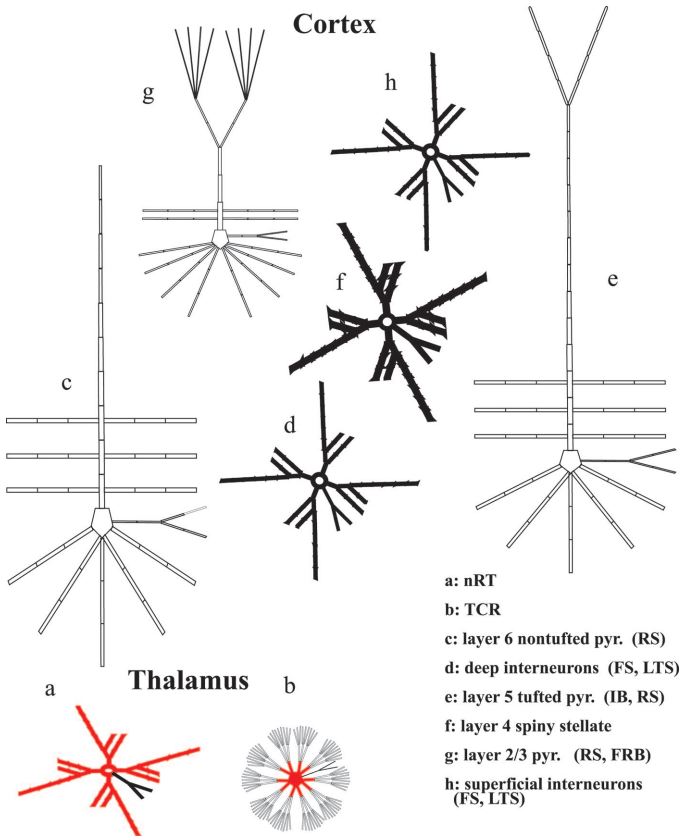

FIG. B10. nRT neurons contact dendritic regions of each other, and also the somata and proximal dendrites of TCR neurons (Liu et al. 1995).

all $GABA_A$ conductances, either in cortex alone, or in cortex plus thalamus. AMPA conductances at spiny stellate → spiny stellate connections are set to "low" or "high" values, by multiplying the baseline conductance by 0.25 or 2.0, respectively. In most simulations, all other AMPA conductances are twice the baseline values. Likewise, in most simulations, NMDA conductances to cortical interneurons are multiplied by 0.2, as are NMDA conductances on nRT cells and TCR cells; cortical principal cell (pyramids and spiny stellates) have NMDA conductances multiplied by 2.5. Other rescalings are performed as described in the main text.

Combining synaptic conductances

For a given compartment on a given neuron, and a particular type of synaptic input (e.g., AMPA), synaptic inputs from different presynaptic neurons simply add together linearly. There is a possibility in the program to allow for saturation of NMDA receptors, to avoid having the program generate huge postsynaptic conductances.

Synaptic plasticity is not included in this model. In particular, we did not include, in this first version, the many known effects of short-term depression and facilitation (Feldmeyer et al. 2002; Thomson 1997; Thomson and West 2003). Such effects could well be important during epileptogenesis, given the high firing rates.)

Patterns of electrical coupling

CORTICAL INTERNEURONS. Cortical FS interneurons are densely electrically coupled with each other, as are LTS interneurons (Galarreta and Hestrin 1999; Gibson et al. 1999; Venance et al. 2000), with the coupling site mainly dendrodendritic (Fukuda and Kosaka 2003; Tamás et al. 2000), and coupling conductances estimated in the range of about 0.6 to 1.6 nS [with Fukuda and Kosaka (2003) estimating even higher values of 2.1–5.3 nS]. In the model, we used gap junctions between superficial baskets [average 4.44 per neuron, vs. an average of 5.3 per parvalbumin positive interneuron in Fukuda and Kosaka (2003)], between superficial LTS cells (average 4.44 per neuron), between deep baskets (average 5 per neuron), and between deep LTS cells (average 5 per neuron)—but not between axoaxonic cells. Interneuron gap junctions could be placed on any of 8 compartments in the dendrites, and all had a conductance of 1.0 nS. These gap junctions were included in the model because of evidence that they stabilize and enhance coherence of gamma oscillations (Buhl et al. 2003; Hormuzdi et al. 2001; Traub et al. 2001).

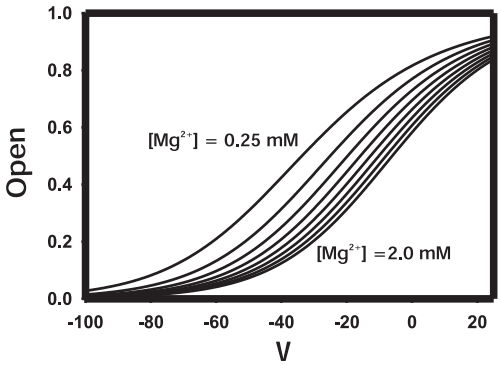

FIG. B11. Fractional opening ["Open" = $g(V, [Mg^{2+}]_o)$] of model NMDA channels as a function of transmembrane potential (abscissa, V) and of $[Mg^{2+}]_o$. Curves are drawn for 0.25-mM steps in $[Mg^{2+}]_o$, from 0.25 to 2.0 mM. Function used is from *Eq. 4A* and Table 1 of Jahr and Stevens (1990); see also Fig. 3 of Traub et al. (1994). Default $[Mg^{2+}]_o$ in the model is 1.5 mM.

CORTICAL PYRAMIDAL CELLS AND SPINY STELLATES. Hippocampal pyramidal cells appear to be electrically coupled, and dye coupled, by their axons (Schmitz et al. 2001). Experimental and modeling evidence furthermore suggests that this type of coupling is necessary for persistent gamma oscillations to occur, both in hippocampus in vitro (Traub et al. 2003) and superficial layers of neocortex in vitro (Cunningham et al. 2004a). Persistent gamma oscillations in entorhinal cortex are also suppressed by carbenoxolone (Cunningham et al. 2004b). Supporting evidence that principal neocortical cells (including spiny stellates) are electrically coupled comes from the observation of spikelets in pyramidal neurons (Cunningham et al. 2004a,b; Deschênes 1981), the staining through layers 2–6 for a putative gap junctional mRNA pannexin2 (Bruzzone et al. 2003; Cunningham et al. 2004a); and the existence of dye coupling between cortical neurons (including pyramidal and stellate), in both superficial and deep layers, with coupling occurring between neurons at similar depths (Gutnick et al. 1985). We therefore placed axonal gap junctions between layer 2/3 pyramidal cells (average 1.44 RS/RS junctions per RS axon, 0.16 FRB/FRB junctions per FRB axon; 0.75 RS/FRB junctions per FRB axon); between spiny stellate cells, average 2 gap junctions per axon; between tufted IB cells, 0.875 per axon; between tufted RS cells, 3.5 per axon; between tufted IB/tufted RS pairs, 0.1 per tufted RS axon; and between nontufted (layer 6) RS axons, average 2 per axon. These gap junctions were not always open in each simulation, however. When gap junctions were open, the conductance was 3.0 nS for layer 2/3 pyramids, 3.0 nS for spiny stellates, and 4.0 nS for deep (layers 5 and 6) pyramids.

NRT CELLS. These GABAergic cells are also electrically coupled (Landisman et al. 2001). We placed an average of 5 gap junctions per cell in the dendrites of nRT cells, each with a conductance of 1 nS.

THALAMOCORTICAL RELAY CELLS. TCR cells are dye coupled and show electrophysiological evidence of being electrically coupled (Hughes et al. 2002 2004). We made the guess that the requisite gap junctions were dendritic because slow, putatively Ca^{2+}-mediated spikes appear as small slow "spikelets" in TCR cells (Fig. 7 of Hughes et al. 2004). In the model, at this stage, TCR gap junctions were usually closed.

All gap junctions in the model had conductances that were voltage-independent and nonrectifying.

AXON CONDUCTION DELAYS. Within the cortical column, and within the nRT/TCR pool, we ignored axon conduction delays. A conduction delay of 1 ms was imposed on thalamocortical connections (Agmon and Connors 1992), and of 5 ms on corticothalamic connections (Gentet and Ulrich 2004). [Note that, in vivo, axonal conduction from cortex to thalamus is much slower than in the reverse direction (Steriade et al. 1990).]

AXON REFRACTORINESS. Axons were not permitted to send spikes to their respective presynaptic terminals at intervals of <1.5 ms.

RANDOM "ECTOPIC" AXONAL ACTION POTENTIALS. The axons of glutamatergic cells generated random action potentials, by independent Poisson processes, usually with mean intervals of 10 s (superficial pyramids) and 1 s (all other glutamatergic neurons, including TCR cells) (see also Cunningham et al. 2004a; Traub et al. 2003).

ESTIMATION OF EXTRACELLULAR FIELDS. We estimated extracellular potentials at depths of 1 and 2 mm, using landmarks for cortical layers in rat auditory cortex (HL), based on a rat brain atlas (Paxinos and Watson 1986). In Plate 23 of that atlas, the approximate thicknesses of the cortical layers were as follows: layer 1: 300 μ; layer 2/3: 1,100 μ; layer 4: 300 μ; layer 5: 400 μ; layer 6: 800 μ. Transmembrane ionic currents were used to estimate fields, using only currents in basal dendrites, soma, and apical dendrites (not oblique dendrites), and only from pyramidal cells: superficial ones and tufted and nontufted pyramids. Any one type of pyramid was assumed to lie at a fixed depth, and homologous compartments were also assumed to lie at the same depth. Thus a defined depth was assigned to each relevant compartment of each type of pyramidal cell. All of the transmembrane currents were then added up, weighted by the inverse distance from the site of "recording." (Thus the resistivity of the extracellular space is assumed constant.) We did not use a specific value for the extracellular resistivity, so that the present fields are without units. When fields at 2 distinct depths are shown, they are plotted on the same scale, for consistency.

APPENDIX B REFERENCES

Agmon A and Connors BW. Correlation between intrinsic firing patterns and thalamocortical synaptic responses of neurons in mouse barrel cortex. *J Neurosci* 12: 319–329, 1992.

Ali AB. Involvement of postsynaptic kainate receptors during synaptic transmission between unitary connections in rat neocortex. *Eur J Neurosci* 17: 2344–2350, 2003.

Bacci A, Rudolph U, Huguenard JR, and Prince DA. Major differences in inhibitory synaptic transmission onto two neocortical interneuron subclasses. *J Neurosci* 23: 9664–9674 2003.

Bannister NJ, Nelson JC, and Jack JJ. Excitatory inputs to spiny cells in layers 4 and 6 of striate cortex. *Philos Trans R Soc Lond B Biol Sci* 357: 1793–1808, 2002.

Bartos M, Vida I, Frotscher F, Geiger JRP, and Jonas P. Rapid signaling at inhibitory synapses in a dentate gyrus interneuron network. *J Neurosci* 21: 2687–2698, 2001.

Beaulieu C. Numerical data on neocortical neurons in adult rat, with special reference to the GABA population. *Brain Res* 609: 284–292, 1993.

Beierlein M, Gibson JR, and Connors BW. Two dynamically distinct inhibitory networks in layer 4 of the neocortex. *J Neurophysiol* 90: 2987–3000, 2003.

Browne SH, Kang J, Akk G, Chiang LW, Schulman H, Huguenard JR, and Prince DA. Kinetic and pharmacological properties of $GABA_A$ receptors in single thalamic neurons and $GABA_A$ subunit expression. *J Neurophysiol* 86: 2312–2322, 2001.

Bruzzone R, Hormuzdi SG, Barbe MT, Herb A, and Monyer H. Pannexins, a family of gap junction proteins expressed in brain. *Proc Natl Acad Sci USA* 100: 13644–13649, 2003.

Buhl DL, Harris KD, Hormuzdi SG, Monyer H, and Buzsáki G. Selective impairment of hippocampal gamma oscillations in connexin-36 knock-out mouse in vivo. *J Neurosci* 23: 1013–1018, 2003.

Buhl EH, Han Z-S, Lörinczi Z, Stezhka VV, Karnup SV, and Somogyi P. Physiological properties of anatomically identified axo-axonic cells in the rat hippocampus. *J Neurophysiol* 71: 1289–1307, 1994.

Cox CL, Huguenard JR, and Prince DA. Nucleus reticularis neurons mediate diverse inhibitory effects in thalamus. *Proc Natl Acad Sci USA* 94: 8854–8859, 1997.

Cunningham MO, Halliday DM, Davies CH, Traub RD, Buhl EH, and Whittington MA. Coexistence of gamma and high-frequency oscillations in the medial entorhinal cortex in vitro. *J Physiol* 559: 347–353, 2004b.

Cunningham MO, Whittington MA, Bibbig A, Roopun A, LeBeau FEN, Vogt A, Monyer H, Buhl EH, and Traub RD. A role for fast rhythmic bursting neurons in cortical gamma oscillations in vitro. *Proc Natl Acad Sci USA* 101: 7152–7157, 2004a.

Deschênes M. Dendritic spikes induced in fast pyramidal tract neurons by thalamic stimulation. *Exp Brain Res* 43: 304–308, 1981.

Eder M, Becker K, Rammes G, Schierloh A, Azad SC, Zieglgänsberger W, and Dodt H-U. Distribution and properties of functional postsynaptic kainate receptors on neocortical layer V pyramidal neurons. *J Neurosci* 23: 6660–6670, 2003.

Feldmeyer D, Egger V, Lübke J, and Sakmann B. Reliable synaptic connections between pairs of excitatory layer 4 neurons within a single "barrel" of developing rat somatosensory cortex. *J Physiol* 521: 169–190, 1999.

Feldmeyer D, Lübke J, Silver RA, and Sakmann B. Synaptic connections between layer 4 spiny neuron-layer 2/3 pyramidal cell pairs in juvenile rat barrel cortex: physiology and anatomy of interlaminar signaling within a cortical column. *J Physiol* 538: 803–822, 2002.

Feldmeyer D and Sakmann B. Synaptic efficacy and reliability of excitatory connections between the principal neurons of the input (layer 4) and output layer (layer 5) of the neocortex. *J Physiol* 525: 31–39, 2000.

Fleidervish IA, Binshtok AM, and Gutnick MJ. Functionally distinct NMDA receptors mediate horizontal connectivity within layer 4 of mouse barrel cortex. *Neuron* 21: 1055–1065, 1998.

Flint AC, Maisch US, Weishaupt JH, Kriegstein AR, and Monyer H. NR2A subunit expression shortens NMDA receptor synaptic currents in developing neocortex. *J Neurosci* 17: 2469–2476, 1997.

Freund TF, Martin KAC, Smith AD, and Somogyi P. Glutamate decarboxylase-immunoreactive terminals of Golgi-impregnated axoaxonic cells and of presumed basket cells in synaptic contact with pyramidal neurons of the cat's visual cortex. *J Comp Neurol* 221: 263–278, 1983.

Fukuda T and Kosaka T. Ultrastructural study of gap junctions between dendrites of parvalbumin-containing GABAergic neurons in various neocortical areas of the adult rat. *Neuroscience* 120: 5–20, 2003.

Gabbott PL and Somogyi P. Quantitative distribution of GABA-immunoreactive neurons in the visual cortex (area 17) of the cat. *Exp Brain Res* 61: 323–331, 1986.

Galarreta M and Hestrin S. A network of fast-spiking cells in the neocortex connected by electrical synapses. *Nature* 402: 72–75, 1999.

Geiger JRP, Lübke J, Roth A, Frotscher M, and Jonas P. Submillisecond AMPA receptor-mediated signaling at a principal neuron-interneuron synapse. *Neuron* 18: 1009–1023, 1997.

Gentet LJ and Ulrich D. Strong, reliable and precise synaptic connections between thalamic relay cells and neurons of the nucleus reticularis in juvenile rats. *J Physiol* 546: 801–811, 2003.

Gentet LJ and Ulrich D. Electrophysiological characterization of synaptic connections between layer VI cortical cells and neurons of the nucleus reticularis thalami in juvenile rats. *Eur J Neurosci* 19: 625–633, 2004.

Gibson JR, Beierlein M, and Connors BW. Two networks of electrically coupled inhibitory neurons in neocortex. *Nature* 402: 75–79, 1999.

Golshani P, Liu XB, and Jones EG. Differences in quantal amplitude reflect GluR4-subunit number at corticothalamic synapses on two populations of thalamic neurons. *Proc Natl Acad Sci USA* 98: 4172–4177, 2001.

Gottlieb JP and Keller A. Intrinsic circuitry and physiological properties of pyramidal neurons in rat barrel cortex. *Exp Brain Res* 115: 47–60, 1997.

Gutnick MJ, Lobel-Yaakov R, and Rimon G. Incidence of neuronal dye-coupling in neocortical slices depends on the plane of section. *Neuroscience* 15: 659–666, 1985.

Gutnick MJ and Prince DA. Dye coupling and possible electrotonic coupling in the guinea pig neocortical slice. *Science* 211: 67–70, 1981.

Hormuzdi SG, Pais I, LeBeau FEN, Towers SK, Rozov A, Buhl EH, Whittington MA, and Monyer H. Impaired electrical signaling disrupts gamma frequency oscillations in connexin 36-deficient mice. *Neuron* 31: 487–495, 2001.

Hughes SW, Blethyn KL, Cope DW, and Crunelli V. Properties and origin of spikelets in thalamocortical neurons in vitro. *Neuroscience* 110: 395–401, 2002.

Huntsman MM and Huguenard JR. Nucleus-specific differences in $GABA_A$-receptor-mediated inhibition are enhanced during thalamic development. *J Neurophysiol* 83: 350–358, 2000.

Jahr CE and Stevens CF. Voltage dependence of NMDA-activated macroscopic conductances predicted by single-channel kinetics. *J Neurosci* 10: 3178–3182, 1990.

Kapur A, Pearce RA, Lytton WW, and Haberly LB. $GABA_A$-mediated IPSCs in piriform cortex have fast and slow components with different properties and locations on pyramidal cells. *J Neurophysiol* 78: 2531–2545, 1997.

Kim HG, Beierlein M, and Connors BW. Inhibitory control of excitable dendrites in neocortex. *J Neurophysiol* 74: 1810–1814, 1995.

Landisman CE, Long MA, Beierlein M, Deans MR, Paul DL, and Connors BW. Electrical synapses in the thalamic reticular nucleus. *J Neurosci* 22: 1002–1009, 2002.

Liu X-B and Jones EG. Predominance of corticothalamic synaptic inputs to thalamic reticular nucleus neurons in the rat. *J Comp Neurol* 414: 67–79, 1999.

Liu X-B, Warren RA, and Jones EG. Synaptic distribution of afferents from reticular nucleus in ventroposterior nucleus of cat thalamus. *J Comp Neurol* 352: 187–202, 1995.

Lübke J, Egger V, Sakmann B, and Feldmeyer D. Columnar organization of dendrites and axons of single and synaptically coupled excitatory spiny neurons in layer 4 of the rat barrel cortex. *J Neurosci* 20: 5300–5311, 2000.

Lübke J, Roth A, Feldmeyer D, and Sakmann B. Morphometric analysis of the columnar innervation domain of neurons connecting layer 4 and layer 2/3 of juvenile rat barrel cortex. *Cereb Cortex* 13: 1051–1063, 2003.

Markram H, Lübke J, Frotscher M, Roth A, and Sakmann B. Physiology and anatomy of synaptic connections between thick tufted pyramidal neurons in the developing rat neocortex. *J Physiol* 500: 409–440, 1997.

Miles R, Tóth K, Gulyás AI, Hajos N, and Freund TF. Differences between somatic and dendritic inhibition in the hippocampus. *Neuron* 16: 815–823, 1996.

O'Kusky J and Colonnier M. A laminar analysis of the number of neurons, glia, and synapses in the adult cortex (area 17) of adult macaque monkeys. *J Comp Neurol* 210: 278–290, 1982.

Paxinos G and Watson C. *The Rat Brain in Stereotaxic Coordinates*. Orlando, FL: Academic Press, 1986.

Perouansky M and Yaari Y. Kinetic properties of NMDA receptor-mediated synaptic currents in rat hippocampal pyramidal cells versus interneurones. *J Physiol* 465: 223–244, 1993.

Pinault D, Smith Y, and Deschênes M. Dendrodendritic and axoaxonic synapses in the thalamic reticular nucleus of the adult rat. *J Neurosci* 17: 3215–3233, 1997.

Reyes A and Sakmann B. Developmental switch in the short-term modification of unitary EPSPs evoked in layer 2/3 and layer 5 pyramidal neurons of rat neocortex. *J Neurosci* 19: 3827–3835, 1999.

Saint Marie SL and Peters A. The morphology and synaptic connections of spiny stellate neurons in monkey visual cortex (area 17): a Golgi-electron microscopic study. *J Comp Neurol* 233: 213–235, 1985.

Salin PA and Prince DA. Spontaneous $GABA_A$ receptor-mediated inhibitory currents in adult rat somatosensory cortex. *J Neurophysiol* 75: 1573–1588, 1996a.

Salin PA and Prince DA. Electrophysiological mapping of $GABA_A$ receptor-mediated inhibition in adult rat somatosensory cortex. *J Neurophysiol* 75: 1573–1588, 1996b.

Sanchez-Vives MV, Bal T, and McCormick DA. Inhibitory interactions between perigeniculate GABAergic neurons. *J Neurosci* 17: 8894–8908, 1997.

Sanchez-Vives MV and McCormick DA. Functional properties of perigeniculate inhibition of dorsal lateral geniculate nucleus thalamocortical neurons in vitro. *J Neurosci* 17: 8880–8893, 1997.

Schmitz D, Schuchmann S, Fisahn A, Draguhn A, Buhl EH, Petrasch-Parwez RE, Dermietzel R, Heinemann U, and Traub RD. Axo-axonal coupling: a novel mechanism for ultrafast neuronal communication. *Neuron* 31: 831–840, 2001.

Segev I, Friedman A, White EL, and Gutnick MJ. Electrical consequences of spine dimensions in a model of a cortical spiny stellate cell completely reconstructed from serial thin sections. *J Comput Neurosci* 2: 117–130, 1995.

Somogyi P, Freund TF, and Cowey A. The axo-axonic interneuron in the cerebral cortex of the rat, cat and monkey. *Neuroscience* 7: 2577–2607, 1982.

Steriade M, Jones EG, and Llinás RR. *Thalamic Oscillations and Signaling*. New York: Wiley–Interscience, 1990.

Stratford KJ, Tarczy-Hornoch K, Martin KA, Bannister NJ, and Jack JJ. Excitatory synaptic inputs to spiny stellate cells in cat visual cortex. *Nature* 382: 258–261, 1996.

Tamás G, Buhl EH, Lörinczi A, and Somogyi P. Proximally targeted GABAergic synapses and gap junctions precisely synchronize cortical interneurons. *Nat Neurosci* 3: 366–371, 2000.

Tamás G, Buhl EH, and Somogyi P. Fast IPSPs elicited via multiple synaptic release sites by different types of GABAergic neuron in the cat visual cortex. *J Physiol* 500: 715–738, 1997.

Tamás G, Somogyi P, and Buhl EH. Differentially interconnected networks of GABAergic interneurons in the visual cortex of the cat. *J Neurosci* 18: 4255–4270, 1998.

Tarczy-Hornoch K, Martin KA, Stratford KJ, and Jack JJ. Intracortical excitation of spiny neurons in layer 4 of cat striate cortex in vitro. *Cereb Cortex* 9: 833–843, 1999.

Thomson AM. Activity-dependent properties of synaptic transmission at two classes of connections made by rat neocortical pyramidal axons in vitro. *J Physiol* 502: 131–147, 1997.

Thomson AM and Bannister AP. Interlaminar connections in the neocortex. *Cereb Cortex* 13: 5–14, 2003.

Thomson AM and Deuchars J. Synaptic interactions in neocortical local circuits: dual intracellular recordings in vitro. *Cereb Cortex* 7: 510–522, 1997.

Thomson AM and West DC. Presynaptic frequency filtering in the gamma frequency band; dual intracellular recordings in slices of adult rat and cat neocortex. *Cereb Cortex* 13: 136–143, 2003.

Traub RD, Cunningham MO, Gloveli T, LeBeau FEN, Bibbig A, Buhl EH, and Whittington MA. GABA-enhanced collective behavior in neuronal

axons underlies persistent gamma-frequency oscillations. *Proc Natl Acad Sci USA* 100: 11047–11052, 2003.

Traub RD, Jefferys JGR, and Whittington MA. Enhanced NMDA conductance can account for epileptiform activity induced by low Mg^{2+} in the rat hippocampal slice. *J Physiol* 478: 379–393, 1994.

Traub RD, Kopell N, Bibbig A, Buhl EH, LeBeau FEN, and Whittington MA. Gap junctions between interneuron dendrites can enhance synchrony of gamma oscillations in distributed networks. *J Neurosci* 21: 9478–9486, 2001.

Venance L, Rozov A, Blatow M, Burnashev N, Feldmeyer D, and Monyer H. Connexin expression in electrically coupled postnatal rat brain neurons. *Proc Natl Acad Sci USA* 97: 10260–10265, 2000.

White EL, Amitai Y, and Gutnick MJ. A comparison of synapses onto the somata of intrinsically bursting and regular spiking neurons in layer V of rat SmI cortex. *J Comp Neurol* 342: 1–14, 1994.

Xiang Z, Huguenard JR, and Prince DA. Synaptic inhibition of pyramidal cells evoked by different interneuronal subtypes in layer V of rat visual cortex. *J Neurophysiol* 88: 740–750, 2002.

Zhang SJ, Huguenard JR, and Prince DA. $GABA_A$ receptor-mediated Cl^- currents in rat thalamic reticular and relay neurons. *J Neurophysiol* 78: 2280–2286, 1997.

Zhu Y, Stornetta RL, and Zhu JJ. Chandelier cells control excessive cortical excitation: characteristics of whisker-evoked synaptic responses of layer 2/3 nonpyramidal and pyramidal neurons. *J Neurosci* 24: 5101–5108, 2004.

Zonta M and Carmignoto G. Calcium oscillations encoding neuron-to-astrocyte communication. *J Physiol* (*Paris*) 96: 193–198, 2002.

APPENDIX C

Computer science aspects

Here we describe the computing platform and the organization of the code. [Further details may be obtained by contacting roger.traub@downstate.edu.] We assume the reader is familiar with the basic principles of simulating membrane electrophysiology in compartmental neurons (Koch and Segev 1998; Traub and Miles 1991).

Simulations were run on a Linux cluster, an IBM e1350, purchased with a combination of National Institutes of Health funds and funds from the SUNY Downstate equipment matching program. The cluster consists of a management/user node and a number of compute nodes. Each compute node contains a dual-processor Intel P4 Xeon 2.4-GHz cpu (central processing unit), with 512 Kbytes of L2 cache; or, more recently, an e1350 Blade 1, at 2.8 GHz. The operating system was Redhat Linux version 7.3. The Linux cluster was used so that the computation could be broken in pieces, each of which runs on its own cpu; the parallel computing allowed simulations to be run in times that were not too unreasonable. Parallel computing on the system was managed by PBS (portable batch system) software.

Code was written in Fortran, which is highly efficient for parallel applications. The **mpi** protocol was used so as to allow the various cpus to run independently, and yet *1*) be able to share data (such as firing times of all the axons in the network), and *2*) to maintain synchrony among the cpus, even though some cpus are handling more computational work than others.

The code was organized so that the numerical integration of each cell type (14 in all) ran on a separate cpu. This organization has a major disadvantage, in that some cpus are loaded more than other cpus, and the overall simulation can run only as fast as the most loaded cpu. On the other hand, the chosen organization makes the code reasonably intelligible, and—we believe—allows for the easiest expansion, to include more cell types, and to allow for extension to multiple columns. In addition, because gap junction connections are mostly between cells of the same type (e.g., superficial LTS interneurons, deep nontufted pyramidal cells), having all cells of a given type on a single cpu will lessen some of the between-cpu message passing. Unfortunately, this relative advantage will be lessened as the number of neurons increases, when it happens that not all cells (even of a given type) can be handled on a single cpu.

To reiterate the cell types, one cpu each is assigned to each cell type as follows: superficial pyramidal RS, superficial pyramidal FRB, superficial basket, superficial axoaxonic, superficial LTS interneuron, layer 4 spiny stellates, tufted layer 5 IB pyramids, tufted layer 5 RS pyramids, nontufted deep pyramids, deep basket, deep axoaxonic, deep LTS interneuron, TCR cells, and nRT cells. Each of these cell types had its own integration program, using a uniform integration step ($dt = 2\ \mu s$), and an explicit 2nd-order Taylor series integration method. Each integration subroutine calls a special subroutine that specifies the voltage and $[Mg^{2+}]_o$ dependency of NMDA conductances (see Fig. B11 in APPENDIX B).

To explain in more detail the organization of the main (highest level) program, we shall list a series of blocks of code that are either **common** (run identically on each cpu) or **cpu-specific** (in which each cpu executes its own code, code specific to the type of neuron "living" on that cpu). The structure of the main program, at a coarse-grained level, is as follows:

1. COMMON. Define the basic network parameters, including these: the number of neurons of each type; the number of synaptic inputs each neuron of one type receives from neurons of any other type; the number of compartments, and their identity, where a synaptic connection from a neuron of *type 1* to a neuron of *type 2* can be placed (for all ordered pairs [*type 1*, *type 2*]); the compartmental locations of possible gap junctions, the density of gap junctions, and which types of cells can couple to which; synaptic conductance scaling factors and time constants; gap junction conductances, and so forth.

2. COMMON. Define a series of tables that specify all the synaptic interconnections (i.e., a cell of *type 1* contacts compartment *x* on another cell of *type 2*); likewise for gap junction interconnectivity; specify tonic driving currents, and the noise parameters for ectopic spikes, and other parameters.

3. COMMON. Allow for special sorts of weightings applied to synaptic conductances of one class or another, for example, to simulate the effects of NBQX, APV, or picrotoxin, or to disconnect the thalamus from the cortex; or to examine the effects of some particular manipulation, such as increasing the extent to which nRT cells inhibit TCR cells.

4. CPU-SPECIFIC. Update the values of time-dependent synaptic conductances, using the latest tables of axonal activity. This is done every 50 time steps. Determine also which axons are to generate new ectopic spikes.

5. CPU-SPECIFIC. Each cpu calls the integration program appropriate for the cell type "living" on that cpu. The subroutine call passes parameters that include: how many time steps have been integrated; the number of neurons of the appropriate type; the present (and to be calculated at the next time step) values of all the voltages and $[Ca^{2+}]_i$; tonic driving currents; synaptic conductance values (for AMPA, NMDA, $GABA_A$); $[Mg^{2+}]_o$; gap junction conductances and connectivity tables. (Synaptic connectivity tables need not be passed to the subroutine, as the relevant information for the integration routine is contained in the actual present values of the conductances, which have been computed in step 4.)

In the very first call of each integration subroutine, that subroutine calls additional subroutines that establish—for the type of neuron handled in the integration subroutine—the basic neuronal structural parameters: compartmental topology, membrane conductance densities (e.g., for fast g_{Na}), electrotonic parameters (R_M, R_i, C_M), the scaling constant for coupling $[Ca^{2+}]_i$ in each compartment to Ca^{2+}-dependent conductances in that compartment; and rate functions for the time-dependent membrane state variables. Each of the 14 cpus performs numerical integration on its cells in order (*cell 1*, *cell 2*, etc.)

6. CPU-SPECIFIC. If the neurons on cpu *k* are electrically coupled to neurons on another cpu, say cpu *l*, then—every 5 time steps—cpu *k* must broadcast the membrane voltages at those compartments (for neurons living on cpu *k*) at which gap junctions might be located. To do this, cpu *k* broadcasts the voltages to all other cpus, so that cpu *l* receives the necessary data. For example, the cpu handling superficial pyramidal RS cells will have to broadcast voltages at some axonal site(s) to all other cpus, so that the cpu handling superficial pyramidal FRB cells can be kept informed.

7. CPU-SPECIFIC. Every 50 time steps, each cpu broadcasts (for its own neurons) the voltages at that distal axon compartment used for the calculation of synaptic inputs to other neurons.

8. COMMON. Update the tables of distal axonal activity. These tables are used in step 4.

9. CPU-SPECIFIC. Every 50 time steps, each cpu writes data about its own neurons, including voltages at selected compartments of selected neurons; total AMPA, NMDA, and $GABA_A$ synaptic input received by one neuron; an average of all the somatic potentials of the neurons on the respective cpu; and the estimated contribution made—by that cpu's neurons—to the extracellular potential at various levels in the cortex.

Steps 4 through 9 are repeated until the simulation is finished. Simulating 1.6 s of network activity took about 30 h, about 18.75 h per second of simulation, with the Xeon nodes. A 6-s simulation took about 127 h (about 21.2 h per second of simulation), with the Blade nodes.

Integration method

We used an explicit 2nd-order Taylor series method with fixed time step (2 μs). This is the same method as used in previous studies (Traub and Miles 1991).

Compilation of the main program—the one with calls to the mpi parallel computing subroutines—was performed with an Intel Fortran parallel compiler, using the call **mpif77**, and linking to the directory PEPCF90. Nonparallel Fortran subroutines were compiled with the call ifc. All compilations used the O3 optimization option.

Fast Fourier transforms (FFTs)

FFTs were usually performed on 8,142 (2^{13}) data points, representing 814.2 ms of data, most often field potential data. We used an FFT algorithm found in the Intel Fortran library in directory /usr/local/lib/libdfftpack.a, with calls to subroutines ZFFTI and ZFFTF.

APPENDIX C REFERENCES

Koch C and Segev I. Editors. *Methods in Neuronal Modeling.* Cambridge, MA: MIT Press, 1998.

Traub RD, Jefferys JGR, and Whittington MA. *Fast Oscillations in Cortical Circuits.* Cambridge, MA: MIT Press, 1998.

Traub RD and Miles R. *Neuronal Networks of the Hippocampus.* Cambridge, UK: Cambridge Univ. Press, 1991.